The Atmospheric Oxidizing Capacity in China: Part 2. Sensitivity to emissions of primary pollutants

Jianing Dai[a], Guy P. Brasseur[a,e,f], Mihalis Vrekoussis[b,g,h], Maria Kanakidou[b,d], Kun Qu[b], Yijuan Zhang[b], Hongliang Zhang[c], Tao Wang[f]

[a] Environmental Modelling Group, Max Planck Institute for Meteorology, Hamburg, 20146, Germany
[b] Institute of Environmental Physics (IUP), University of Bremen, Bremen, 28359, Germany
[c] Department of Environmental Science and Engineering, Fudan University, Shanghai, 200433, China
[d] Environmental Chemical Processes Laboratory, Department of Chemistry, University of Crete, Heraklion, 70013, Greece
[e] National Center for Atmospheric Research, Boulder, Colorado, 80307, USA
[f] Department of Civil and Environmental Engineering, The Hong Kong Polytechnic University, Hong Kong, China
[g] Center of Marine Environmental Sciences (MARUM), University of Bremen, Bremen, 28359, Germany
[h] Climate and Atmosphere Research Center (CARE-C), The Cyprus Institute, Nicosia, Cyprus

Correspondence to: Guy P. Brasseur (guy.brasseur@mpimet.mpg.de)

Formatted: Font color: Text 1

Formatted: Font color: Text 1

Abstract

The Atmospheric Oxidation Capacity (*AOC*), often referred to as the self-cleansing ability of the atmosphere, considerably affects the concentrations of photochemical air pollutants. Despite substantial reductions in anthropogenic emissions of key chemical compounds in China, the mechanisms that determine the changes in the atmospheric oxidation capacity are still not sufficiently understood. Here, a regional chemical transport model is employed to quantify the sensitivity of air pollutants and photochemical parameters to specified emission reductions in China for conditions of January and July 2018 as representative. The model simulations show that, in winter, a 50% decrease in nitrogen oxides (NO_x) emissions leads to an 8-10 ppbv (15-20%) increase in surface ozone concentrations across China. In summer, the ozone concentration decreases by 2-8 ppbv (3-12%) in NO_x-limited areas, while ozone increases by up to 12 ppbv (15%) in volatile organic compounds (VOCs)-limited areas. This ozone increase is associated with a reduced NO_x-titration effect and higher levels of hydroxyl (OH) and hydroperoxyl (HO_2) radicals due to reduced loss reacted with nitrogen dioxide (NO_2) and decreased aerosol uptake. ~~This ozone increase is associated with a reduced NO_x titration effect and higher levels of hydroperoxyl (HO_2) radical due to decreased aerosol uptake.~~ With an additional 50% reduction in anthropogenic VOCs emission, the predicted ozone concentration decreases by 5-12 ppbv (6-15%) in the entire geographic area of China, with an exception in the areas, where the role of BVOCs is crucial to ozone formation. Further, the adopted reduction in NO_x emission leads to an increase of *AOC* by 18% in VOC-limited areas. This specific increase is associated with the combined effect of enhanced radical cycles associated with the photolysis of oxidized VOCs (OVOCs) and the oxidation of alkenes by hydroxyl (OH) radical and O_3. ~~A large reduction of daytime *AOC* in summer results from the reduction in anthropogenic VOCs emission, with a dominant contribution from the reaction of OH radical with reduced alkenes, followed by the reactions with depleted aromatics and OVOCs.~~ This study highlights that photolysis of OVOCs and oxidation of alkenes and aromatic in urban areas when NO_x emission is reduced leads to an increase in O_3. To mitigate ozone rises in urban areas, a joint reduction in the emission of NO_x and specific VOCs species, including alkenes, aromatics and ~~aromatics and~~ unsaturated~~photodegradable~~ OVOCs, including methanol and ~~should~~ethanol, should be implemented.

Keywords: ozone pollution, emission reduction, nitrogen chemistry, *AOC*

Formatted: Font color: Text 1
Formatted: Subscript
Formatted: Subscript
Formatted: Subscript
Formatted: Font color: Text 1
Formatted: Font color: Text 1
Formatted: Font color: Text 1
Formatted: Not Highlight
Formatted: Font color: Text 1

1. Introduction

To effectively reduce air pollution in China, the government of the country has implemented stringent actions between 2013 and 2020 (Liu et al., 2020; Liu et al., 2023). In the initial phase, from 2013 to 2017, the control of primary pollutants was particularly effective, with a dramatic decrease in the anthropogenic emissions of fine particles ($PM_{2.5}$), sulfur dioxide (SO_2), and nitrogen oxides (NO_x) (Liu et al., 2020). After that, a sustained reduction in the emission of SO_2, NO_x, and $PM_{2.5}$ was achieved with continuous emission control from 2018 to 2020 (Liu et al., 2023). The implementation of the emission control policies has greatly improved China's air quality. However, a significant increase in the surface ozone (O_3) concentration was observed from 2013 to 2019, with the rising trend slowing down from 2020 to 2021, but rebounding in 2022 (Liu et al., 2023; China Air 2023). Some studies have documented the explanations for the significantly increasing trend in the surface O_3 concentration, including the reduction of NO_x emissions and atmospheric aerosol loading (Li et al., 2019a; Liu et al., 2020). During and after the recent COVID-19 lockdown, ozone pollution has also been reported to happen, which is believed to be favored by the sharp reduction of NO_x and high emissions of VOCs (Li et al., 2021). Looking through these changes over the past decade, we can learn that rapid reductions of emissions may lead to varied ozone chemistry and, thereby, complex changes in ozone concentrations in China.

The response of ozone to reduced NO_x emissions varies with the local photochemical environment and is different in VOC-limited, NO_x-limited, or transition regimes (Ou et al., 2016; Dai et al., 2023). In VOC-sensitive regimes, the reduction of NO_x tends to increase ozone formation due to the weakening of NO nitration and the competition between NO_2 and VOC for OH radicals (Ou et al., 2016). In NO_x-sensitive regimes, NO_x emission reduction decreases the photolysis of NO_2, leading to less ozone formation (Ou et al., 2016). Several studies using satellite observations (Wang et al., 2021) and regional models (Zhang S. et al., 2023) have shown that the reduction in anthropogenic emissions has generated a change in the geographical distribution of the ozone formation regimes in China. The shift of ozone sensitivity regimes from VOC-sensitive to transition and/or NO_x-sensitive in many metropolitan and suburban regions of East China was also reported by these studies. This shift enables efficient ozone control in NO_x-sensitive areas in response to the continuous decrease in NO_x emissions. In VOC-sensitive and transition areas, NO_x emission reduction fails to effectively mitigate ozone pollution, while a coordinated reduction in anthropogenic VOCs (AVOCs) emissions should effectively limit the ozone formation and should therefore be implemented (Liu et al., 2023; Zhang S. et al., 2023). The source of NO_x in VOC-sensitive areas is mainly from fossil fuel combustion, while AVOCs emissions have a range of sources.

Formatted: Font color: Text 1

Formatted: Font color: Text 1

Formatted: Font color: Text 1

Formatted: Font color: Text 1

To establish a cost-effective control over AVOCs emission, the assessment of the contribution of different VOCs species to ozone formation should be accurately estimated for different areas of China.

~~Aerosol decreases associated with the reduction of primary emissions are expected to continuously affect the effectiveness of ozone control (Liu et al., 2023). Following the successful controls on anthropogenic emissions since 2013, a substantial reduction in $PM_{2.5}$ concentration was observed in China (Zhai et al., 2019). The reduction in the emission of NO_x, SO_2, and ammonia (NH_3), as the gaseous precursors of secondary inorganic aerosol (SIA, the sum of sulfate (SO_4^{2-}), nitrate (NO_3^-), and ammonium (NH_4^+)), leads to a decrease in the SIA concentration (Meng et al., 2022). The decrease in AVOCs emissions will lead to a decrease in the concentration of secondary organic aerosol (SOA), given the gas-phase photochemical oxidation of VOCs plays an important role in SOA formation (Yuan et al., 2013; Li et al., 2022). However, the increasing trends of OH radicals will positively influence SOA formation (Wang W. et al., 2022; Wang W. et al., 2023) and provide an increasing portion of the secondary formation in aerosol compositions (An et al., 2019).~~ The interaction of aerosol and O_3 formation has been discussed in many modeling studies (Li et al., 2019; Liu et al., 2020). However, the influences of aerosol on O_3 production can be varied due to counteracted aerosol effects and different aerosol concentrations (Tan et al., 2022; Dai et al., 2023). Understanding the changes in aerosol effects on ozone formation when the primary emissions are further reduced is still necessary to implement an efficient air quality control policy.

Recent observational studies combined with a source apportionment approach using observation-based models have highlighted the role of specific VOCs species, including the alkenes, aromatics, and several OVOCs, in mitigating summertime ozone formation in the urban areas of China (Shi et al., 2023; Wang W. et al., 2022). The notable contributions of OVOCs to *AOC* as well as the formation of SOA in China have been of concern in many studies (Li et al., 2022; Wang et al., 2023). Since the oxidation of biogenic VOCs (BVOCs) can significantly contribute to the formation of secondary pollutions, the important role of BVOCs in *AOC* and the formation of SOA has also been highlighted in vegetated and highly greening regions in China (Cao et al., 2022; Zhang et al., 2023). However, a comprehensive evaluation of the influence of different VOCs species on *AOC* and ozone chemistry in different regions of China is still needed. Considering the necessity of implementing coordinated actions among large areas to further alleviate air pollution in China, regional chemical transport models are appropriate tools to assess the quantitative response of various VOCs species and *AOC*-related chemical parameters to emission changes.

In the companion paper (Part 1; Dai et al., 2023), we used a regional chemical-meteorological model to quantify the relative contribution of different photochemical processes to the formation and destruction of near-surface RO_x and O_3 in different chemical environments in China. In Part 2 of the study, with the evaluated model, we assess the response of the photo-oxidative species and related parameters to the reduction of primary emissions. This paper is

Formatted: Font color: Text 1

structured as follows. Section 2 introduces the setups of the model system and describes the simulations performed for specified reductions in the emissions of primary pollutants. In Section 3, we first analyze the response in the near-surface concentration of ozone precursors and intermediate to primary emission reductions. We ~~discuss~~ also discuss the changes in the ozone formation regime. ~~resulting from emission reductions.~~ Further, we derive the associated changes in ozone, and aerosols to emission reductions. ~~We also derive the associated changes in the radical and ozone budgets. Further, we analyzed the response in the near-surface concentration of ozone precursors, ozone, and aerosols to emission reductions.~~ Finally, we describe the sensitivity of ~~the photochemical parameters and~~ the atmospheric oxidative capacity (*AOC*) to the reduction in emissions. A summary and implication for policy making of our study is provided in Sec. 4.

2. Method

2.1. Model setting

We use the WRF-Chem model version 4.1.2 (Skamarock et al., 2019), coupled with the gas-phase chemistry mechanism MOZART and the aerosol module MOSAIC, to simulate the meteorological fields as well as the transport, the chemical and physical transformations of trace gases and aerosols. The months of January and July of 2018 were selected as representative months to conduct the simulations and investigate the changes in secondary pollution and *AOC* in response to emission reductions during winter and summer, respectively. Compared to the standard version of the chemical mechanism, several updates of heterogeneous uptake over the ambient aerosol were made (Dai et al., 2023). As for SOA formation in the selected chemical mechanism, the main pathways result from the gas-phase oxidation of VOCs by atmospheric oxidants (OH, O_3, and NO_3) and the heterogeneous formation of glyoxal SOA over the ambient aerosol. The model domain covers the whole geographical area of China. Analyses of modeling results at four urban ~~eight~~ sites~~, including four urban sites~~ (Beijing, Shanghai, Guangzhou, and Chengdu) ~~, two rural sites (Wangdu and Heshan), and two remote sites (Waliguan and Hok Tsui),~~ were also performed in this study. More detailed information on the model configuration, the model validation, and the sites selected for our analysis can be found in Part 1 of our paper by Dai et al. (2023).

We used the Multi-resolution Emission Inventory (MEIC v1.3; http://www.meicmodel.org/) to represent anthropogenic emissions in China and the CAMS-GLOB-ANT v4.2 inventory (https://eccad.aeris-data.fr/) provided by the Copernicus Atmosphere Monitoring Service (CAMS) for anthropogenic emissions in the Asian areas outside China. To explore the sensitivity of secondary pollution and *AOC* to emission reduction, sensitivity experiments were designed to separately assess the influence of reduced NO_x, AVOCs, and other emissions. As shown in Table S1, NO_x emissions include the emissions of NO_2 and NO, and AVOCs emissions include these of ~~alkenes (C_2H_4, C_3H_6, and BIGENE (alkenes with carbon number $\geq$ 4)),~~ alkanes [~~(~~ethane (C_2H_6~~,~~), propane (C_3H_8~~,~~), and BIGALK (alkanes with carbon number $\geqslant$ 4))~~)~~, alkenes [ethene (C_2H_4), propene (C_3H_6), and BIGENE (alkenes with carbon number$\geqslant$ 4)], aromatics [~~(~~benzene (C_6H_6), toluene ($C_6H_5CH_3$), and xylene ($C_6H_4(CH_3)_2$))~~)~~, alkyne (C_2H_2),

Formatted: Font color: Text 1
Formatted: Font color: Text 1
Formatted: Font color: Text 1, Not Highlight
Formatted: Font color: Text 1
Formatted: Font color: Text 1
Formatted: Font color: Text 1
Formatted: Font color: Text 1
Formatted: Font color: Text 1
Formatted: Font color: Text 1
Formatted: Font color: Text 1
Formatted: Font color: Text 1
Formatted: Font color: Text 1
Formatted: Subscript
Formatted: Subscript
Formatted: Font color: Text 1
Formatted: Subscript
Formatted: Subscript
Formatted: Subscript
Formatted: Font color: Text 1
Formatted: Subscript
Formatted: Subscript
Formatted: Subscript
Formatted: Subscript

isoprene (C_5H_8), terpenes ($C_{10}H_{16}$), aand OVOCs (~~CH_3CHO,~~methanol (CH_3OH), ethanol (~~-~~C_2H_5OH), acetaldehyde (CH_3CHO), ~~CH_3OH, $C_{10}H_{16}$,~~ acetone (CH_3COCH_3), methyl acrylate CH_2CCH_3CHO (MACR), and methyl vinyl ketone $CH_2CHCOCH_3$ (MVK)). For other emissions, the emissions of NH_3, SO_2, and carbon monoxide (CO) were considered.

2.2. Design of numerical experiment

To explore the sensitivity of secondary pollutants to emissions changes, five numerical experiments are conducted in both January and July of 2018 (Table 1). In the baseline case, denoted as "*BASE*", we adopted emissions as described in Sect. 2.1. The concentrations of the key species modeled in this case have been validated in our companion study (Dai et al., 2023). To quantify the sensitivity of pollutants to the reduction of NO_x and AVOCs emissions, we applied arbitrary reductions in the surface emissions of primary pollutants; In the first two cases, a 50% reduction is applied separately to the baseline NO_x and AVOCs emissions in whole geographical areas of China. These two sensitivity cases are labeled "*NO_x*" and "*AVOCs*", respectively. A third case in which 50% reduction is applied to both NO_x and AVOCs emissions is referred to as "*N+A*". ~~The simulation labeled "*TOTAL*" assumes that all anthropogenic emissions (NO_x, AVOCs, and other primary pollutants including CO, SO_2, and NH_3) are reduced by 50%.~~ The difference between modeled concentrations of pollutants and chemical parameters in the sensitivity cases and the baseline case provides an estimate of the response of secondary pollution and chemistry to different emission reductions.

Additionally, a ~~The~~ simulation labeled "*TOTAL*" assumes that all anthropogenic emissions under consideration (NO_x, AVOCs, and other primary pollutants including CO, SO_2, and NH_3) are reduced by 50%. This case is used to explore the impact of reduction in the emission of CO, as an ozone precursor, and of SO_2 and NH_3, as aerosol precursors, on ozone formation. The spatial distribution of the emission fluxes changes for the different cases is shown in Fig. S1.

~~3. Model results~~

~~3.1. Changes in ozone regimes~~

~~In order to display the impact of emission reduction on the changes in the ozone regimes, we first show the geographical distribution of NO_x-limited or VOC-limited ozone formation regimes. We adopt the ratio between the production rate of hydrogen peroxide (H_2O_2) and that of nitric acid (HNO_3) [$P(H_2O_2)/P(HNO_3)$] as the indicator to distinguish these regimes. An area is assumed to be VOC-limited or NO_x-limited if $P(H_2O_2)/P(HNO_3) < 0.06$ or $P(H_2O_2)/P(HNO_3) > 0.2$, respectively (Zhang et al., 2009). The regions with ratios between these two limits represent transition situations (Dai et al., 2023).~~

~~Figure 1 shows how the spatial distribution of ozone regimes varies in response to applied emission reductions in both January and July. Under baseline conditions (BASE case), during January, ozone formation in a large part of China, including the north, east, and~~

Formatted: Font color: Text 1
Formatted: Font color: Text 1
Formatted: Font color: Text 1
Formatted: Font color: Text 1
Formatted: Font color: Text 1
Formatted: Font color: Text 1
Formatted: Font color: Text 1
Formatted: Font color: Text 1
Formatted: Subscript
Formatted: Subscript
Formatted: Font color: Text 1
Formatted: Font: Bold, Font color: Text 1
Formatted: List Paragraph, Line spacing: single, Outline numbered + Level: 1 + Numbering Style: 1, 2, 3, … + Start at: 1 + Alignment: Left + Aligned at: 0.63 cm + Indent at: 1.27 cm, Border: Top: (No border), Bottom: (No border), Left: (No border), Right: (No border), Between : (No border)
Formatted: Font color: Text 1
Formatted: Indent: Left: 0.63 cm
Formatted: Indent: Left: 0.63 cm, Border: Top: (No border), Bottom: (No border), Left: (No border), Right: (No border), Between : (No border)

~~central areas, as well as the southeastern coastline and PRD regions, is controlled by the availability of VOC (Fig. 1a). In contrast, ozone formation in western China is under the control of NO_x, while a small area in southern China is located in transition areas. Generally, ozone regimes change mainly in the southern part of China when emissions are reduced. With a 50% reduction in NO_x emissions (Fig. 1c), transition or VOC-limited regimes in the south and southwest China tends to become NO_x-limited for ozone production. With a 50% reduction in AVOCs emissions, some transition areas of southern China are converted to VOC-limited areas (Fig. 1e). With the combined reduction in NO_x and AVOCs emissions (Fig. 1g) as well as in all anthropogenic emissions (Fig. 1i), the VOC-limited regions evolve towards transition or NO_x-limited regions in southern China.~~

~~During July, for baseline conditions (BASE case) (Fig. 1b), a large fraction of the Chinese territory corresponds to NO_x-limited conditions; VOC-limited conditions are found in urban areas including the North China Plain (NCP), the Yangzi River Delta (YRD), the Pearl River Delta (PRD), and the Si Chuan Basin (SCB). The changes in ozone regimes with emission reductions are found mainly in VOC-limited areas and surroundings. With the reduction of NO_x emissions, VOC-limited areas shrink and become more concentrated in a smaller fraction of metropolitan areas (Fig. 1d). With the reduction of AVOCs emissions, VOC-limited areas expand to the surroundings near the metropolitan areas (Fig. 1f). With the combined 50% reduction in the emissions of NO_x and AVOCs (N+A case; Fig. 1h) and of all species (TOTAL case; Fig. 1j), the calculated change pattern of ozone sensitivity is similar, with a smaller VOC-limited area relative to the BASE case.~~

~~At the specific sites examined here (see Sect. 2.1), emission reduction does not modify ozone sensitivity regimes at the urban and rural sites in January (Fig. S2), remaining in VOCs-limited regimes. Except for the remote site Waliguan, at this site, the ozone production is still located in the transition regimes in AVOCs case, while in other cases changing to NO_x-limited regime. However, the change in ozone regimes is notable in July (Fig. 2). During this season, in the baseline case, the four urban sites and the rural site of Wangdu are VOC-limited; the Heshan site is located in the transition regime and the two remote sites are located in the NO_x-limited area. With a 50% reduction in NO_x emissions, only the Guangzhou site remains in a VOC-limited region, but also with the value of the $P(H_2O_2)/P(HNO_3)$ ratio increasing from 0.008 to 0.045. The other three urban sites shift from VOC-limited regimes to transition areas. With a 50% cut in AVOCs emission, ozone sensitivity at the Hok Tsui site shifts from VOC-limited to transition conditions. If we apply a combined 50% reduction to the emissions of NO_x and AVOCs (N+A case) and all emissions (TOTAL case), the three sites of Beijing, Chengdu, and Wangdu shift from a VOC-limited to a transition area.~~

3.~~2~~1. Changes in precursors and intermediates in ozone formation ~~Changes in the budgets of radicals and ozone~~

Formatted: Font color: Text 1

Formatted: Indent: Left: 0.63 cm

Formatted: Font color: Text 1

Formatted: Left, Indent: Left: 0.63 cm, Border: Top: (No border), Bottom: (No border), Left: (No border), Right: (No border), Between : (No border)

~~In Part 1 of the present study (Dai et al., 2023), we found that the production of RO_x radicals in China results primarily from the photolysis of O_3, nitrous acid (HONO), and different OVOCs, with a relatively minor role from the ozonolysis of alkenes. Besides, the destruction of RO_x radicals results from the termination reactions between different RO_x radicals and between RO_x radicals and nitric oxide as well as from the heterogeneous uptake of HO_2 on aerosol surfaces. The production rate of odd oxygen (O_x = O_3 + NO_2) is associated with recurrent radical reaction chains involving the oxidation of hydrocarbons in the presence of NO_x. The photochemical destruction of O_x results from several processes, including the photolysis of O_3, followed by the reaction between the electronically excited oxygen atom $O(^1D)$ and water vapor (H_2O). Other O_x loss mechanisms include the reactions of ozone with OH, HO_2, and different alkenes. In the presence of NO_x, additional O_x losses are provided by the titration of O_3 by NO, followed by the conversion of NO_2 to nitric acid (HNO_3).~~

~~In Part 1 of the present study (Dai et al., 2023), we found that the production of RO_x radicals in China results primarily from the photolysis of O_3, nitrous acid (HONO), and different OVOCs, with a relatively minor role from the ozonolysis of alkenes. Besides, the destruction of RO_x radicals results from the termination reactions between different RO_x radicals and between RO_x radicals and nitric oxide as well as from the heterogeneous uptake of HO_2 on aerosol surfaces. The production rate of odd oxygen (O_x = O_3 + NO_2) is associated with recurrent radical reaction chains involving the oxidation of hydrocarbons in the presence of NO_x. The photochemical destruction of O_x results from several processes, including the photolysis of O_3, followed by the reaction between the electronically excited oxygen atom $O(^1D)$ and water vapor (H_2O). Other O_x loss mechanisms include the reactions of ozone with OH, HO_2, and different alkenes. In the presence of NO_x, additional O_x losses are provided by the titration of O_3 by NO, followed by the conversion of NO_2 to nitric acid (HNO_3).~~

~~3.2.1. Production and destruction rates of RO_x~~

~~Figure 3 shows the spatial distribution of the changes in the averaged daytime (06:00-19:00 Local Standard Time) production rate of RO_x radicals ($P(RO_x)$) near the surface resulting from a 50% decrease in NO_x and AVOCs emissions for conditions representative of January and July 2018, respectively.~~

~~In January, with a 50% reduction in NO_x emission, the resulting reduction in $P(RO_x)$ is of the order of 0.3-0.7 ppbv h^{-1} (30-33%) in the urban areas, including in the NCP, YRD, and PRD regions (Fig. 3a). The effect of the reduction in AVOCs emissions on the daytime value of $P(RO_x)$ is less significant than the effect of NO_x emission reduction, with decreases of $P(RO_x)$ by only 0.1-0.4 ppbv h^{-1} (10-25 %) in the NCP, YRD and SCB (Fig. 3c), but by up to 0.8 ppbv h^{-1} (35%) in the PRD. More notable effects of AVOCs emission reduction on $P(RO_x)$ in the PRD are mainly attributed to the reduced contribution from the photolysis of OVOCs (see the results at the Heshan and Hok Tsui sites in Fig. 4). Under the combined reduction in NO_x and AVOCs emissions, the decrease of $P(RO_x)$ ranges within 0.5-0.9 ppbv h^{-1} (30-42%), which is overall larger than the sum of the separated effects of NO_x and AVOCs emission reduction (Fig. 3e). With a further decrease in the emissions of other pollutants, the reduction in the daytime $P(RO_x)$ value, by 0.4-0.8 ppbv h^{-1} (25-35%; Fig. 3g), is slightly lower than the~~

Formatted: Font color: Text 1, Strikethrough

Formatted: Font color: Text 1

Formatted: Border: Left: (No border)

Formatted: Font color: Text 1

Formatted: Font color: Text 1

Formatted: Font color: Text 1

Formatted: Font color: Text 1

Formatted: Font color: Text 1

Formatted: Font color: Text 1

Formatted: Font color: Text 1

Formatted: Font color: Text 1

Formatted: Font color: Text 1

Formatted: Border: Left: (No border)

combined effect of NO_x and AVOCs emissions reduction. The weakened effect on $P(RO_x)$ is related to the higher concentration of HONO, HCHO, non-HCHO OVOCs, and ozone (see Sec. 3.3.1), due to the higher level of oxidants caused by the lower consumption of CO, SO_2, and NH_3, whose emissions are assumed to be reduced.

In July, the decline of $P(RO_x)$ due to the reduction in NO_x emissions is larger than in winter (Fig. 3b), with a maximum decrease of 1.2 ppbv h^{-1} (28%) in urbanized areas. The reduction in AVOCs emissions leads to a reduction in $P(RO_x)$ that reaches 0.8 ppbv h^{-1} (18%) in urbanized areas of East China (Fig. 3d). Under the combined reduction of NO_x and AVOCs emissions, the reduced value of $P(RO_x)$ is also larger than when considering their separated effects, which ranges from 0.5 to 1.2 ppbv h^{-1} (12-28%; Fig. 3f). When the reduction is applied to emissions of other species, the production rate of RO_x decreases by 0.4 to 1.0 ppbv h^{-1} (9-22% Fig. 3h).

Figure 4 shows the averaged value of daytime $P(RO_x)$ at eight monitoring sites in all the cases for January and July, respectively. In January, with the 50% reduced NO_x emissions, the reduction of $P(RO_x)$ is predominantly attributed to the reduced contribution from the photolysis of HONO at urban and rural sites (larger than 70%), which acts as a source of OH. As HONO mainly emanates from the heterogeneous conversion of NO_2 in polluted East China (Zhang et al., 2021), the reduced contribution from HONO is associated with the reduced concentrations of NO_2. In July, the reduced contribution from the HONO photolysis (due to reduced NO_x emissions) is also an important factor in explaining the decrease in the $P(RO_x)$ values (larger than 70%) in urban areas. When considering the decrease in AVOCs emissions, the reduced value in daytime $P(RO_x)$ results to a large extent from the reduction in the photolysis rates of OVOCs in both seasons.

Figure S3 shows the spatial distribution of the average daytime changes in the destruction rate of RO_x radicals ($D(RO_x)$) due to the emission reductions applied in January and July conditions. The reduction in NO_x emissions has a higher effect on $D(RO_x)$ than the reduction in AVOCs emissions. The dominant reason for the decrease in the value of $D(RO_x)$ is due to the reduced destruction rate of OH by nitrogen oxides (NO_2 and NO) in January and July (Fig. S4). A higher contribution from the HO_2 uptake by aerosol, increasing from 3-5% to 5-10% in January and July, is owing to the higher concentration of HO_2 due to reactions with reduced NO and less aerosol uptake (See Sec. 3.3.3).

3.2.2. Production and Destruction Rates of O_x

Figure S5 shows the spatial distribution of the changes in the mean daytime production rate of odd oxygen [$P(O_x)$] during January and July 2018 resulting from emission changes/reductions. In January, with the reduction of NO_x emissions, the calculated decrease in $P(O_x)$ is the largest in southern and eastern China (by 1.5-2.0 ppbv h^{-1} (15-20%); Fig. S5a). Some positive changes in the O_x production rates are simulated in the metropolitan areas of the YRD and SCB, with an increase of 0.8-1.5 ppbv h^{-1} (7-15%). These positive values are attributed to the increase in the concentration of HO_2 and RO_2 radicals, as $P(O_x)$ is strongly contributed by the reaction rates of NO with the HO_2 and RO_2 radicals. With the reduction in AVOCs emissions, $P(O_x)$

Formatted: Font color: Text 1

decreases by up to 4.5 ppbv h^{-1} (42%) in the PRD region (Fig. S5c). When considering combined reductions of the NO_x and AVOCs emissions, the calculated daytime value of $P(O_x)$ is reduced by 2-3 ppbv h^{-1} (30-60%; Fig. S5e) in the whole of China. When the reduction in all anthropogenic emissions is considered, the ozone production rate decreases by 3-5 ppbv h^{-1} (30-70%; Fig. S5g). In different monitoring sites, the highest reduced value of $P(O_x)$ is up to 4.2 ppbv h^{-1} (40%) at the Guangzhou site, followed by 2.8 ppbv h^{-1} (55%) in the Shanghai site, in the effect of AVOCs emission reduction only (Fig. S6).

The decrease of $P(O_x)$ for summer conditions is more significant than for winter conditions. With NO_x emissions reduced by 50% (Fig. S5b), the reduction in the O_x production rate is within the range of 15-20 ppbv h^{-1} (20-50%). As shown in Fig. S6, the value of $P(O_x)$ decreases by 50% in Guangzhou, 45% in Shanghai, 30% in Chengdu, and 25% in Beijing. In response to a 50% reduction in AVOCs emissions, the decrease in the value of $P(O_x)$ (5-10 ppbv h^{-1} (10-28%); Fig. S5d) is smaller than the decrease resulting from the reduction in NO_x emission. We also found a decrease of P(Ox) by 28% in Guangzhou, by 10% in Shanghai, by 25% in Chengdu, and by 20% in Beijing (Fig. S6). When the reduction in both NO_x and AVOCs emissions is applied, the reduced value of $P(O_x)$ is around 16-25 ppbv h^{-1} (22-55%; Fig. S5f). With further reduction of other emissions, the values of $P(O_x)$ decrease by 15-22 ppbv h^{-1} (20-52%; Fig. S5h).

Figure S7 shows the corresponding changes in the destruction rate of odd oxygen ($D(O_x)$). The decrease of $D(O_x)$ resulting from the 50% reduction of NO_x is in the range of 0.1-0.5 ppbv h^{-1} (20-30%) in winter (Fig. S7a), with the highest reduction simulated in the PRD regions. In summer, the reduction of $D(O_x)$ reaches 1.0-2.0 ppbv h^{-1} (15-25%), with the largest decrease occurring in the NCP (Fig. S7b). The decrease of $D(O_x)$ due to the reduction in AVOCs emissions is most prominent in the urbanized areas, with the highest decrease reaching 0.2 ppbv h^{-1} in winter (25%, Fig. S7c) and 0.8 ppbv h^{-1} (10%) in summer (Fig. S7d).

The budgets of radicals and ozone are important indicators for the formation potential of ozone and other secondary pollutants (Tan et al., 2019). The decrease in the values of the summertime $P(RO_x)$ and $P(O_x)$ provides some information that can be useful to mitigate secondary photochemical pollution. The changes in the budgets due to emission reduction suggest that the most effective way to reduce summertime $P(RO_x)$ and $P(O_x)$ is to reduce NO_x emissions. When applying a combined reduction in the NO_x and AVOCs emissions, the decrease of the $P(RO_x)$ and $P(O_x)$ values is further enhanced. Thus, reductions in specific AVOCs emissions are needed to conduct the effective mitigation of air pollution in China.

3.3. Changes in the concentrations of ozone and other secondary pollutants

Tropospheric ozone is a secondary pollutant, and its formation is largely affected by the levels of ozone precursors, including NO_x, VOCs, and CO (Wang et al., 2022). The reduction in the emissions of these primary species leads to changes in the photochemical formation of ozone. The formation of secondary inorganic aerosols (SIA), including particulate nitrate (NO_3^-), sulfate (SO_4^{2-}), and ammonium (NH_4^+), is associated with the level of their gas phase

Formatted: Border: Left: (No border)

Formatted: Font color: Text 1

Formatted: Border: Left: (No border)

~~precursors, such as NO_2, SO_2, and NH_3, and oxidants (Zheng et al., 2015). The oxidizing processes of AVOCs, including benzene, xylene, and toluene, play an important role in the formation of anthropogenic secondary organic aerosol (SOA) (Hu et al., 2017). Owing to high uncertainties in the chemical mechanisms adopted in chemical transport models, only limited studies have assessed the impact of reduced primary emissions on the tropospheric concentration of SOA (Hu et al., 2017; Li et al., 2022). In this section, we quantify the response of ozone precursors, ozone, and secondary aerosols to the reduction in the emissions of primary pollutants.~~

~~3.3.1. Precursors and intermediates in ozone formation~~

Firstly, we describe the changes in the surface concentration of ozone ~~ozone~~ precursors and ~~and~~ intermediates, including NO, NO_2, OH radical, HO_2 radical, and specific species of hydrocarbons and ~~and~~ OVOCs, ~~-~~in response to different reductions in surface emissions. We show the results for January and July of 2018, as representative for winter and summer conditions. ~~-~~To support the discussion of radical changes induced by emissions reduction, we examine the changes in two parameters. One is the production of RO_x radicals ($P(RO_x)$), resulting from the photolysis of O_3, nitrous acid (HONO), and of different OVOCs, and from the ozonolysis of alkenes. Another parameter is the destruction of RO_x radicals ($D(RO_x)$), resulting from the termination reactions between different RO_x radicals and between RO_x radicals and nitric oxide, as well as from the heterogeneous uptake of HO_2 on aerosol surfaces. Detailed estimates of $P(RO_x)$ and $D(RO_x)$ can be found in Part 1 of the present study (Dai et al., 2023).

3.1.1. Changes in radicals

Winter condition. Figure ~~5.~~ 1 displays the spatial distribution of the changes in the surface mixing ratios of ~~responses of~~OH and HO_2 radicals ~~the ozone precursors and intermediate to~~ resulting from the 50% reduction in the ~~of~~ NO_x, AVOCs, and combined NO_x and AVOCs emissions for ~~in~~January of 2018 ~~the daytime~~. With the reduction in NO_x emissions~~The calculated mixing ratio of surface OH radical decreases by 0.05 pptv (40%) in southern China (Fig. 5e)~~, the calculated mixing ratio of surface OH radical is significantly decreased in southern China by up to 40% (0.05 pptv, Fig. 1a), with a relatively lower decrease in the central and western parts of China. The decreases in the NO_2 concentration (Fig. S2a), resulting from the reduced NO_x emissions ~~(Fig. SX)~~, lead to reduced formation of ozone. As a result, the oxidation capacity and levels of oxidants are reduced (see Sect. 3.3). At the same time, an increase in the concentration of the OH radical is found in urban areas, including the North China Plain (NCP), Yangzi River Delta (YRD), Pearl River Delta (PRD), and Si Chuan Basin (SCB) regions, with the maximum increase of 24% in PRD regions. This increase is explained by the reduced destruction of the OH radical by the reaction with NO_2 (Fig. S2b). For the HO_2 radical, a distinct increase in its surface mixing ratio is derived in southern China (by up to 5 pptv (60%), Fig. 1b). This~~is~~ enhancement is related to the increased OH radical in urban areas, leading to enhanced HO_2 via VOCs oxidation, and ~~with caused by~~ reduced loss of HO_2 via the

Formatted: Font color: Text 1
Formatted: Font color: Text 1
Formatted: Font color: Text 1
Formatted: Font: Italic
Formatted: Font color: Text 1
Formatted: Font color: Text 1
Formatted: Font color: Text 1
Formatted: Font color: Text 1
Formatted: Font color: Text 1, Not Strikethrough
Formatted: Font color: Text 1
Formatted: Not Strikethrough
Formatted: Font color: Text 1
Formatted: Font: Italic
Formatted: Font color: Text 1
Formatted: Font color: Text 1
Formatted: Font color: Text 1, Subscript
Formatted: Font color: Text 1
Formatted: Font color: Text 1
Formatted: Font color: Text 1
Formatted: Font color: Text 1, Subscript
Formatted: Font color: Text 1
Formatted: Font color: Text 1
Formatted: Font color: Text 1, Subscript
Formatted: Font color: Text 1
Formatted: Font color: Text 1
Formatted: Font color: Text 1
Formatted: Font color: Text 1
Formatted: Subscript
Formatted: Font color: Text 1
Formatted: Not Highlight
Formatted: Font color: Text 1
Formatted: Font color: Text 1
Formatted: Subscript
Formatted: Subscript

aerosol uptake, which is associated with a decrease in the aerosol load (see Sect. 3.2.3), and hence in HO_2 uptake (Song et al., 2021).

For the 50% decrease in AVOCs emissions, the mixing ratio of OH is reduced by 4-12% (0.005-0.015 pptv, Fig. 1c) and the mixing ratio of HO_2 radicals is reduced by 20-~~up to~~ 36% (1-3pptv, Fig. 1d) in the southern part of China. The decreases in these radicals are related to the reduced oxidation of VOCs, due to the reduction in AVOCs emissions. ~~decreased~~ Simultaneously, a slight increase in the mixing ratio of OH radical is derived in the southern part of China. This increase in the OH radical is related to the reduced extinction of radiation associated with the decreased aerosol load due to AVOCs emission reduction.

~~with are calculated with emission reduction~~

When the 50% emission reduction in NO_x is combined with 50% reduction in AVOCs emissions, the distribution of changes in OH radical ~~changes~~ are similar to the pattern induced by the emissions reduction in NO_x alone. However, weakened increase are calculated, as the increase in OH radical with reduced NO_x emissions is largely compensated by the decreased radicals due to the AVOCs emission reduction~~ to radical concentration~~. ~~–~~As shown in Fig. 1e, the maximum increase in urban China is also lowered to 12% (from 40%). Besides that, the increase in HO_2 radicals is also largely reduced to 20% (from 60%) by the lowered ~~with~~AVOCs emissions, with only a mild increase of HO_2 distributed in the southern coast of China (Fig. 1f).

With accounting in addition to the reduction of other anthropogenic emissions (NH_3, SO_2, and CO), the mixing ratio of OH radical is positively modified, relative to the results in the combined case (N+A case). As shown in Fig. S5a, the mixing ratio of OH radical is increasing in the PRD and SCB regions (by up to 22%). This increase is due to the reduced consumption of the OH radical by CO (Fig. S4a), due to reduced CO emissions (Fig. S1d). For the HO_2 radicals, the additional ~~emissions~~ reduction in other emissions also contributes to a larger mixing ratio, with a pronounced increase in southern China ~~in January~~ (by up to 18%, Fig. S5b). This increase in HO_2 radical mixing ratio is due to the increase in the oxidation of VOCs by OH radical and the reduced aerosol uptake of HO_2, associated with the decrease in aerosol load. ~~, where the ozone sensitivity is controlled by NO_x (Fig. 1c), is due to the decrease in the oxidation capacity of atmospheric (See Sec.3.4.2). At the same time, a relatively strong increase of OH is found in the PRD region (by 0.03 pptv; 24%), due to less consumption by the reduction in NO_x and more production from the photolysis of enhanced OVOCs (Fig. 6g). An increase in the surface mixing ratio of the HO_2 radical is derived in southern China (by up to 5 pptv (60%); Fig. 5g), which is associated with a decrease in the aerosol load (see Sect. 3.3.3), and hence in reduced HO_2 uptake (Song et al., 2021).In January, a decrease of NO (by up to 6 ppbv (40%); Fig. 5a) and NO_2 (by up to 8 ppbv (25%); Fig. 5c) is derived in the metropolitan regions of China, which is consistent with the spatial distribution of reduction in NO_x emissions (Fig. S1a). The calculated mixing ratio of surface OH radical decreases by 0.05 pptv (40%) in southern China (Fig. 5e), where the ozone sensitivity is controlled by NO_x (Fig. 1c), is due to the decrease in the oxidation capacity of atmospheric (See Sec.3.4.2). At the same time, a relatively strong increase of OH is found in the PRD region (by 0.03 pptv; 24%), due to less consumption by the reduction in NO_x and more production from the photolysis of~~

Formatted: Not Highlight
Formatted: Font color: Text 1
Formatted: Font: (Asian) +Body Asian (SimSun), (Asian) Chinese (Simplified, Mainland China)
Formatted: Font: (Asian) +Body Asian (SimSun), Font color: Text 1, (Asian) Chinese (Simplified, Mainland China)
Formatted: Font color: Text 1
Formatted: Font color: Text 1
Formatted: Font color: Text 1
Formatted: Font color: Text 1
Formatted: Font color: Text 1
Formatted: Font color: Text 1
Formatted: Font color: Text 1
Formatted: Font color: Text 1
Formatted: Font color: Text 1
Formatted: Subscript
Formatted: Subscript
Formatted: Subscript
Formatted: Font color: Text 1
Formatted: Subscript
Formatted: Subscript
Formatted: Not Highlight
Formatted: Font color: Auto
Formatted: Font color: Auto
Formatted: Font color: Auto
Formatted: Subscript
Formatted: Subscript
Formatted: Font color: Text 1
Formatted: Font color: Text 1
Formatted: Font color: Text 1
Formatted: Font color: Text 1
Formatted: Font color: Text 1

enhanced OVOCs (Fig. 6g). An increase in the surface mixing ratio of the HO_2 radical is derived in southern China (by up to 5 pptv (60%); Fig. 5g), which is associated with a decrease in the aerosol load (see Sect. 3.3.3), and hence in reduced HO_2 uptake (Song et al., 2021).

In July, the decrease in the concentration of NO (4 ppbv (50%); Fig. 5b) and NO_2 (6 ppbv (35%); Fig. 5d) due to the reduction in the NO_x emission is smaller than in winter, which is related with the smaller reduction in summertime NO_x emissions (Fig. S1g). The level of summertime decreases in OH radicals (by up to 0.15 pptv (30-40%); Fig. 5f) is larger than the decrease derived in winter and displayed in broader areas. The spatially varied distribution in the changes of OH and HO_2 radicals in two seasons can be explained by the seasonal variations of UV, water vapor, and solar radiation, with high values concentrated in southern China only in winter and evenly distributed in the whole of China in summer (Dai et al., 2023). An increase in the surface mixing ratio of HO_2 radical is derived in the NCP (6-8 pptv; 15-20%) and is due to the decreased uptake by the aerosol surfaces. An increase of alkene is calculated in July by 0.2-0.5 ppbv (10-20%), owing to the reduced consumption by decreased OH radicals.

For the 50% decrease in AVOCs emissions, the calculated surface concentration of alkenes decreased by up to 3.0-4.0 ppbv (30-40%; Fig. 7a) in urban China in January. At the same time, a decrease is calculated in the mixing ratio of OH (by 0.005-0.015 pptv (4-12%); Fig. 7c) and HO_2 radicals (by 3pptv (36%); Fig. 7e) in the southern part of China. Reasons for the decreases in these radicals are the declined contributions from the VOCs oxidation and OVOCs photolysis. Owing to the reduced consumption of hydrogenated radicals, an increase of NO (by 1.2-2.0 ppbv (7-12%)) is derived in the urban areas of China (Fig. S8a). In July, the calculated decrease of alkenes is estimated to be 1.0-2.0 ppbv (30-50%; Fig. 7b). The reduction in VOCs also leads to a summertime decrease in radicals in urban areas, with the decrease of OH by 0.03-0.05 pptv (8-12%) and HO_2 radicals by 3-5 pptv (6-10%). The relevant summertime enhancement in NO concentration is 0.8-1.0 ppbv (10-15%; Fig. S8b).

When applying the combined 50% reduction in NO_x and AVOCs emissions, the changes in the spatial distribution of radicals are similar to the changes derived when a reduction was applied only to the NO_x emissions alone. Compared with the results in the reduction NO_x emissions alone, a smaller increase of OH radical is provided in urban China in January (by 0.01 pptv (12%); Fig. 8a) and in July (by 0.07 pptv (15-20%); Fig. 8b), which is attributable to the less production of OH radical from the VOCs oxidation due to reduction in AVOCs emission. The decrease of OH radical is also suppressed to 0.02 pptv (16%) in January and 0.1 pptv (10-12%) in July, which is due to the lower destruction rate of OH from the reaction with reduced HO_2 radicals. As the negative effects of declined VOCs oxidation due to AVOCs emissions reduction, the enhanced HO_2 radicals in the NO_x emission reduction case are largely offset. As shown in Fig. 8c and d, the combined case derived less than 1 pptv (12%) of wintertime enhancement in the southern coastal areas of China and 3 pptv (6%) of summertime increase in the urban areas.

When applying a 50% reduction to NO_x, AVOCs, and other anthropogenic emissions, the mixing ratio of OH radical is positively varied compared with the results in the combined case

Formatted: Font color: Text 1

Formatted: Font color: Text 1

Formatted: Font: (Asian) 新細明體, (Asian) Chinese (Traditional, Taiwan)

Formatted: Font color: Text 1

Formatted: Font color: Text 1

~~(N+A case). A distinct increase of wintertime OH radical is derived in the PRD and SCB regions (by up to 0.03 pptv; Fig.8e). This increase is owing to the lower consumption of OH radical by the reduced concentration of NH_3, SO_2, and CO, due to their reduced emissions. In July, the increase of OH radical is also enhanced to 0.01 pptv (Fig. 8f) in VOC-limited areas. At the same time, the decreases of OH radicals in NO_x-limited areas are suppressed in both winter and summer, indicating the increasing atmospheric oxidative capacity in these areas. For HO_2 radicals, the additional emissions reduction also contributed to an increase in its mixing ratio, with a pronounced increase in southern China in January (by 1.5 pptv (18%) Fig 8g) and in the NCP region in July (by 6 pptv (12%); Fig. 8h). The enhancement in HO_2 radicals is caused by less HO_2 loss via the aerosol uptake, as a decrease is derived in aerosol concentration due to the reduction in the precursor of secondary inorganic aerosols (See Sec. 3.3.3).~~

Formatted: Font color: Text 1

Summer condition. Figure 2 displays the spatial distribution of the changes in OH and HO_2 radicals due to the reduction of NO_x, AVOCs, and combined NO_x and AVOCs emissions for July 2018. Compared with the wintertime variation in radicals, which is limited to southern China, the geographical area covered by these changes is broader during summertime and covers a large fraction of northern China. When applying a reduction in NO_x emission by 50%, a decrease in the concentration of OH radicals is derived in large parts of China, with the maximum decrease reaching 40% (0.15 pptv, Fig. 2a). The concentration od the OH radical increases in the metropolitan areas, including in the YRD and PRD regions. Simultaneously, the surface mixing ratio of HO_2 radical increases by 6 to 8 pptv (15-20%, Fig. 2d) in the North China plain. These changes are affected by the meteorological parameters including the temperature, the water vapor abundance, and the solar radiation intensity, which are involved in the oxidative processes (Dai et al., 2023).

Formatted: Font: Italic

When AVOCs emissions are reduced by 50%, the concentration of the radicals in urban areas, including in the NCP, YRD, and PRD regions, decreases on the average by 8-12% in the case of OH (0.03-0.05 pptv, Fig. 2b) and by 6-10% (3-5 pptv, Fig. 2e) in the case of HO_2. Simultaneously, a comparable increase in the OH radical is calculated in non-urban areas, due to potential effect by the aerosol light extinction. When applying the combined 50% emissions reduction in AVOCs with NO_x, the distribution pattern of OH radical changes are similar to the distribution derived for the reduction in NO_x emissions alone, but it is also compensated by the offset effect from AVOCs emissions, like in winter conditions. As shown in Fig.2c, the maximum increase in OH radical is weakened to 20% (from 40%) and the maximum decrease is also reduced to 12% (from 30%). The offset effect of AVOCs emissions reduction is also shown in the enhanced abundance of HO_2 radicals (Fig.2f), with less than 6% (from 15-20%) increases in the urban areas.

With an additional 50% reduction to other anthropogenic emissions, the mixing ratio of OH radical is increased (Fig. S4c), relative to the results obtained in the combined case, with the highest increase occurring in the NCP region.

Formatted: Font color: Text 1

3.1.2 Changes in OVOCs

Oxygenated hydrocarbons (OVOCs) originate from direct surface emissions (primary source), and from the oxidation of primary hydrocarbons (secondary source) in the atmosphere (Wang W. et al., 2022).

Winter condition. Figure 3 shows the spatial distribution of calculated changes in total OVOCs due to the 50% reduction in NO_x, AVOCs and in combined NO_x and AVOCs emissions for January of 2018. With a reduction in NO_x emission, the OVOCs concentration decreases in the non-urban areas in southern China and increases in urbanized China (Fig. 3a), which is consistent with the changes in the mixing ratio OH radical. The highest increase in OVOCs concentration is approximately10% (2 ppbv), in the urban areas of the YRD and PRD regions; it includes a significant increase in the concentration of formaldehyde (HCHO, Fig. S6a), followed by peroxyacetyl nitrate (PAN, Fig. S6b), and alcohols (CH_3OH+C_2H_5OH, Fig. S6c). At four city sites under consideration, the highest increase in OVOCs is calculated in the site of Shanghai and Guangzhou, with concentrations increasing by about 12% (1.8 ppbv, Fig. 3e) and 8% (1.2 ppbv, Fig. 3f), respectively.

When AVOCs emissions are reduced, OVOCs are decreased in most regions of China (Fig. 3b), with the highest decrease found in the regions of PRD and SCB. At the four city sites under consideration, the decrease in ketones is the most distinct (Fig. 3d-g). The abundance of these species is reduced by almost a factor of two, followed by HCHO and other aldehydes. When combining the emission reduction of AVOCs and NO_x, the decrease in OVOCs concentration resulting from the AVOCs emission reduction is further strengthened in large parts of China (Fig. 3c). However, an increased concentration of 1~2 ppbv is derived for OVOCs at Guangzhou site (Fig.3f). With additional decreases in other emissions, the OVOCs' concentration is enhanced by 2~4 ppbv in whole China (Fig. S5e), which is consistent with the increased abundance of the OH radical resulting from a reduction in the NH_3, SO_2, and CO emissions.~~relevant dwith ionfroms~~~~OVOCs are both contributed by the primary source, their direct emissions, and the secondary source, the oxidation of hydrocarbons (Wang W. et al., 2022). With the reduction in emissions, the concentrations of OVOCs also change substantially. Figure 6 g and h displays the spatial distribution of the changes in total OVOCs due to the 50% reduction in NO_x emissions in January and July of 2018. During January, there is an increase in the calculated concentration of OVOCs in the NCP, YRD, and PRD. In these areas, the highest wintertime increases in the concentration of OVOCs reach about 0.5-1.0 ppbv (5-10%; Fig. 6g). At specific sites, the highest increase in OVOCs concentrations is calculated at the Shanghai and Guangzhou sites. As shown in Fig. 9, at these two urban sites, the reduction in NO_x emissions leads to an increase in OVOCs concentration by 1.8 ppbv (12%) and 1.2 ppbv (8%), respectively, which is mainly contributed by the increase of HCHO (Fig. 6e) due to the higher secondary formation from the oxidation of VOCs (Li et al., 2021). When AVOCs emissions are reduced, a decrease in OVOCs concentration is simulated in most regions of East China (by up to 8 ppbv (12%); Fig. 7g), especially the SCB~~up to (X%)~~ and PRD regions~~by up to (X %)~~, with the ~~(Fig. SX)~~highest decrease in ketones (by 2-3 ppb (10-

Formatted ...

Formatted ...

~~15%); Fig. 9). However, a rebounded OVOCs is derived at Guangzhou site by 1~2 ppbv (Fig.). further~~

~~In summer, with the 50% NO_x emission reduction, the increases of simulated OVOCs concentrations in North China are more pronounced than in the wintertime, with an increase of 0.5-1.5 ppbv (10-15%; Fig. 6h). These OVOCs increases in NO_x-limited areas are associated with the enhanced hydrocarbons concentration, including alkenes (Fig. 6d) and isoprene (Fig. S10a) due to less loss via the oxidation by OH radicals. While, in VOC-limited areas, the increase of OVOCs can be attributed to the increased mixing ratio of OH radical (Fig. 5f) due to less titration effect. With the 50% AVOCs emission reduction, similarly with the wintertime change, the simulated OVOCs decrease reaches up to about 5 ppbv (20%; Fig. 7h), with the largest contribution calculated in ketones (by 1~3 ppbv (8-15%); Fig. 9). Limited changes (less than 5%) are found in the concentration of OVOCs in the sub-rural sites Heshan, which is relevant to the major contribution of BVOCs, which are not notably influenced by anthropogenic emissions, to the secondary OVOCs formation at this site (Dai et al., 2023).~~

~~Quantification of the impact of emissions reduction on OVOCs abundance provides an important indicator of its impacts on the atmospheric oxidative capacity since the photolysis of OVOCs produces HO_x radicals that drive fast ozone production and accelerate further VOC oxidation (Li et al., 2021). Li et al., (2021) reported that the fast photochemical production of ozone during the Covid-19 lockdown was attributed to the sharp reduction of the NO_x emissions in urban China and the high VOCs emissions, driving ozone production through HCHO photolysis. The study also suggests extending the VOC emission controls year round to avoid the spread of ozone pollution outside the summer season. In our study, with the 50% reduction of NO_x emissions, the increased concentration of OVOCs, including HCHO, is simulated in both winter and summer, which is supportive of Li et al., (2021). The discussion in the following sections explores the changes in other secondary pollutants, including ozone and secondary aerosols.~~

~~the Simultaneouslythe summertime increases~~3.3.2. ~~Ozone~~

Summer conditions. Figure 4 displays the spatial distribution of the changes in total OVOCs due to a 50% reduction in NO_x, AVOCs and in the combined NO_x and AVOCs emissions for July 2018. ~~In summer, W~~with a ~~conducting the~~ 50% reduction in NO_x emissions ~~reduction~~, the changes in OVOCs concentration do not resemble with changes in the OH radical. A decrease in the OVOCs is derived in southern China. However, in central and northern China, the level of OVOCs generally increases and this increase is not limited to metropolitan areas~~similar with the impact of changes in OH radical on OVOCs concentration during winter, the increases of simulated OVOCs concentrations in North China are more pronounced than in the wintertime, with an increase of 0.5-1.5 ppbv (10-15%; Fig. 6h).~~ (Fig. 4a). ~~also .~~For specific OVOCs, the changes in HCHO, glyoxal, and PAN (Fig. S7a-c) are consistent with the changes calculated for the OH radical. However, for aldehydes and alcohols, (Fig. S8a-b), an increased concentration is derived in the entire geographical area of China, with a consistent distribution

Formatted: Font: Italic
Formatted: Font color: Text 1
Formatted: Font color: Text 1
Formatted: Font color: Text 1
Formatted: Font color: Text 1
Formatted: Font color: Text 1
Formatted: Font color: Text 1
Formatted: Font color: Text 1
Formatted: Font color: Text 1
Formatted: Font color: Text 1
Formatted: Font color: Text 1
Formatted: Font color: Text 1
Formatted: Font color: Text 1
Formatted: Font color: Text 1
Formatted: Font color: Text 1, Not Highlight
Formatted: Font color: Text 1
Formatted: Font color: Text 1
Formatted: Font color: Text 1
Formatted: Font color: Text 1, Not Highlight
Formatted: Font color: Text 1
Formatted: Font color: Text 1
Formatted: Font color: Text 1
Formatted: Font color: Text 1

of changes in the level of alkenes (Fig. S8c) and isoprene (Fig. S8d). In summer, the temperature-dependent emissions of biogenic VOCs from vegetations are high. The reduced production rate of OVOCs, resulting from the reduced AVOCs emissions, is compensated to a certain extent by the high natural emissions of BVOCs species.

~~due to the While, in winter, the change of isoprene is ignorable. These OVOCs increases in NO_x-limited areas are associated with the enhanced hydrocarbons concentration, including alkenes (Fig. 6d) and isoprene (Fig. S10a) due to less loss via the oxidation by OH radicals. While, in VOC-limited areas, the increase of OVOCs can be attributed to the increased mixing ratio of OH radical (Fig. 5f) due to less titration effect.~~ With a ~~the~~ 50% reduction in AVOCs emission~~-reduction, similarly with the wintertime change,~~ ~~the significant the simulated decreases in~~ OVOCs concentrations are significantly reduced ~~decrease is simulated~~ in the NCP and SCB regions~~, with the maximum decrease by~~ reaches up to about 5 ppbv (20% ~~;~~ Fig. 4b~~7h~~), ~~, with the largest contribution calculated in ketones (by 1~3 ppbv (8-15%); Fig. 9).~~ Different~~similarly~~ with what is occurring in ~~large~~ winter (~~time decrease in~~ OVOCs concentration reduced by about (~~~~, 50%), ~~wintertime change,~~the response of OVOCs concentration to AVOCs emissions reduction is milder in summer, with the largest decrease reduced to ~~suppressed to~~ 30%. This is explained by the more effective secondary formation of OVOCs during summertime. ~~Limited changes (less than 5%) are found in the concentration of OVOCs in the sub-rural sites Heshan, which is relevant to the major contribution of BVOCs, which are not notably influenced by anthropogenic emissions, to the secondary OVOCs formation at this site (Dai et al., 2023).~~

~~Quantification of the impact of emissions reduction on OVOCs abundance provides an important indicator of its impacts on the atmospheric oxidative capacity since the photolysis of OVOCs produces HO_x radicals that drive fast ozone production and accelerate further VOC oxidation (Li et al., 2021). Li et al., (2021) reported that the fast photochemical production of ozone during the Covid-19 lockdown was attributed to the sharp reduction of the NO_x emissions in urban China and the high VOCs emissions, driving ozone production through HCHO photolysis. The study also suggests extending the VOC emission controls year-round to avoid the spread of ozone pollution outside the summer season. In our study, with the 50% reduction of NO_x emissions, the increased concentration of OVOCs, including HCHO, is simulated in both winter and summer, which is supportive of Li et al., (2021). The discussion in the following sections explores the changes in other secondary pollutants, including ozone and secondary aerosols.~~

~~Figure 10 shows the changes in surface daytime ozone concentrations resulting from the 50% emissions reduction for January and July conditions. In winter, the reduction in NO_x emission leads to an increase in the surface ozone concentrations, which is the largest in the YRD and PRD regions (8-10 ppbv (15-20%); Fig. 10a). During wintertime, as shown in Fig. 1a, a large part of China is under a VOC-sensitive regime. In this NO_x-reduced case, the weakened titration effect due to the decrease in NO_x concentrations favors ozone formation. In AVOCs emissions reduction case, a reduction in the surface ozone concentration, ranging from 2.0 to~~

Formatted: Font color: Text 1
Formatted: Font color: Text 1
Formatted: Font color: Text 1
Formatted: Font color: Text 1
Formatted: Font color: Text 1
Formatted: Font color: Text 1
Formatted: Font color: Text 1
Formatted: Font color: Text 1, Not Highlight
Formatted: Font color: Text 1
Formatted: Font color: Text 1, Not Highlight
Formatted: Font color: Text 1
Formatted: Font color: Text 1, Not Highlight
Formatted: Font color: Text 1, Not Highlight
Formatted: Font color: Text 1, Not Highlight
Formatted: Font color: Text 1, Not Highlight
Formatted: Font color: Text 1
Formatted: Font color: Text 1
Formatted: Font color: Text 1, Not Highlight
Formatted: Font color: Text 1
Formatted: Font color: Text 1
Formatted: Font color: Text 1
Formatted: Font color: Text 1

~~8.0 ppbv (4-10%; Fig. 10c), is calculated in the southern part of China. This ozone decrease is owing to the decelerated ozone production rate attributed to the decrease in the concentration of hydrocarbons (Fig. 7a) (Jacob et al., 1995) and lower HO_x radicals originating from the photolysis of reduced OVOCs concentration (Fig. 7g).~~

~~In the combined emission reduction case, the wintertime ozone changes in a large part of China have primarily followed the ozone changes with NO_x emissions reduction, with an ozone increase of 3.0-7.5 ppbv (4-9%; Fig. 10e) in VOC-limited areas. As the distribution of ozone response mainly depends on the sensitive areas, in this combined case, a large part of China, including North China and some urban regions in South China, is located in VOC-limited areas (Fig. 1g). Thus, in these areas, the ozone response mainly follows the positive changes in the NO_x reduction case. Simultaneously, a slight ozone decrease (by 2.0-4.5 ppbv; 5-8%) is derived by the model over the southern coast of China. In these areas, the ozone sensitivity is under the control of the NO_x. Therefore, the ozone decrease is relevant to the negative ozone response in AVOCs emissions reduction case. Compared with the combined case, with further emission reduction in other species, including CO, SO_2, and NH_3, a smaller ozone increase (by 3-5 ppbv; 4-6%) is calculated in the southern part of China (Fig. 10g). One of the reasons for the higher ozone formation is the reduced CO concentration, as an ozone precursor, due to the CO emission reduction. Besides, a higher level of HO_2, resulting from less aerosol uptake due to emission reduction of NH_3 and SO_2 (See Sec. 3.3.3), can also lead to higher ozone formation.~~

~~In summer, an increase in the surface ozone concentration by up to 12 ppbv (10~20%) is only calculated in the urbanized NCP, YRD, and PRD (Fig. 10b), under the effect of NO_x emissions reduction. These areas are typically located in VOC-limited conditions (Fig. 1b); thus, ozone increase can be well explained by reduced ozone titration. At the same time, in NO_x-limited areas, the calculated surface ozone concentration is reduced by 2 to 8 ppbv (3-10%). This ozone decrease is associated with less photochemical formation from reduced NO (Fig. 5b) and NO_2 (Fig. 5d) concentrations. With the reduction of AVOCs emissions, the surface ozone concentration decreases in whole areas of China by up to 8.0-12.0 ppbv (8-20%; Fig. 10d). Unlike wintertime ozone decrease, which primarily occurs in southern China, the summertime ozone decline shifts from the southern regions to the northern ones, including the NCP, the PRD, and the YRD regions. This spatial variation is consistent with the distribution of model-derived HO_2 radicals' changes (Fig. 7f), indicating the importance of AVOCs to the formation of HO_2 radicals.~~

~~In the combined 50% reduction case of the NO_x and AVOCs emissions, the surface ozone concentration decreases by up to 12 ppbv (15%; Fig. 10f) in NO_x-sensitive areas due to the influence of the reduction in the NO_x and AVOCs emissions. In VOC-sensitive areas, the increase of ozone associated with the positive impact of the reduction in NO_x emissions is largely compensated by the negative effect of the reduction in AVOCs emissions. An ozone decrease is derived in almost all areas of China and ranges from about 5 to 12 ppbv (6-15%). One exception is found at the Guangzhou site, where ozone slightly increases by 0.5 ppbv (Fig. S11). The important contribution of BVOCs to the formation of ozone in the PRD region has been documented in many studies (Zhang et al., 2023). One reason can be the role of BVOCs~~

Formatted: Font color: Text 1

species, such as isoprene, becomes more important to ozone formation in this area, when NO_x and AVOCs emissions are reduced (see Sec. 3.4.1).

When emission reduction is conducted to all species, the largest ozone decrease is slightly rebounded to 10 ppbv (15%) in NO_x limited conditions and 11 ppbv (13%) in VOCs limited conditions (Fig. 10h).

This change in two season indicates less sensitive of OVOCs formation to the reduction in AVOCs emissions during summer than during winter. Nevertheless, Besides that , a more pronounced distinct decrease in OVOCs is found in North China. For example, aAt the Beijing site, the decreases in OVOCs concentration increased toreaches 10 ppbv (28%10 ppbv compared to the) from the decrease in winter by 5 ppbv (45%5 ppbv derived in winter), which is consistent with the higher concentration of summertime OVOCs (~34 ppbv) relative to winter (~11 ppbv). When the cCombined reduction in the emissions reduction inof AVOCs with NO_x are considered, a lower decrease of OVOCs is can be found in the whole geographical area of China (Fig. 4cX), which is relevant to the reduced decrease in the level of the OH radical.compared with the results with only AVOCs emission reduction, indicating a more significant impact of OH radical with isoprene when AVOCs emission reduced. The effect on With additional reduction in other emissions, the changes in OVOCs concentration of the reduced emissions in the other species under consideration are mildlysmall (Fig. 4SfFig. S).

3.2. Changes in secondary pollutants to emissions reduction

Following the changes in ozone precursors and intermediate, the formation of ozone and secondary aerosol will also be affected by the reduction in emissions. The formation of ozone and secondary aerosol is affected by the changes in the emissions of primary species and in the concentration of ozone precursors and intermediate species. The production rate of odd oxygen ($O_x = O_3 + NO_2$) is associated with recurrent radical reaction chains involving the oxidation of hydrocarbons in the presence of NO_x. The photochemical destruction of O_x results from several processes, including the photolysis of O_3, followed by the reaction between the electronically excited oxygen atom $O(^1D)$ and water vapor (H_2O). Other O_x loss mechanisms include the reactions of ozone with OH, HO_2, and different alkenes. In the presence of NO_x, additional O_x losses are provided by the titration of O_3 by NO, followed by the conversion of NO_2 to nitric acid (HNO_3).

In order to highlight the regional differences in the response of the existing photochemical regimes to emissions reduction, we first show the changes in the distributions of the areas where the ozone formation is either NOx- or VOC-limited. In order to display the impact of emission reduction on the changes in the ozone regimes, we first show the geographical distribution of NO_x limited or VOC limited ozone formation regimes. We distinguish the two regions from adopt the calculated ratio between the production rate of hydrogen peroxide (H_2O_2) and that of nitric acid (HNO_3) [$P(H_2O_2)/P(HNO_3)$] as the indicator to distinguish these regimes. An area is assumed to be VOC-limited or NO_x-limited if the adopted indicator $P(H_2O_2)/P(HNO_3)$ is

Formatted: Font: (Asian) 新細明體, Font color: Text 1, (Asian) Chinese (Traditional, Taiwan)
Formatted: Border: Top: (No border), Bottom: (No border), Left: (No border), Right: (No border), Between : (No border)
Formatted: Font color: Text 1
Formatted: Font color: Text 1
Formatted: Font color: Text 1
Formatted: Font color: Text 1
Formatted: Font color: Text 1
Formatted: Font color: Text 1
Formatted: Font color: Text 1, Subscript
Formatted: Font color: Text 1
Formatted: Font color: Text 1, Not Highlight
Formatted: Font color: Text 1
Formatted: Font color: Text 1
Formatted: Font color: Text 1
Formatted: Font color: Text 1, Not Highlight
Formatted: Font color: Text 1, Not Highlight
Formatted: Font: (Asian) +Body Asian (SimSun), Font color: Text 1, (Asian) Chinese (Simplified, Mainland China)
Formatted: Font color: Text 1
Formatted: Font color: Text 1
Formatted: Font color: Text 1
Formatted: Font color: Text 1
Formatted: Font color: Text 1
Formatted: Font color: Text 1

smaller than~~<~~ 0.06 or if it is larger than ~~$P(H_2O_2)/P(HNO_3) >$~~ 0.2, respectively (Tonnesen and Dennis, 2000)~~(Zhang et al., 2009)~~. The regions with ratios between these two limits represent transition situations (Dai et al., 2023). ~~-~~The production rate of odd oxygen (O_x = O_3 + NO_2), associated with recurrent radical reaction chains involving the oxidation of hydrocarbons in the presence of NO_x, and the photochemical destruction of O_x, is also adopted here to support the analysis of the underlying reasons for ozone changes.

3.2.1 Response of ozone sensitivity regimes to emissions reduction

~~In order to display the impact of emission reduction on the changes in the ozone regimes, we first show the geographical distribution of NO_x-limited or VOC-limited ozone formation regimes. We adopt the ratio between the production rate of hydrogen peroxide (H_2O_2) and that of nitric acid (HNO_3) [$P(H_2O_2)/P(HNO_3)$] as the indicator to distinguish these regimes. An area is assumed to be VOC-limited or NO_x-limited if $P(H_2O_2)/P(HNO_3)$ < 0.06 or $P(H_2O_2)/P(HNO_3)$ > 0.2, respectively (Zhang et al., 2009). The regions with ratios between these two limits represent transition situations (Dai et al., 2023).~~

Figure ~~1~~5 displays the spatial distribution of ozone regimes in response to applied emission reductions in the combined emissions in NO_x and AVOCs emissions in ~~both~~ January and July ~~and July~~.

Winter conditions. In January, ~~Under baseline conditions (BASE case), during January, ozone formation in a large part of China, including the north, east, and central areas, as well as the southeastern coastline and PRD regions, is controlled by the availability of VOC (Fig. 1a). In contrast, ozone formation in western China is under the control of NO_x, while a small area in southern China is located in transition areas. Generally, ozone regimes change mainly in the southern part of China when emissions are reduced.~~ with a 50% reduction in NO_x emissions (Fig. 5b), transition or VOC-limited regimes in the south and southwest of China (in BASE case, Fig. 5a) tend to be converted into NO_x-limited for ozone production regimes. The change in ozone sensitivity regimes is consistent with (1) the decreased concentration in the simulated HNO_3 (Fig. S9a) due to less NO_2 reacting with OH, and (2) the increased H_2O_2 concentration (Fig. S9e), due to the reduced aerosol HO_2 uptake by aerosols, ~~e changes in H2O2 and HNO3;~~ With a 50% reduction in AVOCs emissions, some transition areas of southern China are converted to VOC-limited areas (Fig. 5c). A relevant decrease in H_2O_2 concentration also derived in southern China and is attributed to the decrease in the calculated HO_2 concentration. When considering the combined reduction in NO_x and AVOCs emissions as well as all anthropogenic emissions, the VOC-limited regions of southern China evolve towards transition regions or even NO_x-limited regions (Fig. 5d, Fig. S10a). In these two last cases, the changes in ozone sensitivity regimes are determined by the decrease in the calculated HNO_3 concentrations.

At ~~the~~ the urban sites~~specific sites examined here (see Sect. 2.1)~~, the emission reduction does not modify the wintertime ozone sensitivity regimes ~~at the urban and rural sites in January~~ (Fig. S11~~2~~), which remain~~ing~~ in VOC~~s~~-limited regimes. ~~Except for the remote site Waliguan, at this~~

Formatted ...

Formatted: Font color: Text 1

Formatted: Font: (Asian) +Body Asian (SimSun), Font color: Text 1, (Asian) Chinese (Simplified, Mainland China)

Formatted ...

Formatted ...

Formatted ...

~~site, the ozone production is still located in the transition regimes in AVOCs case, while in other cases changing to NO_x-limited regime.~~

Summer conditions. In July, ~~for baseline conditions (BASE case) (Fig. 1b), a large fraction of the Chinese territory corresponds to NO_x-limited conditions; VOC-limited conditions are found in urban areas including the North China Plain (NCP), the Yangzi River Delta (YRD), the Pearl River Delta (PRD), and the Si Chuan Basin (SCB). t~~The changes in ozone regimes related to emission reductions are found mainly in VOC-limited areas and their surroundings. With the reduction of NO_x emissions, the size of VOC-limited areas (Fig. 5e) shrinks and becomes a smaller fraction of metropolitan areas (Fig. 5f). With the reduction in AVOCs emissions, the VOC-limited areas expand to the surroundings of the metropolitan areas (Fig. 5g). Finally, when considering the combined 50% reduction in the emissions of NO_x and AVOCs (N+A case; Fig. 5h) as well as the reduction of all other emitted species (TOTAL case; Fig. S10b), the calculated change pattern of ozone sensitivity is similar to the pattern corresponding to the NOx emissions, with a smaller VOC-limited area relative to the BASE case. In baseline case, the ozone sensitivity of ~~At~~ the four urban sites under consideration~~,~~ are located in VOC-limited areas. ~~w~~The 50% reduction in NO_x emissions shifts the Beijing sites to NO_x-limited areas (Fig. 5i). The sites of Shanghai (Fig. 5j) and Chengdu (Fig. 5l) are shifted to Transition. Only the Guangzhou site remains in a VOC-limited region (Fig. 5k). When considering N+A and TOTAL cases, the sites of Beijing and Chengdu shift to a transition condition, while the Guangzhou and Shanghai sites remain affected by VOC-limited conditions.

3.2.2 Response of ozone concentrations to emissions reduction

Figure ~~6~~6~~10~~ shows the changes in surface daytime ozone concentrations resulting from a 50% reduction of the NO_x and AVOCs emissions in the January ~~and July~~ and July of~~in~~ 2018.

Winter condition. In January, the 50% reduction in NO_x emission enhances the surface ozone concentrations, with the largest increase derived in the YRD and PRD regions (15-20% (8-10 ppbv); Fig. 6~~S~~a). During wintertime, ~~As During wintertime, as shown in Fig. 1a,~~ a large part of China is under a VOC-sensitive regime. -Therefore~~during wintertime~~,~~.~~ ~~In this NO_x-reduced case, the~~ the reduced titration of ozone by reduced NO (Fig. S13a; Fig. S2c) ~~in this NO_x-reduced case~~ favors an increase in the ozone concentration. If AVOCs emissions are reduced by 50%, the surface ozone is reduced by 4-10% (2.0 to 8.0 ppbv; Fig. 6b) in the southern part of China. This ozone decrease is associated with the reduced concentration of HO_x radicals and hence a reduction in the ozone production by the HO_2 + NO reaction (Fig. S14a).

In the combined emission reduction case, ~~Thus, in these areas,~~ the ozone response in VOC-limited areas ~~mainly~~ follows the positive changes found in the NO_x-reduction case, ~~.~~with an ozone increase of 3.0-7.5 ppbv (4-9%) in North ~~(4-9%; Fig. 10e) in VOC-limited areas (Fig. 1g), including North~~ China and some urban regions in South China (Fig. 6c). ~~is located in VOC-limited areas (Fig. 1g).have primarily followed the ozone changes with NO_x emissions reduction, with an ozone increase of 3.0-7.5 ppbv (4-9%; Fig. 10e) in VOC-limited areas. As the distribution of ozone response mainly depends on the sensitive areas, in this combined case,~~

Formatted ...
Formatted ...
Formatted ...
Formatted ...
Formatted ...
Formatted ...
Formatted ...
Formatted ...
Formatted ...
Formatted ...
Formatted ...
Formatted ...
Formatted ...
Formatted ...
Formatted ...
Formatted ...
Formatted ...
Formatted ...
Formatted ...
Formatted ...
Formatted ...
Formatted ...
Formatted ...
Formatted ...
Formatted ...
Formatted ...
Formatted ...
Formatted ...
Formatted ...
Formatted ...
Formatted ...
Formatted ...
Formatted ...
Formatted ...
Formatted ...
Formatted ...
Formatted ...
Formatted ...
Formatted ...
Formatted ...
Formatted ...

~~a large part of China, including North China and some urban regions in South China, is located in VOC-limited areas (Fig. 1g). Thus, in these areas, the ozone response mainly follows the positive changes in the NO_x reduction case.~~ Simultaneously, a slight ozone decrease ~~(by 2.0-4.5 ppbv; 5-8%)~~ is derived over the southern coast of China (~~by~~ 2.0-4.5 ppbv; 5-8%). In these areas, the ozone sensitivity is under the control of the NO_x. The ozone decrease is dominant by the negative ozone response in AVOCs emissions reduction case. ~~Compared with the combined case, W~~with further emission reduction of other species ~~compared with the combined case~~, a higher ozone increase (3-5 ppbv (4-6%); Fig. S5g) relative to the combined case ~~(by 3-5 ppbv; 4-6%)~~ is calculated in the southern part of China. ~~(by 3-5 ppbv (4-6%, concentration of ozone precursorvia aerosols reduction~~

Summer condition. In July, under the ~~effect of~~reduction in the NO_x emissions ~~reduction~~, an increase in the surface ozone concentration of up to 10 ppbv (17%) is calculated in the urbanized regions of NCP, YRD, and PRD (Fig. 6d). ~~under the effect of NO_x emissions reduction.~~ These areas are typically located in VOC-limited areas (Fig. 5); thus, ozone increase is explained by the reduced ozone titration (Fig. S13b). At the same time, in NO_x-limited areas, the calculated surface ozone concentration is reduced by 2 to 8 ppbv (3-10%), as a result of less photochemical formation from reduced NO_x ~~NO (Fig. 5b) and NO_2 (Fig. 5d)~~ concentrations. With the reduction of AVOCs emissions, the surface ozone concentration decreases by up to 8.0-12.0 ppbv (8-20%; Fig. 6e) in whole areas of China. A spatial shift in ozone decrease, from the southern regions in winter to the northern ones in summer, also occurs under this condition, which is relevant with the distribution of model-derived HO_2 radicals' decrease, as it involved in the reaction with NO and contributed to the decreased ozone production rate (Fig. S14b).

When combining the 50% reduction in the NO_x and AVOCs emissions, the surface ozone concentration decreases by up to 12 ppbv (15%; Fig. 6f) in NO_x-sensitive areas. In VOC-sensitive areas, the increase of ozone associated with the positive impact of the reduction in NO_x emissions is also surpassed by the negative effect of the reduction in the AVOCs emissions. In other words, the reduced destruction of ozone associated with the reduced NO level is less important than the decreased production of ozone resulting from the reduced mixing ratio of HO_x radical. This is explained by the fact that the consumed ozone can be rapidly compensated by the photochemically ozone formation processes, since the ozone production rate is accelerated by high temperature and photolysis rate during summertime (Wang et al., 2022). While the decrease in HO_x radical, due to reduced AVOCs emissions has a stronger impact on the ozone production, as the radicals are fast consumed in the oxidative processes during summer. One exception can be found at the Guangzhou site, where ozone slightly increases by 0.5 ppbv (Fig. S15), which is possibly explained by the increasingly important role of naturally emitted BVOCs species in the oxidation processes when anthropogenic emissions are reduced. When emission reduction is applied to all species, the largest ozone decrease is slightly increased to 10 ppbv (15%) in NO_x-limited conditions and 11 ppbv (13%) in VOCs-limited conditions (Fig. S5h) relative to combined cases, due to the increase in the mixing ratio of OH and HO_2 radicals.

Formatted ...

Formatted: Font color: Text 1

Formatted ...

Formatted ...

3.2.3. Response of aerosols to emissions reduction ~~and its potential effects on ozone 7T ()T, which is largely contributed~~

Figure 7 shows the changes in the average concentrations of secondary aerosol due to emissions reduction in January and July of 2018.

Winter condition. In January, the 50% reduction of NO_x leads to a large decrease of aerosol load (10-18 μg m^{-3} or 12-20%; Fig. 7a) in central and southern China. The aerosol decrease is predominantly results from the decrease in the NO_3^- abundance (Fig. S16a) linked to the reduced concentration of NO_2, followed by NO_4^+ (Fig. S16b). A slight increase in the abundance of secondary organic aerosols (SOA) is derived in the urban areas of NCP, YRD, and PRD regions (1-2 μg m^{-3} or 3-5%; Fig. S16c), which is consistent with the increase in the level of oxidants, including ozone and OH radicals. With a 50% reduction of AVOCs emissions, the changes in aerosol concentration are smaller than with the 50% reduction in NO_x emissions reduction, with a decrease of less than 5 μg m^{-3} (4%; Fig. 7b), which is predominantly resulting from the reduction in SOA (Fig. S17a). With a joint reduction in NO_x and AVOCs (Fig. 7c), the aerosol decrease is larger than the separated effect by emissions decrease, as the increase in SOA by reduced NO_x emissions is compensated by the reduced AVOCs emissions.

With further reduction in other emissions, the decrease in the concentration of aerosol is deeply enhanced; this is the case for the concentration of NH_4^+ (Fig. S19a), SO_4^{2-} (Fig. S19b), and NO_3^- (Fig. S19c). Conversely, the concentration of their precursors, NH_3 and SO_2, are largely reduced, which can also affect the process of acid replacement and then the level of NO_3^-. An overestimation in the concentration of NO_2 and $PM_{2.5}$ has been simulated in the baseline condition, which can possibly lead to a higher reduction in aerosol concentration, especially in the concentration of NO_3^-. This overestimation can also potentially affect the aerosol-related changes in ozone formation.

Summer condition. In July, the aerosol decrease due to the emissions reduction is much smaller than the decrease in winter. The decreased values range from 1.5 to 5 μg m^{-3} (Fig. 7d), from 2 to 6 μg m^{-3} (Fig. 7e), from 4 to 7 μg m^{-3} (Fig. 7f) and from 8 to 10 μg m^{-3} (Fig. 7g), for a reduction in NO_x, AVOCs, combined NO_x and AVOCs, and TOTAL emissions, respectively. The simulated reductions in aerosols undergo a spatial shift, from the southern part of China in winter to the northern China Plain in summer. This shift is consistent with the calculated changes in oxidants, hydrocarbons, and other gaseous aerosol precursors. The higher decrease in the aerosols loads for the combined case also indicates that the reduction in AVOCs emission will increase the efficiency of the aerosol decrease produced by the reduced NO_x emission.

~~In July~~

The aerosol effect on ozone formation has been discussed in several modeling studies (Li et al., 2019; Liu et al., 2020; Dai et al., 2023). Our results show that the reduction in primary emissions results in a large decrease in aerosol concentrations. The major contribution to aerosol decrease is from the reduction in NO_x emissions, with a strengthened effect on aerosol

Formatted: Font color: Text 1

Formatted ...

Formatted: Font color: Text 1, (Asian) Chinese (Simplified, Mainland China)

Formatted ...

Formatted: Font color: Text 1

Formatted ...

Formatted: Font color: Text 1

decrease when combined with the reduction in AVOCs emissions. This aerosol decrease weakens the aerosol extinction effect and therefore enhances the photochemical formation rate of radicals and ozone. As shown in Fig. S20 a-d, the photolysis rate increases (by 5-20%) in southern and central China in winter due to aerosol decrease induced by emission reduction. The highest increase in photolysis rate results from the joint emissions reduction in NO_x and AVOCs (Fig. S20). The increase of photolysis rate in summer is not as distinct as the increase during wintertime, due to the less decrease of aerosol. The increase in photolysis rate, such as for HONO, can also well explain the increased level of OH radical (Fig. 1b) in AVOCs case in south China, with a potentially positive effect on ozone formation.

Besides that, the aerosol decreases can also decline the aerosol uptake of NO_2 and HO_2 radicals, which indirectly resulting in an enhancement in the mixing ratio of OH and HO_2 radicals (Dai et al., 2023). The increased level of HO_x (Fig. S5 a-d) due to the emissions reduction in NH_3 and SO_2 can be caused by the less aerosol uptake, associated with a large decrease in the calculated concentration of NH_4^+ and SO_4^{2-}. When conducting the emission reduction in NOx or AVOCs emissions, the increase in HO_x radicals can also result from the less destruction by reduced NO_2 or VOCs oxidations. However, the aerosol effect, with decrease in aerosol load, on the contribution to the HO_x radicals is supportive to the ozone formation. This result indicates a need to consider the aerosol effect on ozone formation even with stringent emissions reduction.

3.3.3. Aerosols

Figure 11 shows the changes in the daytime average concentrations of secondary inorganic aerosol (SIA; the sum of NO_3^-, NH_4^+, and SO_4^{2-}) due to emissions reduction in January and July. In January, the 50% reduction of NO_x leads to a large wintertime decrease of SIA by up to 10-18 μg m^{-3} (12-20%; Fig. 10a), with a dominant contribution from the decrease in NO_3^- (by 5-12 μg m^{-3}; Fig. S12a) due to reduced concentration of NO_2 (Fig. 5c), followed by NH_4^+ (by 2-4 μg m^{-3}; Fig. S13a) due to reduced NO_3^- concentration (Meng et al., 2022). In July, the decrease of SIA due to NO_x emission reduction is smaller than during wintertime, with a decrease of 2-3 μg m^{-3} (6-10%; Fig. 11b). With a 50% reduction of AVOCs emissions, the simulated reduction in concentration of SIA is limited, with the decrease less than 4 μg m^{-3} (4%; Fig. 11c) and 1.5 μg m^{-3} (5%; Fig. 11d) in winter and summer, respectively. With a combined 50% emission reduction in NO_x and AVOCs in winter, as shown in Fig. 11e, the decrease in SIA is larger than the decrease affected by separated emission reduction. This enhanced decrease is also derived from the decrease of NO_3^- (Fig. S12e), NH_4^+ (Fig. S13e), and SO_4^{2-} (Fig. S14e) due to combined emission reduction. In specific sites (Fig. 13), the strengthened aerosol decrease can be found in six sites, except for the Guangzhou and Heshan sites, where BVOCs play an important role in oxidative capacity. This phenomenon indicates that the reduction in AVOCs emission will increase the efficiency of aerosol decrease in winter when NO_x emission is reduced.

With the further reduction in other emissions, including the emissions of NH_3 and SO_2, the decrease in the SIA is largely enhanced. In January, the decrease of the SIA concentration

reaches 15-25 μg m^{-3} (20-38%; Fig. 11g), while in July, it reaches 8-10 μg m^{-3} (30-40%; Fig. 11h). This enhancement in the aerosol decrease is caused to a large extent by the decrease in the concentration of NH_4^+ (Fig. S13 g and h) and SO_4^{2-} (Fig. S14 g and h).

Figure 12 shows the changes in the daytime average concentrations of secondary organic aerosol (SOA) due to emissions reduction in January and July. With 50% NOx emission reduction in winter, a slight increase of SOA (1.0-1.5 μg m^{-3} (3-5%; Fig. 12a)) is derived in the urban areas of NCP, YRD, and PRD regions, which is consistent with the increase in oxidants, including ozone and OH radicals. When AVOC emissions are reduced, the simulated decrease in SOA concentration is about 2-5 μg m^{-3} (5-11%; Fig. 12c) in the southern part of China. In summer, the decreased level of SOA is comparable to the wintertime decrease. However, the simulated reductions in SOA undergo a spatial shift, from the southern part of China in winter to the northern China Plain. Reasons for the seasonal variations in spatial pattern are the spatial distribution of SOA precursors, including oxidants, hydrocarbons, and OVOCs, and the seasonally changing meteorological parameters, such as temperature and solar radiation.

The aerosol effect on ozone formation has been discussed in several modeling studies (Li et al., 2019; Liu et al., 2020; Dai et al., 2023). Our results show that the SIA concentration is largely decreased in winter due to NO_x emissions reduction, while the declined SOA concentration relies more on the reduction of AVOCs emissions. This aerosol decrease weakens the aerosol extinction effect and therefore enhances the ozone photochemical formation rate (Tan et al., 2022). At the same time, aerosol decreases can result in a decline in aerosol uptake through heterogeneous reactions, resulting in an enhanced concentration of NO_2 and HO_2 radicals. Moreover, the formation of HONO will also decline with NO_x emission reduction (Fig. 6 a and b) through the heterogeneous conversion from NO_2, photolysis of NO_3^- and direct emission from transport (Dai et al., 2023). Thus, the atmospheric level of the OH radical will also be reduced, as the photolysis of HONO is an important source of HO_x radicals. However, the effect of the increase of NO_2 and the decrease of OH radical associated with the decrease of aerosol, is negligible, due to the offset effect by the decrease in the concentration of NO_2 when NO_x emissions are reduced. The enhancement in HO_2 radicals, contributed by aerosol decrease, is consistent with the weakened titration effect due to reduced NO_2 concentration by NO_x emission reduction and can favor the formation of secondary pollutants, including O_3 and SOA, in the VOC-limited areas. When combined with a decrease in AVOCs emissions, the increase of secondary pollutants, due to reduced NO_x, can be largely offset by the decrease in hydrocarbons and OVOCs. Exceptions can be found in the areas where high enough UV and temperature for the photochemical oxidation processes of VOCs are lacking, such as the northern part of China during wintertime, and where the role of BVOCs is crucial for the formation of ozone and secondary aerosols, including the PRD region during wintertime. A schematic diagram describing the chemical mechanisms involved in the atmospheric ozone chemical in response to the reduction in NO_x emissions is shown in Fig. 14.

3.43. Changes in the photochemical reactivity and the atmospheric oxidative capacity

Formatted: Font color: Text 1

The changes in photochemical parameters, including the net production rate of odd oxygen (O_x = O_3 + NO_2) OH reactivity and the atmospheric oxidative capacity (*AOC*), in response to the adopted reductions in emissions are discussed in this section. The production rate of odd oxygen (O_x = O_3 + NO_2) is associated with recurrent radical reaction chains involving the oxidation of hydrocarbons in the presence of NO_x. The photochemical destruction of O_x results from several processes, including the photolysis of O_3, followed by the reaction between the electronically excited oxygen atom $O(^1D)$ and water vapor (H_2O). Other O_x loss mechanisms include the reactions of ozone with OH, HO_2, and different alkenes. In the presence of NO_x, additional O_x losses are provided by the titration of O_3 by NO, followed by the conversion of NO_2 to nitric acid (HNO_3).

. The OH reactivity (OH^R) is expressed as the OH loss frequency due to the reactions by VOC (VOC^R) (including CO) and NO_x (NO_x^R). Thus, this parameter can be used to represent the specific role of VOCs, NO_x, as well as CO that determine the photochemical formation of ground-level ozone (Tan et al., 2017, Xue et al., 2016; Wang et al., 2022).

-Atmospheric Oxidizing Capacity (*AOC*) is a parameter that characterizes the self-cleansing ability of the atmosphere (Liu et al., 2022). It and is derived here as the rate at which CO, methane (CH_4), and non-methane hydrocarbons (NMHCs) are oxidized by atmospheric oxidants, including OH, O_3, and NO_3 (Xue et al., 2016; Dai et al., 2023). This parameter allows us to characterize the formation process of removal process of secondary species, including O_3, SIA, and SOA, and therefore, can be used as an indicator to design mitigation control policies for reducing for ozone pollutionsecondary pollutants. A detailed description of these parameters can be found in Part 1 of the paper (Dai et al., 2023).

3.4.1. OH reactivity

Figure 15 displays the daytime changes in OH reactivity for VOCs (VOC^R) in January and July in response to the specified emission reductions. During wintertime, not surprisingly, the response of VOC^R to the NO_x reduction is considerably smaller than the response to the reduction of AVOCs emissions. Reduction in the NO_x emission slightly reduces the value of VOC^R by 0.2–0.5 s^{-1} (<5%) in the YRD and PRD regions (Fig. 15a). The reduction in VOC^R resulting from the 50% reduction in the AVOCs emissions is found to be of the order of 1.5–3 s^{-1} (12–25%; Fig. 15c). In summer, the reduction in the NO_x emission increase VOC^R in the southern and northeastern parts of China (1.5–2 s^{-1} (8–15%); Fig. 15b), which is consistent with the increase in the concentration of reactive VOCs species including alkenes (Fig. 6d) and isoprene (Fig. S11a) due to reduced oxidant. The potentially positive role of isoprene in the VOC^R in this case highlights the increasing importance of BVOCs in the summertime atmospheric oxidative capacity as the anthropogenic emissions are reduced. For reduced AVOCs emissions, a decrease in VOC^R of 2–3 s^{-1} (10–20%) is derived in the four major metropolitan regions of China, i.e. the NCP, YRD, PRD, and SCB (Fig. 15d).

Figure S15 shows the changes in the value of NO_x^R in response to the 50% reductions in NOx emissions for the January and July conditions. The reduction in NO_x emissions leads to a decrease in NO_x^R in the range of 4.0–6.0 s^{-1} (30–50%) during January (Fig. S15a) and of 3.0–4.0 s^{-1} (35–45%) during July (Fig. S15b). The higher decrease in winter is consistent with the

Formatted: Border: Top: (No border), Bottom: (No border), Left: (No border), Right: (No border), Between : (No border)

Formatted: Font color: Text 1

Formatted: Font color: Text 1

Formatted: Font color: Text 1, Not Highlight

Formatted: Font color: Text 1

~~larger wintertime decrease in NO and NO_2. When considering the reduction in AVOCs emissions, the changes in NO_x^R are relatively small (less than 3% in both January and July). When combining the emission reductions, the changes in the OH reactivity are substantially larger than individual impacts. For example, the combined reduction leads to a wintertime decrease in NO_x^R up to 8 s^{-1} (65%; Fig. S15e). For the 50% reduction in total anthropogenic emissions, the OH reactivity further decreases in urban areas, which is attributed to the decrease in the concentration of CO due to the relevant emission reduction (Fig. S16d).~~

~~For different sites, in winter, the largest decrease is found to occur at the Beijing site (Fig. 16a), with a decrease of 50% in OH reactivity in the combined 50% reductions in VOCs and NO_x emissions. In the combined case, the reduction in the OH reactivity is 45% in Shanghai, 40% in Chengdu, 35% in Wangdu, and 30% in Guangzhou. In summer, the highest decrease also occurs at the Beijing site (by 45%) when a 50% reduction is applied to all emissions. Under these conditions, the OH reactivity is reduced by about 30% in Guangzhou, 25% in Chengdu, and 15% in Shanghai. Besides, the contribution of BVOCs to OH^R becomes considerably larger, with the reduction in NO_x emissions. The most significant increase is calculated at the Heshan sites, with the contribution increasing from 18% to 34%. At the Beijing and Guangzhou sites, the contribution also increases from 3-5% to 10-15%. Small reductions of OH^R (less than 3%) are found at background sites (Waliguan), which suggests that the impact of anthropogenic emissions on the background OH reactivity is limited.~~

~~3.4.2. Atmospheric oxidative capacity~~

The changes in the spatial distribution of daytime (06:00 to 19:00 LST) *AOC* resulting from the adopted 50% reduction in the emissions of ozone precursors for January and July of 2018 is depicted in Fig. 8.

Winter conditions. In January, the 50% reduction in NO_x emission leads to a decrease in daytime *AOC* of 10~20% in southern China and an increase of 10~15%in the urban areas, including the PRD, YRD and SCB regions (Fig.9a). With the 50% reduction in AVOCs emissions, the daytime *AOC* is reduced in all the major regions of China (Fig. 9b), with the largest decreases (30%) occurred in the southern part of the country. With a combined emission reduction in NO_x and AVOCs emission (Fig. 9c) and with the additional reduction of the other considered emissions (Fig. 9d), the distribution pattern of the changes in daytime *AOC* are similar with the pattern found in the AVOCs cases but derived with higher levels of decreases in daytime *AOC*.

Based on the changes in the daytime *AOC* at four city sites, as shown in Fig. 9, the increase in daytime *AOC* associated with the reduced NO_x emissions is caused by the enhanced contributions from OH-related reactions, including the reactions of OH with alkenes, followed by OH with OVOCs and aromatics. The reduction in AVOCs emissions leads to a large *AOC* decrease at four city sites, especially at the Guangzhou site (by 50%), followed by the Shanghai (by 48%) and Beijing sites (by 40%). This decrease in *AOC* is mainly attributable to the reduced

Formatted: Font color: Text 1
Formatted: Font: (Asian) +Body Asian (SimSun), (Asian) Chinese (Simplified, Mainland China)
Formatted: Font color: Text 1
Formatted: Font: Italic, Font color: Text 1
Formatted: Font color: Text 1
Formatted: Font color: Text 1
Formatted: Font: Italic
Formatted: Font color: Text 1
Formatted: Font color: Text 1
Formatted: Font color: Text 1, Subscript
Formatted: Font color: Text 1
Formatted: Font: Italic, Font color: Text 1
Formatted: Font color: Text 1
Formatted: Font color: Text 1
Formatted: Font color: Text 1
Formatted: Font color: Text 1
Formatted: Font color: Text 1
Formatted: Font color: Text 1
Formatted: Font: Italic, Font color: Text 1
Formatted: Font color: Text 1
Formatted: Font color: Text 1
Formatted: Font color: Text 1
Formatted: Font color: Text 1
Formatted: Font color: Text 1
Formatted: Font color: Text 1
Formatted: Font color: Text 1, Subscript
Formatted: Font color: Text 1
Formatted: Font color: Text 1
Formatted: Font color: Text 1
Formatted: Font color: Text 1
Formatted: Font color: Text 1
Formatted: Font: Italic, Font color: Text 1
Formatted: Font color: Text 1
Formatted: Font color: Text 1
Formatted: Font color: Text 1
Formatted: Font color: Text 1
Formatted: Font color: Text 1
Formatted: Font color: Text 1
Formatted: Font color: Text 1

contribution from the reactions between OH with alkenes, followed by the reactions of OH with aromatics and with OVOCs.

During nighttime (20:00 to 05:00 LST), an increase in *AOC* of up to 50% results from the reduction in NO_x emissions (Fig. S21a). The increases are contributed by alkenes ozonolysis, with a relevant enhancement in the concentration of ozone (Fig. 6 a) and alkenes (Fig. S8c). The largest increase in the alkene ozonolysis is derived at the sites of Shanghai from 31% to 40% (Fig. S22b). These results highlight the importance of ozonolysis associated with the NO_x emissions reduction.

Summer conditions. During summertime, the decrease in daytime *AOC* is more pronounced than in wintertime. With the 50% reduction in NO_x emissions, *AOC* decreases in large areas of China (ranging from 10% ~ 20%, Fig. 9e), while, in urban areas, a slight increase of 5% is also predicted. In the cases of AVOCs, N+A, and TOTAL, the daytime *AOC* decreases in the whole of geographical China (Fig. 9f-h), with more distinct decreases in North China than in winter conditions.~~Finally, we show the changes in the spatial distribution of daytime *AOC* resulting from the adopted 50% reduction in the emissions for the January and July conditions in 2018. In January, The reduction in NO_x emission leads to an increase in *AOC* (by 0.6 ×10^7 molecules cm^{-3} s^{-1} (18%); Fig. 17a) in the metropolitan areas of the YRD, PRD, and SCB and a decrease in *AOC* in southern China (by 0.9 ×10^7 molecules cm^{-3} s^{-1}; 25%). The increase in the daytime *AOC* of the metropolitan areas is consistent with the increase in the concentration of surface O_3 (Fig. 10a) and SOA (Fig. 12a), which is related to the increase in the concentration of oxidants, including OH and HO_2 radicals, ozone, and OVOCs.~~

At the four city sites, during summertime, the reduced NO_x emissions also increase daytime *AOC*. However, at the Beijing sites, the daytime value of *AOC* decreased, due to the shift in ozone sensitivity regime of the site from VOC-limited to NO_x-limited. During nighttime, the NO_x emissions reduction also leads to an increase in *AOC* due to the alkene ozonolysis (Fig. S21b), with the largest increase derived at Beijing sites (from 10% to 14%, Fig. S22e). With reduction in AVOCs emissions, a smaller decrease of daytime *AOC* than the decrease in winter is derived, especially at Guangzhou site (to 30%). When the emissions of NO_x and AVOCs are jointly reduced, an increasing role of the reaction between OH and BVOCs in the determination of *AOC* is derived at four city sites, with the largest increase (15%) at the Guangzhou sites. This increase results from the enhanced level of OH radicals and from the concentrations of biogenic VOCs.

~~When examining the wintertime impact of NO_x emission reduction at different sites, the largest daytime *AOC* increase occurs at the Shanghai site (by 20%) (Fig. 18b), followed by the sites of Guangzhou (by 18%), Chengdu (by 12%), and Beijing (by 8%). These results are consistent with the wintertime increase of OH radical (Fig. 5e).~~

~~With the reduction in the AVOCs emissions, the daytime *AOC* is reduced in all the major regions of China (Fig. 17c). The large decreases occurred in the southern part of China (by 1.0~~

Formatted: Font: Italic
Formatted: Font color: Text 1
Formatted: Font: Italic, Font color: Text 1
Formatted: Font color: Text 1
Formatted: Font color: Text 1
Formatted: Font color: Text 1, Subscript
Formatted: Font color: Text 1
Formatted: Font: Italic, Font color: Text 1
Formatted: Font color: Text 1
Formatted: Font color: Text 1
Formatted: Font color: Text 1
Formatted: Font color: Text 1
Formatted: Font color: Text 1
Formatted: Font color: Text 1
Formatted: Font color: Text 1
Formatted: Font color: Text 1
Formatted: Font: Italic, Font color: Text 1
Formatted: Font color: Text 1
Formatted: Font color: Text 1
Formatted: Font color: Text 1
Formatted: Border: Top: (No border), Bottom: (No border), Left: (No border), Right: (No border), Between : (No border)
Formatted: Subscript

~~$\times10^7$ molecules cm^{-3} s^{-1}; 30%), which is consistent with the large decrease of HO_x radicals and ozone due to reduced hydrocarbons and OVOCs.~~

~~With the reduction in AVOCs emissions, the largest *AOC* decrease is found at the Guangzhou site (by 50%), followed by the Shanghai (by 48%) and Beijing sites (by 40%). The decrease in *AOC* is mainly attributable to the reduced contribution from the reactions between OH with alkenes, followed by OH with aromatics and OVOCs.~~

~~With a 50% emission reduction in NO_x, AVOCs, and other primary pollutants (Fig. 17g), the level of daytime *AOC* is higher than the level with the decrease in NO_x and AVOCs emissions only (Fig. 17e). The higher level of daytime *AOC* is caused by the enhanced OH and HO_2 radicals (Fig. S9 e and g) resulting from less consumption by the reduced CO, SO_2, and aerosol uptake.~~

~~When examining the wintertime impact of NO_x emission reduction at different sites, the largest daytime *AOC* increase occurs at the Shanghai site (by 20%) (Fig. 18b), followed by the sites of Guangzhou (by 18%), Chengdu (by 12%), and Beijing (by 8%). These results are consistent with the wintertime increase of OH radical (Fig. 5e). With the reduction in AVOCs emissions, the largest *AOC* decrease is found at the Guangzhou site (by 50%), followed by the Shanghai (by 48%) and Beijing sites (by 40%). The decrease in *AOC* is mainly attributable to the reduced contribution from the reactions between OH with alkenes, followed by OH with aromatics and OVOCs.~~

~~During summertime, the decrease in daytime *AOC*, resulting from the reduction in emissions, is more pronounced than in wintertime. With a 50% reduction in NO_x emissions, a decrease in *AOC* is derived in large areas of China (NO_x limited regimes), with a peak decrease of 1.5×10^7 molecular cm^{-3} s^{-1} (20%; Fig. 17b) derived in the NCP region. At the same time, an increase of daytime *AOC* by 2.5×10^7 molecules cm^{-3} s^{-1} (5%) is predicted in urban areas (VOC-limited regimes). The spatial pattern of predicted changes in *AOC* due to reduced NO_2 is consistent with the changes in OH (Fig. 5f), HCHO (Fig. 6f), and O_3(Fig. 10b), indicating the efficient representation of *AOC* in the formation of secondary pollutants. At specific sites, the simulated increase (by 5-7%) is derived in the sites of Guangzhou (Fig. 18c), Shanghai, and Chengdu.~~

~~The decrease of daytime *AOC* due to the reduced AVOCs emissions is most pronounced in urbanized areas with values reaching 2×10^7 molecules cm^{-3} s^{-1} (25%; Fig. 17d), in the NCP, YRD, and PRD. At four urban sites (Fig. 18), the decrease in *AOC* ranges from 15% to 30%.~~

~~When combining the 50% reduction in AVOCs and NO_x emissions, the decrease in *AOC* is derived in the whole of geographical China (Fig. 17f). The decreases in different sites range from 10%-20% at the four city sites, and 16% and 20% at the rural sites; a reduction of around 5% is derived at the two remote sites. When adding the decrease in other emissions, the spatial distribution of daytime *AOC* decrease is not substantially different from the previous cases.~~

Formatted: Font: (Asian) +Body Asian (SimSun), Font color: Text 1, (Asian) Chinese (Simplified, Mainland China)

Formatted: Border: Top: (No border), Bottom: (No border), Left: (No border), Right: (No border), Between : (No border)

Formatted: Justified, Border: Top: (No border), Bottom: (No border), Left: (No border), Right: (No border), Between : (No border)

Formatted: Font color: Text 1

Interestingly, fFor nighttime (20:00 to 05:00 LST) *AOC*, the reduction in NO_x emissions results in an increase of *AOC* by up to 2×10^6 molecules cm^{-3} s^{-1} in both January (50%; Fig. 19a) and July (10%; Fig. 19b) due to the reaction of alkenes with O_3. The increases are mainly located in urban China in winter and in southern and northern China in summer, which is associated with the relevant enhancement in the concentration of ozone (Fig. 10 a and b) and summertime alkenes (Fig. 6 d). Moreover, the most significant increase from the contribution of alkene ozonolysis is also derived in city sites. For example, in January, the contribution of ozonolysis to nighttime *AOC* increases from 31% to 40% in the Shanghai site (Fig. 20b; Fig. S17b) and from 10% to 16% in the Chengdu sites (Fig. 20d; Fig. S17d). In summer, the changes are smaller than in winter, with the increase from 10% to 14% in the Beijing site (Fig. 20a; Fig. S17a).

Notably, as shown in Fig. 18, among all the emission reduction scenarios, the largest decrease in daytime *AOC* at urban sites is provided with a 50% reduction in AVOCs emission. To mitigate the formation of secondary pollution, the reduction in AVOCs emissions needs to be implemented. In practice, a reduction of 50% AVOCs emissions is hard to achieve in the short term, thus efficient control over emissions of key AVOCs species is needed based on their contributions to *AOC*. As shown in Fig. S18, at four metropolitan sites (Beijing, Shanghai, Guangzhou, and Chengdu), the largest contribution to daytime *AOC* is provided by the reaction of OH with alkenes (30-44%), carbon monoxide (28-40%) and aromatics (15-25%) in winter. In summer, a higher contribution from OH with OVOCs (30-40%) is derived at four urban sites, in comparison to the wintertime conditions (12-22%). The contributions from OH with alkenes and aromatics are around 15-30% and 10-20%, respectively. Combined with the consideration of the dominant contribution of alkenes and aromatics to OH reactivity, we suggest that reducing the emissions of alkenes, aromatics, and unsaturated OVOCs should be prioritized in the control of *AOC* and secondary pollutants in urban China. To give more accurate suggestions for AVOCs emission control, more studies on the contribution of specific AVOCs emissions to *AOC* are required.

The aerosol effect on ozone formation has been discussed in several modeling studies (Li et al., 2019; Liu et al., 2020; Dai et al., 2023). Our results show that the SIA concentration is largely decreased in winter due to NO_x emissions reduction, while the declined SOA concentration relies more on the reduction of AVOCs emissions. This aerosol decrease weakens the aerosol extinction effect and therefore enhances the ozone photochemical formation rate (Tan et al., 2022). At the same time, aerosol decreases can result in a decline in aerosol uptake through heterogeneous reactions, resulting in an enhanced concentration of NO_2 and HO_2 radicals. Moreover, the formation of HONO will also decline with NO_x emission reduction (Fig. 6 a and b) through the heterogeneous conversion from NO_2, photolysis of NO_3^- and direct emission from transport (Dai et al., 2023). Thus, the atmospheric level of the OH radical will also be reduced, as the photolysis of HONO is an important source of HO_x radicals. However, the effect of the increase of NO_2 and the decrease of OH radical associated with the decrease of aerosol, is negligible, due to the offset effect by the decrease in the concentration of NO_2 when NO_x emissions are reduced. The enhancement in HO_2 radicals, contributed by aerosol decrease, is consistent with the weakened titration effect due to reduced NO_2 concentration by NO_x emission reduction and can favor the formation of secondary pollutants,

Formatted: Not Highlight

Formatted: Justified, Border: Top: (No border), Bottom: (No border), Left: (No border), Right: (No border), Between : (No border)

Formatted: Font color: Text 1

Formatted: Font color: Text 1

Formatted: Font color: Text 1

Formatted: Font color: Text 1

Formatted: Font: (Asian) 新細明體, Font color: Text 1, (Asian) Chinese (Traditional, Taiwan)

~~including O_3 and SOA, in the VOC-limited areas. When combined with a decrease in AVOCs emissions, the increase of secondary pollutants, due to reduced NO_x, can be largely offset by the decrease in hydrocarbons and OVOCs. Exceptions can be found in the areas where high enough UV and temperature for the photochemical oxidation processes of VOCs are lacking, such as the northern part of China during wintertime, and where the role of BVOCs is crucial for the formation of ozone and secondary aerosols, including the PRD region during wintertime.~~

~~A schematic diagram describing the chemical mechanisms involved in the atmospheric ozone chemical in response to the reduction in NO_x emissions is shown in Fig. 14.~~

~~Notably, as shown in Fig. 18, among all the emission reduction scenarios, the largest decrease in daytime *AOC* at urban sites is provided with a 50% reduction in AVOCs emission. To mitigate the formation of secondary pollution, the reduction in AVOCs emissions needs to be implemented. In practice, a reduction of 50% AVOCs emissions is hard to achieve in the short term, thus efficient control over emissions of key AVOCs species is needed based on their contributions to *AOC*. As shown in Fig. S18, at four metropolitan sites (Beijing, Shanghai, Guangzhou, and Chengdu), the largest contribution to daytime *AOC* is provided by the reaction of OH with alkenes (30-44%), carbon monoxide (28-40%) and aromatics (15-25%) in winter. In summer, a higher contribution from OH with OVOCs (30-40%) is derived at four urban sites, in comparison to the wintertime conditions (12-22%). The contributions from OH with alkenes and aromatics are around 15-30% and 10-20%, respectively. Combined with the consideration of the dominant contribution of alkenes and aromatics to OH reactivity, we suggest that reducing the emissions of alkenes, aromatics, and unsaturated OVOCs should be prioritized in the control of *AOC* and secondary pollutants in urban China. To give more accurate suggestions for AVOCs emission control, more studies on the contribution of specific AVOCs emissions to *AOC* are required.~~

~~A schematic diagram describing the chemical mechanisms involved in the atmospheric ozone chemical in response to the reduction in NO_x emissions is shown in Fig. 14.~~

The distribution pattern of changes in daytime *AOC* due to emissions reduction is almost consistent with the relevant changes in the mixing ratio of OH radicals and the concentration of OVOCs, ozone, and SOA in both winter and summer. These consistent patterns suggest that the *AOC* is an appropriate indicator to characterize the changes in secondary pollutants attributed to emissions reduction. One exception is found when considering the changes in the ozone concentration resulting from the reduction in the NO_x emission during winter. During this season, a comparison between the values of *AOC* with the changes in the ozone concentration (Fig. 5a) shows that the change in daytime *AOC* is reflecting primarily the changes in the net production rate of odd oxygen (Fig. S23); this can be explained by the important role played by NO_2 in the wintertime formation of ozone.

~~3.~~ Summary and Policy Implications

~~4.~~

Formatted: Font color: Text 1

Formatted: Not Highlight

Formatted: Font color: Text 1

Formatted: Justified

Formatted: Font: (Asian) 新細明體, Bold, Font color: Text 1

Formatted: Font: (Asian) 新細明體, Bold, Font color: Text 1

Formatted: Outline numbered + Level: 1 + Numbering Style: 1, 2, 3, … + Start at: 1 + Alignment: Left + Aligned at: 0.63 cm + Indent at: 1.27 cm

In this study, several model simulations have been conducted to explore the response of radicals, of ozone, and of the atmospheric oxidative processes to a 50% reduction in primary emissions of key pollutants. Our analysis provides insight into the changes in ozone chemistry and in the oxidizing processes to be expected in China in response to future emission reduction.

In winter, as most areas are VOC-limited (saturated in NOx) a 50% reduction in NO_x emissions leads to an ozone concentration increase of up to 8-10 ppbv (15-20%) in all geographical regions of China; this increase results from of the reduced titration of ozone by nitric oxide. When combining this NO_x reduction with a 50% reduction in AVOCs emissions, the ozone enhancement found in the rural areas and resulting from the reduced NO_x is considerably reduced. However, in urban areas (VOC-limited), the ozone increase, although weakened, still exists (by 3.0-7.5 ppbv).

In summer, as most rural areas become NOx-limited, the geographical regions covered by the ozone increase in response to the 50% emission reduction in NO_x shrink and cover primarily the VOC-limited metropolitan areas. In these urban environments, the ozone increase reaches a maximum of 10 ppbv or 17%. When the NOx emission reduction is combined with a 50% VOC emission reduction, the increase in ozone almost disappears in all areas of China. This is explained by the significant decrease in ozone production resulting from the reduced level of hydrocarbons. However, in the rural areas where hydrocarbons are dominated by the emissions of biogenic VOCs, the ozone concentration (linked to the photochemical degradation of isoprene) still slightly increases.~~Our analyses of the model results provide insight into the changes in the atmospheric oxidizing capacity and chemistry in China in response to reductions of anthropogenic emissions.~~

Paths to mitigation. We conclude this paper by highlighting a few chemical paths that should be considered when designing a mitigation policy for a reduction of ozone in urban areas of China. Figure 10 presents a schematic description of the chemical mechanisms involved in the chemical production of atmospheric ozone and highlights how different reaction paths tend to change the ozone abundance in urban areas in response to a reduction in NO_x and anthropogenic VOC (AVOCs) emissions. This graph shows that a reduction in NO_x emissions tends to increase the ozone concentration by (1) reducing the rate of the NO + O_3 reaction (ozone titration); (2) by increasing the rate of the HO_2 + NO reaction due to an increase in the HO_2 level associated with the reduced uptake of this radical by a lowered aerosol load; (3) by an increase in the atmospheric oxidizing capacity (*AOC*) though the OH- and ozone-related reactions. The graph also shows that a decrease in AVOCs emissions tends (1) to reduce the level of the HO_x radical and hence the ozone production by the HO_2 + NO reaction; (2) to enhance the level of HO_x due to the reduced aerosol uptake and (3) to reduce the *AOC* with a negative effect on the ozone concentration. The relative importance of these different chemical mechanisms varies with location and environmental conditions.

Formatted: Font: (Asian) +Body Asian (SimSun), Font color: Text 1, (Asian) Chinese (Simplified, Mainland China)

Formatted: Normal

Formatted: Subscript

Formatted: Font color: Text 1, (Asian) Chinese (Simplified, Mainland China)

We conclude that in winter when the background concentration is low, the reduction of NO_x emissions tends to increase the ozone concentration, while the reduction in AVOC emissions has the opposite effect. This conclusion applies both in rural and in urban areas. A combined reduction in the emissions of these two primary pollutants tends to decrease the level of ozone in rural areas, but to increase ozone in urban areas. Thus, in urban areas during winter, an effective approach to reduce the surface ozone concentration is through a strong limitation in the emissions of volatile organic compounds.

In summer when the ozone level is generally high, the reduction of NO_x emissions is an effective action to reduce the ozone concentration in rural areas, but this measure is counterproductive in urban areas where ozone is controlled by VOCs. In fact, in urban areas during this season, the mechanisms involved in ozone mitigation are complex. For example, when NO_x emissions are reduced, the atmospheric OH concentration is enhanced because of its reduced destruction by NO_2. Following this increase in the OH concentration, an increase in the level of OVOCs, whose photolysis is an important source of HO_x radicals, also leads to accelerated ozone production and further amplifies the oxidation of VOC. In addition, the increase in *AOC*, linked to the reaction of OH and ozone with alkenes and the reactions of OH with OVOCs also contributes to an increase in ozone production. Further, the reduction in the aerosol load resulting from a reduction in the emissions of aerosol precursors promotes ozone formation by decreasing the aerosol extinction and by reducing the uptake of HO_2. If combined with a 50% reduction in AVOCs, the increase in OVOCs and *AOC*, due to reduced NO_x emissions, can be offset. However, the aerosol-related promotion in the level of OH and HO_2 radicals can even be exaggerated, indicating the complexity in mitigating summertime ozone pollution in urban areas.

Table 2 provides quantitative information on the response of ozone at different urban locations for January and July. In short in urban areas, the reduction in the level of surface ozone requires a reduction in the emissions of anthropogenic VOCs. However, in practical terms, a 50% reduction in AVOCs emissions, as assumed in our study, is difficult to implement over a short period of time. With the known contribution of the VOCs-related reactions to the *AOC*, the reduction in the emissions of alkenes, aromatics, and unsaturated OVOCs, especially the aldehydes and alcohols, should be a priority. The development of efficient mitigation strategies based on the reduction of AVOCs emissions requires, however, more detailed investigations on the reactivity of individual VOCs and on their potential impact on the ozone formation.

~~With a 50% reduction in NO_x emissions, the production rate of radicals and odd oxygen decreases substantially in both January and July. These decreases are larger in summer (by 0.5–1.2 ppbv h^{-1} (12–28%) and 15–20 ppbv h^{-1} (20–50%)) than in winter (by 0.3–0.7 ppbv h^{-1} (30–33%) and 1.5–2.0 (15–20%) ppbv h^{-1}) and can be attributed to the reduction in the concentrations of nitrogen oxides and OH radicals. During wintertime, however, an increase by 0.8–1.5 ppbv h^{-1} (7–15%) is derived to produce odd oxygen in the PRD region, which is related to the increasing concentration of the HO_2 radical resulting from the increase in the OVOCs concentration and the reduction in the aerosol load. Moreover, during summertime, the simulated concentration of surface ozone decreases in NO_x limited areas (up to 2–8 ppbv~~

Formatted: Justified

Formatted: Font color: Text 1

(3-12%)) and increases in VOC-limited areas (up to 12 ppbv (15%)). The increasing ozone concentration in VOC-limited areas is attributed to the reduced titration by NO_x decrease. In the NO_x-limited areas, the decrease in the ozone concentration results from the reduced photochemical ozone formation associated with the reduction in the concentration of NO_x with considerate effects from reduced HO_x radicals, due to less formation from the photolysis of HONO and OVOCs.

With the AVOCs emissions lowered by 50%, a lower concentration of alkenes by up to 4.0 ppbv (40%) in January and by 2.0 ppbv (50%) in July is derived in urban China areas. The concentrations of OVOCs are reduced by 2.0-5.0 ppbv (8-20%) in January and by 3.0-5.0 ppbv (12-20%) in July due to the reduced primary emissions and secondary formations from the oxidation of hydrocarbons. Results show that, with a 50% reduction in AVOCs emissions, the RO_x and O_x production rates also reduce; the decreases reach 0.1-0.8 ppbv h^{-1} (10-35%) and 1.0-4.5 ppbv h^{-1} (20-42%), respectively, during winter, and 0.3-0.8 ppbv h^{-1} (7-18%) and 5.0-10.0 ppbv h^{-1} (10-28%), respectively, during summer. It is attributed to a decrease in the concentration of HO_2 radicals, associated with a decrease in the oxidation of hydrocarbons and photolysis of OVOCs. The simulated ozone concentrations are reduced by 2.0-8.0 ppbv (4-15%) in southern China during winter and by 8.0-12.0 ppbv (9-20%) in urbanized areas during summer.

With the combined 50% reduction in NO_x and AVOCs emissions, the geographic patterns of the simulated ozone changes in January resemble more the patterns associated with NO_x emission reduction than those with AVOCs emission reduction. Generally, the surface ozone concentration increases by 5-12 ppbv (6-15%) in urbanized areas. In summer, the changes in the ozone concentrations in VOC-limited areas are affected positively by the reduction in NO_x emissions and negatively by the reduction in AVOCs emissions. The net effect is an ozone reduction in almost all areas of China except the PRD region, where the role of biogenic VOCs emissions is considered to be comparable to or more important than anthropogenic emissions.

For aerosol response to primary emissions reduction, a large decrease (up to 20%) in SIA concentrations is derived with a 50% NO_x emissions reduction in winter, dominantly contributed by decreases in NO_3^-, followed by NH_4^+. With a 50% reduction in AVOCs

Formatted: Font color: Text 1

Formatted: Justified

Formatted: Justified

Formatted: Border: Top: (No border), Bottom: (No border), Left: (No border), Right: (No border), Between : (No border)

Formatted: Justified

emissions, the simulated SIA decrease is limited (less than 5%) during wintertime. However, when combining the emissions reduction in NO_x with AVOCs, a strengthened effect can be found in the decrease of each composition of SIA (NO_3^-, NH_4^+, and SO_4^{2-}), indicating the necessity of a joint reduction in NO_x and AVOCs emissions in an efficient reduction in the aerosol concentration in the future. The decrease of SOA is more sensitive to AVOCs emissions reduction, as the oxidation of several AVOCs is an important source of SOA formation. A geographical shift can be found in the spatial distribution of SOA decrease, with large decreases in southern China during wintertime and in the NCP region during summertime. This shift is consistent with the seasonally varied distribution of HO_x radicals. With the aerosol decrease, the effect of the associated enhancement of HO_2 will be consistent with the weakened nitration effect by NO_x emission reduction and lead to an enhancement in secondary pollutants. When combined with the reduction in AVOCs, the positive effect of aerosol enhanced HO_2 will still be important to ozone formation in northern China during wintertime and PRD regions during summertime, due to the relatively small influence of AVOCs.

Regarding the OH reactivity from VOCs in urban areas, we find that a 50% decrease in the NO_x emission leads to a decrease of 0.2–0.5 s^{-1} (<5%) and 0.6–3.0 s^{-1} (5–20%) in January and July, respectively. During summertime, an increase of 3.0 s^{-1} of VOC-related OH reactivity by up to 3.0 s^{-1} is found in southern and northeastern China. This increase is associated with an increase in the concentrations of alkenes and biogenic VOCs (e.g. isoprene), due to less consumption of these reactive VOCs by the reduced OH radical. Regarding the OH reactivity from NO_x, a slight increase is derived during wintertime in the specific case where AVOCs emissions are reduced by 50%. This increase is attributed to the increase in the calculated NO_2 concentrations.

For atmospheric oxidative capacity (*AOC*), a reduction in NO_x emissions during January leads to a slight decrease (0.2–0.4 $\times10^7$ molecules cm^{-3} s^{-1}; 3–6%) in the daytime *AOC* value of southern China and a distinct increase (1.0×10^7 molecules cm^{-3} s^{-1}; 18%) in the PRD region, due to the enhanced HO_x radical from the increase alkenes ozonolysis and OVOCs photolysis. In July, *AOC* decreases by 0.4–1.5 $\times10^7$ molecules cm^{-3} s^{-1} (7–20%) in the NO_x-limited areas and increases by 2.0×10^7 molecules cm^{-3} s^{-1} (25%) in the VOC-limited areas when NO_x emissions are reduced by 50%. These changes are linked to the corresponding changes in the levels of OH radicals and ozone. A reduction in the AVOCs emissions leads to a reduction in the daytime *AOC* by 1.0×10^7 molecules cm^{-3} s^{-1} (13%) in January and 2.0×10^7 molecules cm^{-3} s^{-1} (25%) in July. Specifically, the summertime decreases result predominantly from the weakening of the reaction between OH and alkenes, followed by the reaction of OH with aromatics and OVOCs.

Our results suggest that a substantial reduction in the NO_x emissions and associated effects in the aerosols decrease, the photolysis of OVOCs and ozonolysis of alkenes will lead to an enhancement in surface ozone concentration, OH reactivity from VOCs and *AOC* parameters in urbanized areas. A coordinated strategy for the reduction in NO_x and AVOCs emissions is required to efficiently reduce the ozone levels in metropolitan areas. More detailed

Formatted: Justified

~~investigations to characterize the contribution of individual VOCs to summertime ozone formation are required to develop efficient mitigation strategies against rising ozone concentrations and the related change in the oxidative capacity of the atmosphere in China.~~

Code and data availability. The WRF-Chem model is publicly available at https://www2.mmm.ucar.edu/wrf/users/. The air quality data at surface stations are publicly available at the website of the Ministry of Ecology and Environment of the People's Republic of China at http://english.mee.gov.cn/.

Author contributions. JD and GB designed the structure of the manuscript, performed the numerical experiments, analyzed the results, and wrote the manuscript. JD analyzed the data and established the figures. All co-authors provided comments and reviewed the manuscript.

Competing interests. The authors declare that they have no conflict of interest.

Acknowledgments. The present joint Sino-German study was supported by the German Research Foundation (Deutsche Forschungs Gemeinschaft DFG), the National Science Foundation of China (NSFC) under Air-Changes grant no. 4487-20203, the Research Grants Council– University Grants Committee (grant no. T24-504/17-N) and the NSFC (grant no.42293322). The National Center for Atmospheric Research (NCAR) is sponsored by the US National Science Foundation. We would like to acknowledge the high-performance computing support from NCAR Cheyenne.

Formatted: Font color: Text 1
Formatted: Justified
Formatted: Font color: Text 1
Formatted: Font color: Text 1
Formatted: Font color: Text 1
Formatted: Font color: Text 1
Formatted: Font color: Text 1

Formatted: Font color: Text 1

Formatted: Font color: Text 1

References

An, Z. S., Huang, R. J., Zhang, R. Y., Tie, X. X., Li, G. H., Cao, J. J., Zhou, W. J., Shi, Z. G., Han, Y. M., Gu, Z. L., and Ji, Y. M.: Severe haze in northern China: A synergy of anthropogenic emissions and atmospheric processes, P. Natl. Acad. Sci. USA, 116, 8657–8666, https://doi.org/10.1073/pnas.1900125116, 2019.

Cao, J., Situ, S., Hao, Y., Xie, S., and Li, L.: Enhanced summertime ozone and SOA from biogenic volatile organic compound (BVOC) emissions due to vegetation biomass variability during 1981–2018 in China, Atmos. Chem. Phys., 22, 2351–2364, https://doi.org/10.5194/acp-22-2351-2022, 2022.

China Air 2023, Air Pollution Prevention and Control Progress in Chinese Cities. http://www.allaboutair.cn/uploads/231027/ChinaAir2023EN.pdf

Dai, J., Brasseur, G. P., Vrekoussis, M., Kanakidou, M., Qu, K., Zhang, Y., Zhang, H., and Wang, T.: The atmospheric oxidizing capacity in China – Part 1: Roles of different photochemical processes, Atmos. Chem. Phys., 23, 14127–14158, https://doi.org/10.5194/acp-23-14127-2023, 2023.

Hu, J., Wang, P., Ying, Q., Zhang, H., Chen, J., Ge, X., Li, X., Jiang, J., Wang, S., Zhang, J., Zhao, Y., and Zhang, Y.: Modeling biogenic and anthropogenic secondary organic aerosol in China, Atmos. Chem. Phys., 17, 77–92, https://doi.org/10.5194/acp-17-77-2017, 2017.

Jacob, D. J., Horowitz, L. W., Munger, J. W., Heikes, B. G., Dickerson, R. R., Artz, R. S., and Keene, W. C.: Seasonal transition from NOx - to hydrocarbon-limited conditions for ozone production over the eastern United States in September, J. Geophys. Res.-Atmo., 100, 9315–9324, https://doi.org/10.1029/94JD03125, 1995.

Li, C., Liu, Y., Cheng, B., Zhang, Y., Liu, X., Qu, Y., Feng, M.: A comprehensive investigation on volatile organic compounds (VOCs) in 2018 in Beijing, China: Characteristics, sources and behaviours in response to O3 formation. Sci. Total Environ, 806, 150247https://doi.org/10.1016/j.scitotenv.2021.150247, 2022.

Li, J., Xie, X., Li, L., Wang, X., Wang, H., Jing, S. A., Hu, J.: Fate of Oxygenated Volatile Organic Compounds in the Yangtze River Delta Region: Source Contributions and Impacts on the Atmospheric Oxidation Capacity. Environ. Sci., Technol., 56(16), 11212-11224.https://doi.org/10.1021/acs.est.2c00038, 2022.

Li, K., Jacob, D. J., Liao, H., Shen, L., Zhang, Q., Bates, K. H.: Anthropogenic drivers of 2013−2017 trends in summer surface ozone in China. Proc. Natl. Acad. Sci., 116 (2), 422−427, https://doi.org/10.1073/pnas.1812168116, 2019.

Li, K., Jacob, D. J., Liao, H., Qiu, Y., Shen, L., Zhai, S., Kuk, S. K.: Ozone pollution in the North China Plain spreading into the late-winter haze season. Proc. Natl. Acad. Sci., 118(10), e2015797118, https://doi.org/10.1073/pnas.2015797118, 2021.

Liu, T., Hong, Y., Li, M., Xu, L., Chen, J., Bian, Y., Yang, C., Dan, Y., Zhang, Y., Xue, L., Zhao, M., Huang, Z., and Wang, H.: Atmospheric oxidation capacity and ozone pollution mechanism in a coastal city of southeastern China: analysis of a typical photochemical episode by an observation-based model, Atmos. Chem. Phys., 22, 2173–2190, https://doi.org/10.5194/acp-22-2173-2022, 2022.

Liu, Y., Geng, G., Cheng, J., Liu, Y., Xiao, Q., Liu, L., Zhang, Q.: Drivers of Increasing Ozone during the Two Phases of Clean Air Actions in China 2013–2020. Environ. Sci., Technol., https://doi.org/10.1021/acs.est.3c00054, 2023

Liu, Y., and Wang Tao: Worsening urban ozone pollution in China from 2013 to 2017 – Part 2: The effects of emission changes and implications for multi-pollutant control, Atmos. Chem.

Formatted: Font color: Text 1, Not Highlight
Formatted: Not Highlight
Formatted: Font color: Text 1
Formatted: Font color: Text 1, Not Highlight
Formatted: Font color: Text 1
Formatted: Not Highlight
Formatted: Font color: Text 1
Formatted: Font color: Text 1
Formatted: Font color: Text 1
Formatted: Not Highlight
Formatted: Font color: Text 1
Formatted: Font color: Text 1
Formatted: Font color: Text 1
Formatted: Not Highlight
Formatted: Font color: Text 1
Formatted: Font color: Text 1
Formatted: Font color: Text 1
Formatted: Font color: Text 1
Formatted: Font color: Text 1
Formatted: Font color: Text 1, Not Highlight
Formatted: Not Highlight
Formatted: Font color: Text 1, Not Highlight
Formatted: Font color: Text 1
Formatted: Font color: Text 1, Not Highlight
Formatted: Font color: Text 1
Formatted: Font color: Text 1, Not Highlight
Formatted: Font color: Text 1
Formatted: Not Highlight
Formatted: Font color: Text 1

Phys., 20, 6323-6337, https://doi.org/10.5194/acp-206323, 2020.

Meng, F., Zhang, Y., Kang, J., Heal, M. R., Reis, S., Wang, M., Liu, L., Wang, K., Yu, S., Li, P., Wei, J., Hou, Y., Zhang, Y., Liu, X., Cui, Z., Xu, W., and Zhang, F.: Trends in secondary inorganic aerosol pollution in China and its responses to emission controls of precursors in wintertime, Atmos. Chem. Phys., 22, 6291–6308, https://doi.org/10.5194/acp-22-6291-2022, 2022.

Ou, J., Yuan, Z., Zheng, J., Huang, Z., Shao, M., Li, Z., Louie, P. K.: Ambient ozone control in a photochemically active region: short-term despiking or long-term attainment? Environ. Sci., Technol., *50* (11), 5720-5728, https://doi.org/10.1021/acs.est.6b00345, 2016.

Shi, Y., Ren, J., Xi, Z., Simayi, M., Xie, S.: Identification of key anthropogenic VOC species and sources controlling summer ozone formation in China. Atmos. Environ., 298, 119623, https://doi.org/10.1016/j.atmosenv.2023.119623, 2023

Skamarock, W.C., Klemp, J.B., Dudhia, J., Gill, D.O., Liu, Z., Berner, J., Wang, W., Powers, J.G., Duda, M.G., Barker, D.M.: A Description of the Advanced Research WRF Model Version 4; Mesoscale and Microscale Meteorology Laboratory NCAR: Boulder, CO, USA, 2019.

Song, H., Lu, K., Dong, H., Tan, Z., Chen, S., Zeng, L., Zhang, Y.: Reduced aerosol uptake of hydroperoxyl radical may increase the sensitivity of ozone production to volatile organic compounds. Environ. Sci., Technol. Lett., 9(1), 22-29. https://doi.org/10.1021/acs.estlett.1c00893, 2021.

Tan, Z., Lu, K., Hofzumahaus, A., Fuchs, H., Bohn, B., Holland, F., Liu, Y., Rohrer, F., Shao, M., Sun, K., Wu, Y., Zeng, L., Zhang, Y., Zou, Q., Kiendler-Scharr, A., Wahner, A., and Zhang, Y.: Experimental budgets of OH, HO_2, and RO_2 radicals and implications for ozone formation in the Pearl River Delta in China 2014, Atmos. Chem. Phys., 19, 7129–7150, https://doi.org/10.5194/acp-19-7129-2019, 2019.

Tan, Z., Lu, K., Ma, X., Chen, S., He, L., Huang, X., Zhang, Y.: Multiple Impacts of Aerosols on O3 Production Are Largely Compensated: A Case Study Shenzhen, China. Environ. Sci., Technol., 56(24), 17569-17580, https://doi.org/10.1021/acs.est.2c06217, 2022.

Tonnesen, G. S., and R. L. Dennis.: Analysis of radical propagation efficiency to assess ozone sensitivity to hydrocarbons and NO_x: 2. Long-lived species as indicators of ozone concentration sensitivity, *J. Geophys. Res.*, 105(D7), 9227–9241, https://doi.org/10.1029/1999JD900372, 2000.

Wang, T., Xue, L., Feng, Z., Dai, J., Zhang, Y., Tan, Y.: Ground-level ozone pollution in China: a synthesis of recent findings on influencing factors and impacts. Environ. Res. Letters, 17(6), 063003. https://doi.org/10.1088/1748-9326/ac69fe, 2022.

Formatted: Font color: Text 1
Formatted: Font color: Text 1
Formatted: Font color: Text 1, Not Highlight
Formatted: Font color: Text 1
Formatted: Font color: Text 1, Not Highlight
Formatted: Not Highlight
Formatted: Font color: Text 1, Not Highlight
Formatted: Font color: Text 1
Formatted: Font color: Text 1, Not Highlight
Formatted: Font color: Text 1
Formatted: Font color: Text 1, Not Highlight
Formatted: Not Highlight
Formatted: Font color: Text 1
Formatted: Font color: Text 1
Formatted: Font color: Text 1
Formatted: Font color: Text 1
Formatted: Font color: Text 1
Formatted: Font color: Text 1
Formatted: Font: (Default) Times New Roman, 12 pt
Formatted: Font: (Default) Times New Roman, 12 pt
Formatted: Font: (Default) Times New Roman, 12 pt
Formatted: Default Paragraph Font, Font: (Default) Times New Roman, 12 pt, Pattern: Clear
Formatted: Font color: Text 1, (Asian) Chinese (Simplified, Mainland China)
Formatted: Font color: Text 1
Formatted: Font color: Text 1

Wang, H., Wang, H., Lu, X., Lu, K., Zhang, L., Tham, Y. J., Zhang, Y.: Increased night-time oxidation over China despite widespread decrease across the globe. Nat. Geosci., 1-7. https://doi.org/10.1038/s41561-022-01122-x, 2023.

Wang J, Zhang Y, Xiao S, Wu Z, Wang X.: Ozone Formation at a Suburban Site in the Pearl River Delta Region, China: Role of Biogenic Volatile Organic Compounds. Atmosphere, 14 (4):609. https://doi.org/10.3390/atmos14040609, 2023.

Wang, W., van der A, R., Ding, J., van Weele, M., and Cheng, T.: Spatial and temporal changes of the ozone sensitivity in China based on satellite and ground-based observations, Atmos. Chem. Phys., 21, 7253–7269, https://doi.org/10.5194/acp-21-7253-2021, 2021.

Wang, W., Fang, H., Zhang, Y., Ding, Y., Hua, F., Wu, T., Yan, Y.: Characterizing sources and ozone formations of summertime volatile organic compounds observed in a medium-sized city in Yangtze River Delta region. Chemosphere, 328, 138609 https://doi.org/10.1016/j.chemosphere.2023.138609, 2023.

Wang, W., Li, X., Cheng, Y., Parrish, D. D., Ni, R., Tan, Z., Liu, Y., Lu, S., Wu, Y., Chen, S., Lu, K., Hu, M., Zeng, L., Min, S., Huang, C., Tian, X., Leung, K., Chen, L., Fan, M., Zhang, Q., Rohrer, F., Wahner, A., Pöschl, U., Su, H., Zhang, Y.: Ozone pollution mitigation strategy informed by long-term trends of atmospheric oxidation capacity. Nat. Geosci., 1-6. https://doi.org/10.1038/s41561-023-01334-9, 2023.

Xue, L., Gu, R., Wang, T., Wang, X., Saunders, S., Blake, D., Louie, P. K. K., Luk, C. W. Y., Simpson, I., Xu, Z., Wang, Z., Gao, Y., Lee, S., Mellouki, A., and Wang, W.: Oxidative capacity and radical chemistry in the polluted atmosphere of Hong Kong and Pearl River Delta region: analysis of a severe photochemical smog episode, Atmos. Chem. Phys., 16, 9891–9903, https://doi.org/10.5194/acp-16-9891-2016, 2016.

Yuan, B., Hu, W. W., Shao, M., Wang, M., Chen, W. T., Lu, S. H., Zeng, L. M., and Hu, M.: VOC emissions, evolutions and contributions to SOA formation at a receptor site in eastern China, Atmos. Chem. Phys., 13, 8815–8832, https://doi.org/10.5194/acp-13-8815-2013, 2013

Zhai, S., Jacob, D. J., Wang, X., Shen, L., Li, K., Zhang, Y., Gui, K., Zhao, T., and Liao, H.: Fine particulate matter ($PM_{2.5}$) trends in China, 2013–2018: separating contributions from anthropogenic emissions and meteorology, Atmos. Chem. Phys., 19, 11031–11041, https://doi.org/10.5194/acp-19-11031-2019, 2019.

Zhang, S., Sarwar, G., Xing, J., Chu, B., Xue, C., Sarav, A., Ding, D., Zheng, H., Mu, Y., Duan, F., Ma, T., and He, H.: Improving the representation of HONO chemistry in CMAQ and examining its impact on haze over China, Atmos. Chem. Phys., 21, 15809–15826, https://doi.org/10.5194/acp-21-15809-2021, 2021.

Formatted: Font color: Text 1
Formatted: Font color: Text 1
Formatted: Font color: Text 1
Formatted: Font color: Text 1
Formatted: Font color: Text 1
Formatted: Font color: Text 1
Formatted: Font color: Text 1
Formatted: Font color: Text 1
Formatted: Font color: Text 1
Formatted: Font color: Text 1
Formatted: Font color: Text 1
Formatted: Font color: Text 1

Zhang, Y., Dai, J., Li, Q., Chen, T., Mu, J., Brasseur, G., Wang, T., Xue, L.: Biogenic volatile organic compounds enhance ozone production and complicate control efforts: Insights from long-term observations in Hong Kong. Atmos. Environ., 309, 119917, https://doi.org/10.1016/j.atmosenv.2023.119917, 2023.

Zhang, Y., Wen, X.-Y., Wang, K., Vijayaraghavan, K., and Jacobson, M. Z.: Probing into regional O3 and particulate matter pollution in the United States: 2. An examination of formation mechanisms through a process analysis technique and sensitivity study, J. Geophys. Res., 114, 1–31, https://doi.org/10.1029/2009jd011900, 2009.

Zheng, B., Zhang, Q., Zhang, Y., He, K. B., Wang, K., Zheng, G. J., Duan, F. K., Ma, Y. L., and Kimoto, T.: Heterogeneous chemistry: a mechanism missing in current models to explain secondary inorganic aerosol formation during the January 2013 haze episode in North China, Atmos. Chem. Phys., 15, 2031–2049, https://doi.org/10.5194/acp-15-2031-2015, 2015.

Zheng, B., Tong, D., Li, M., Liu, F., Hong, C., Geng, G., Li, H., Li, X., Peng, L., Qi, J., Yan, L., Zhang, Y., Zhao, H., Zheng, Y., He, K., and Zhang, Q.: Trends in China's anthropogenic emissions since 2010 as the consequence of clean air actions, Atmos. Chem. Phys., 18, 14095–14111, https://doi.org/10.5194/acp-18-14095-2018, 2018

Zhu, S., Ma, J., Wang, S., Sun, S., Wang, P., Zhang, H.: Shifts of formation regimes and increases of atmospheric oxidation led to ozone increase in North China Plain and Yangtze River Delta from 2016 to 2019. J. Geophys. Res.: Atmos., e2022JD038373, https://doi.org/10.1029/2022JD038373, 2023.

Table 1. Sensitivity experiments

Model Experiments	Description
BASE	Without emission reduction
NOx	With emission reduction in NO_x[a] by a factor of 2

AVOCs	With emission reduction in anthropogenic VOCs[a] by a factor of 2
N+A	With emission reduction in NO_x[a] and anthropogenic VOCs[a] by a factor of 2
TOTAL	With emissions reduction in all species[a] by a factor of 2

[a] Relevant species is shown in Table S1.

Table 2. Ozone changes due to reduction in emissions (in percentage)

Site type	Location	Sites name	Ozone changes in winter condition (Mean ± SD)			
			NOx[a]	AVOCs[b]	N+A[c]	TOTAL[d]
Urban sites	North	Beijing	35.0 ± 25.2[e]	-2.5 ± 1.3	40.0 ± 32.8	30.0 ± 19.5
	East	Shanghai	63.6 ± 35.3	-18.2 ± 13.5	31.8 ± 20.5	32.7 ± 18.8
	South	Guangzhou	31.4 ± 22.6	-17.1 ± 11.2	7.1 ± 3.2	10.0 ± 3.5
	West	Chengdu	31.3 ± 23.8	-9.4 ± 8.5	14.1 ± 8.3	20.3 ± 13.5
non-Urban sites[f]	North	Wangdu	45.0 ± 35.0	-2.5 ± 1.8	40.0 ± 28.8	35.0 ± 28.9
	South	Heshan	34.3 ± 28.2	-24.3 ± 19.2	5.7 ± 4.2	7.1 ± 5.8

Site type	Location	Sites name	Ozone changes in summer condition (Mean ± SD)			
			NOx	AVOCs	N+A	TOTAL
Urban sites	North	Beijing	6.4 ± 3.8	-21.8 ± 19.2	-5.5 ± 4.2	-7.3 ± 5.0
	East	Shanghai	17.1 ± 12.8	-22.9 ± 20.8	-2.9 ± 2.1	-2.6 ± 1.5
	South	Guangzhou	15.0 ± 13.1	-14.5 ± 13.5	1.3 ± 1.0	1.3 ± 0.9
	West	Chengdu	5.5 ± 4.5	-14.5 ± 10.2	-5.5 ± 2.0	-4.5 ± 1.9
non-Urban sites	North	Wangdu	2.0 ± 1.2	-17.0 ± 15.8	-5.6 ± 4.2	-7.0 ± 5.2
	South	Heshan	-3.3 ± 2.8	-13.3 ± 10.9	-6.7 ± 3.9	-16.7 ± 3.9

a-d. Sensitivity cases with a 50% reduction in NO_x emissions (NOx), AVOCs emissions (AVOCs), NOx and AVOCs (N+A), and other species (NOx, AVOCs, CO, NH_3, SO_2) under consideration (TOTAL).

e. values are displayed in the average ozone changes during daytime (06:00-19:00) in percentage with the standard deviation as the error bar. (ozone changes = (case value -base-line case) *100).

f. two non-Urban sites in North (Wangdu) and South China (Heshan) were selected, detailed information of these two sites can be found in the Part 1 of the paper (Dai et al., 2023).

Formatted: Font: 12 pt
Formatted: Font: 12 pt
Formatted: Font: (Asian) +Body Asian (SimSun), 12 pt
Formatted: Font: 12 pt
Formatted: Font: 12 pt
Formatted: Font: (Asian) +Body Asian (SimSun), Font color: Text 1, (Asian) Chinese (Simplified, Mainland China)
Formatted: Font: (Asian) +Body Asian (SimSun), Font color: Text 1
Formatted: Subscript
Formatted: Subscript
Formatted: Subscript
Formatted: Font: (Asian) +Body Asian (SimSun), Font color: Text 1, (Asian) Chinese (Simplified, Mainland China)
Formatted: Font: (Asian) +Body Asian (SimSun), Font color: Text 1, (Asian) Chinese (Simplified, Mainland China)

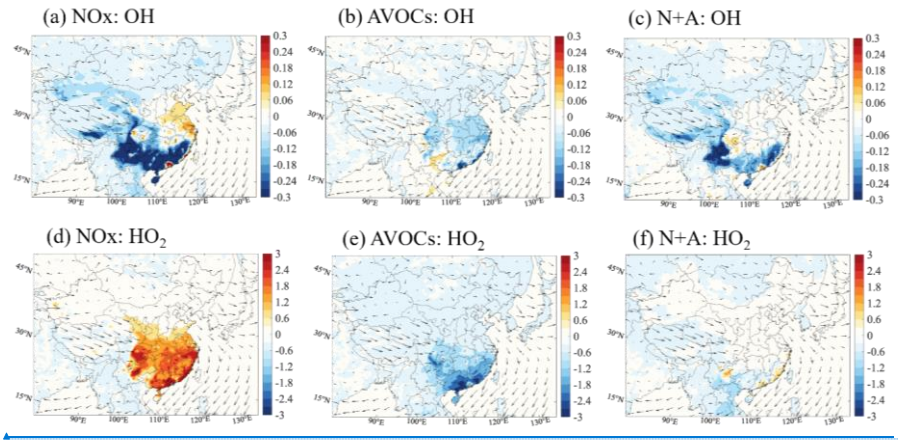

Figure 1. Changes in the averaged daytime surface mixing ratio of OH radical (a-c, Unit: 0.1 pptv) and HO_2 radical (d-f, Unit: pptv) response to the a 50% reduction in NO_x emissions (a, d; NOx case), in anthropogenic VOCs (AVOCs) emissions (b, e; AVOCs case) and in NO_x and AVOCs emissions (c, f; N+A case) relative to BASE case for January of 2018. Arrows represent the wind speed and wind direction.

Formatted: Font color: Text 1

Formatted: Font: (Asian) +Body Asian (SimSun), Font color: Text 1, (Asian) Chinese (Simplified, Mainland China)

Formatted: Centered

Formatted: Font: (Asian) 新細明體, (Asian) Chinese (Traditional, Taiwan)

Formatted: Font color: Text 1

Formatted: Font color: Text 1

1875

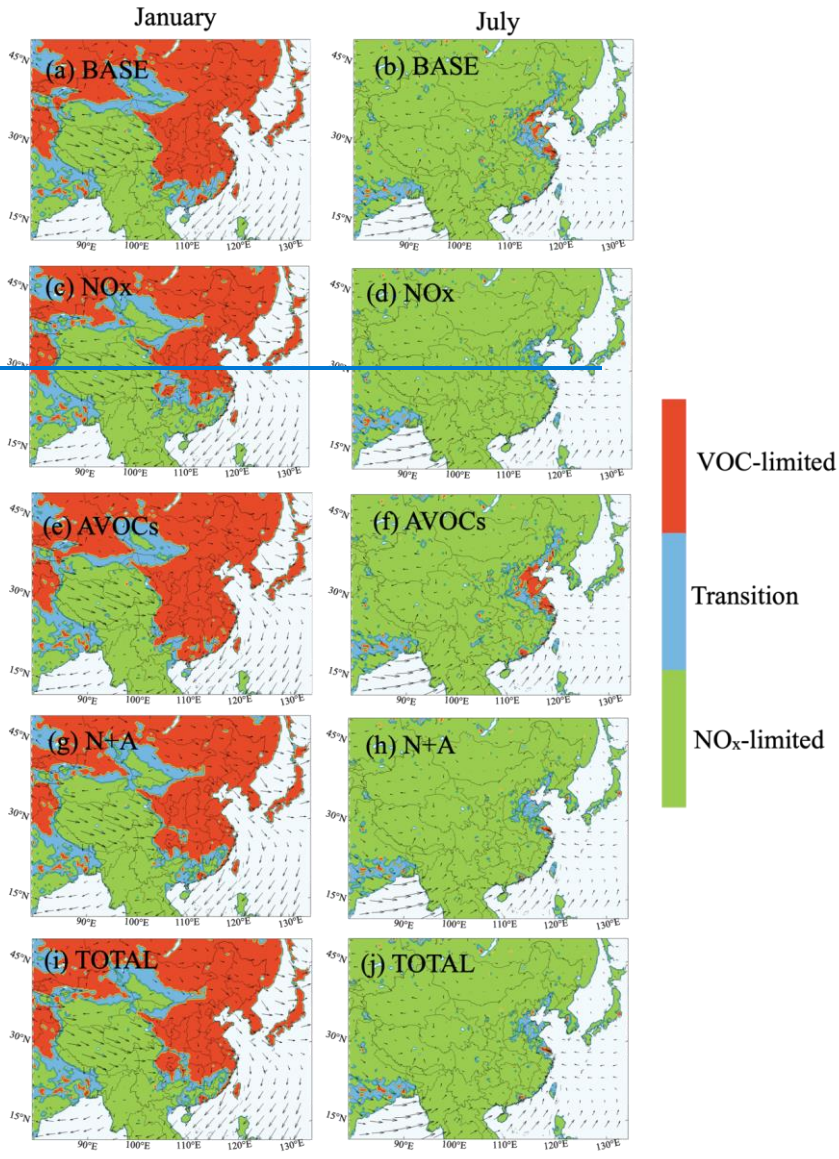

Formatted: Font: (Asian) 新細明體, Font color: Text 1, (Asian) Chinese (Traditional, Taiwan)

Formatted: Font color: Text 1

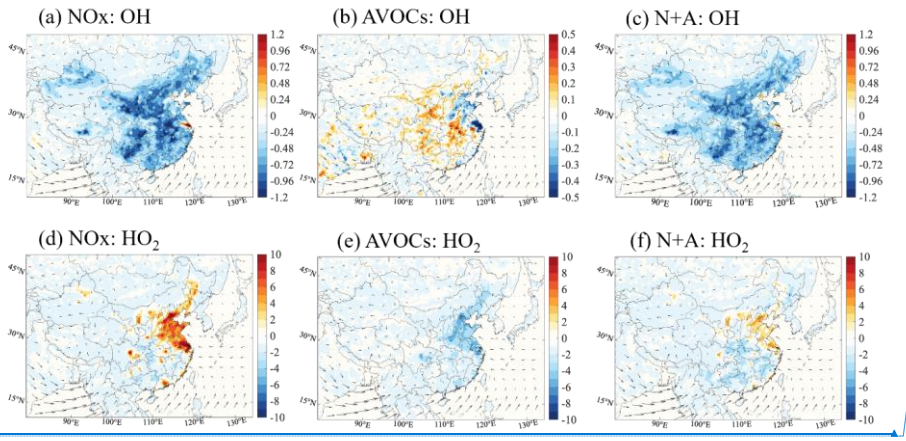

Figure 2. Same as Fig.1 but for July of 2018. Notice the inconsistency in the scale of Figure 2b.

Formatted: Font color: Text 1
Formatted: Font color: Text 1
Formatted: Font: 12 pt, Font color: Text 1
Formatted: Font color: Text 1
Formatted: Font: 12 pt, Font color: Text 1
Formatted: Font color: Text 1
Formatted: Font: 12 pt, Font color: Text 1
Formatted: Font color: Text 1
Formatted: Left
Formatted: Font: 12 pt, Font color: Text 1
Formatted: Font: (Asian) +Body Asian (SimSun), Font color: Text 1, (Asian) Chinese (Simplified, Mainland China)

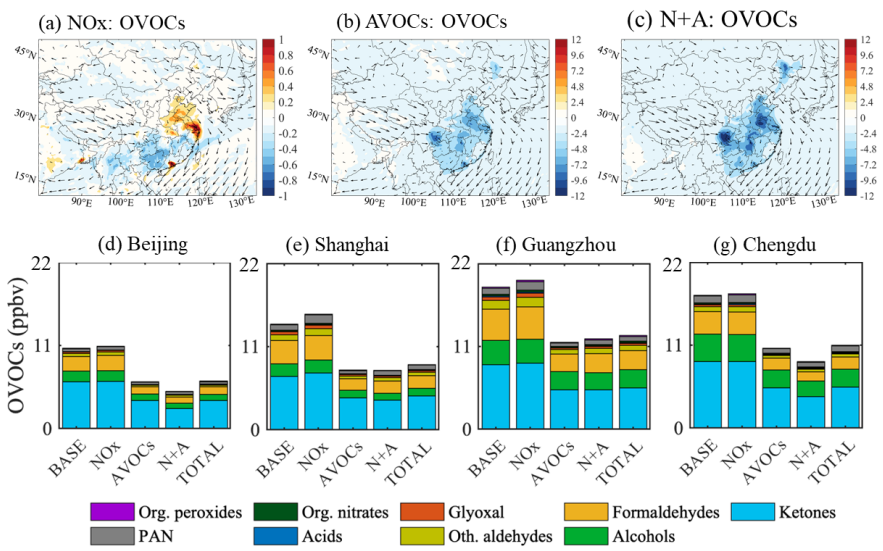

Figure 3. Changes in the surface mixing ratio of total oxidized VOCs (OVOCs) for January of 2018. (a-c) Changes in total OVOCs (Unit: ppbv) response to the reduction in NOx, AVOCs, and combined NOx and AVOCs emissions relative to the BASE case. (d-g) Contributions of averaged concentration of OVOC by different species at four city sites (Beijing, Shanghai, Guangzhou, and Chengdu) in China (c-f) in five cases (BASE, NOx, AVOCs, N+A, and TOTAL cases). Arrows in a-c represent the wind speed and wind direction. Notice the inconsistency in the scale of Figure 3a.

Formatted: Font color: Text 1

Formatted: Font color: Text 1

Formatted: Font color: Text 1

Formatted: Font color: Text 1

Formatted: Font color: Text 1

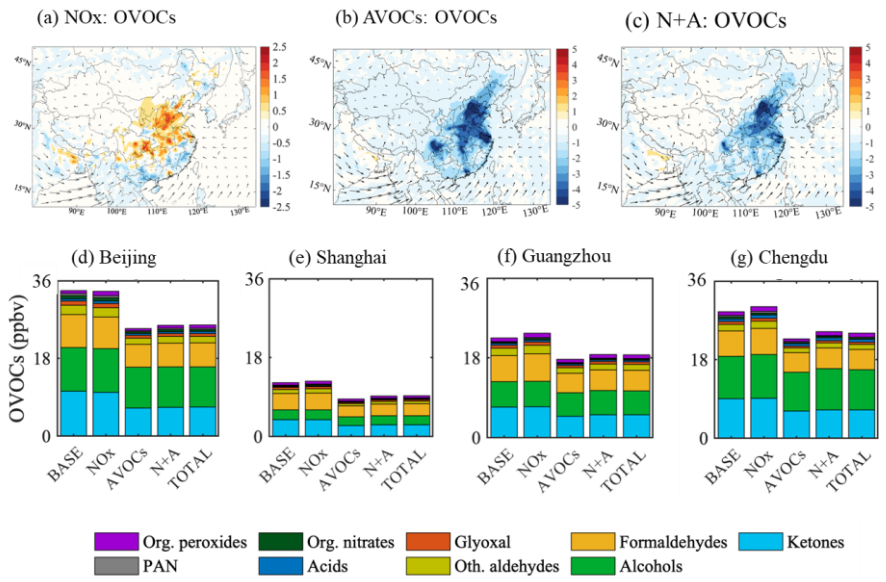

Figure 4. Same as Fig.3 but for July of 2018. Notice the inconsistency in the scale of Figure 4a.

~~Figure 1. Display of regions in which ozone production is limited by the availability of nitrogen oxides (NO_x limited, in green), and volatile organic components (VOC limited, in red) from the BASE case (a, b), the NOx case (c, d), the AVOCs case (e, f), the N+A case (g, h), and the TOTAL case (i, j) in January (a, c, e, g, i) and July (b, d, f, h, j) of 2018. The regions where ozone production is controlled by the availability of both NO_x and VOCs (transition) are shown in blue. The indicator used to define these regions is the ratio between the production rate of hydrogen peroxide (H_2O_2) and nitric acid (HNO_3).~~

Formatted: Font color: Text 1
Formatted: Font color: Text 1
Formatted: Font: 12 pt, Font color: Text 1
Formatted: Font color: Text 1
Formatted: Font: 12 pt, Font color: Text 1
Formatted: Font color: Text 1
Formatted: Font: 12 pt, Font color: Text 1
Formatted: Font color: Text 1
Formatted: Font: (Asian) 新細明體, 12 pt, Font color: Text 1, (Asian) Chinese (Traditional, Taiwan)
Formatted: Font color: Text 1

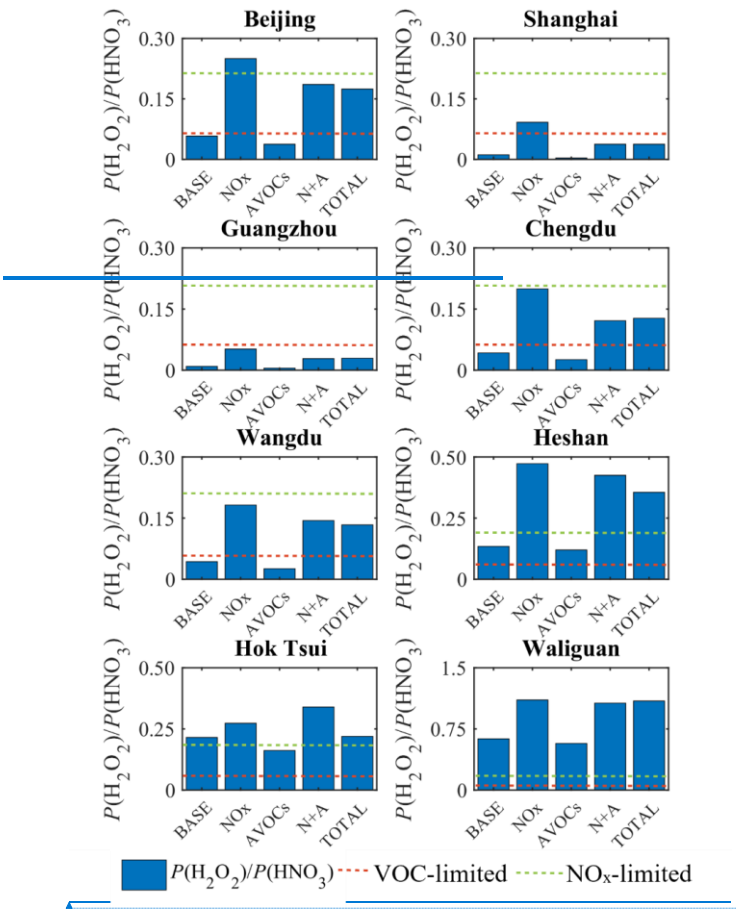

Figure 2. The daytime (06:00 to 19:00 Local Standard Time (LST)) value of ratio between the production rate of hydrogen peroxide (H_2O_2) and nitric acid (HNO_3) [$P(H_2O_2)/P(HNO_3)$] in different regions of China for July 2018. The value of [$P(H_2O_2)/P(HNO_3)$] below the dotted line in red (0.06), above the dotted line in green (0.2), and in between represents the control by VOCs, NO_x, and in transition.

Formatted: Font color: Text 1

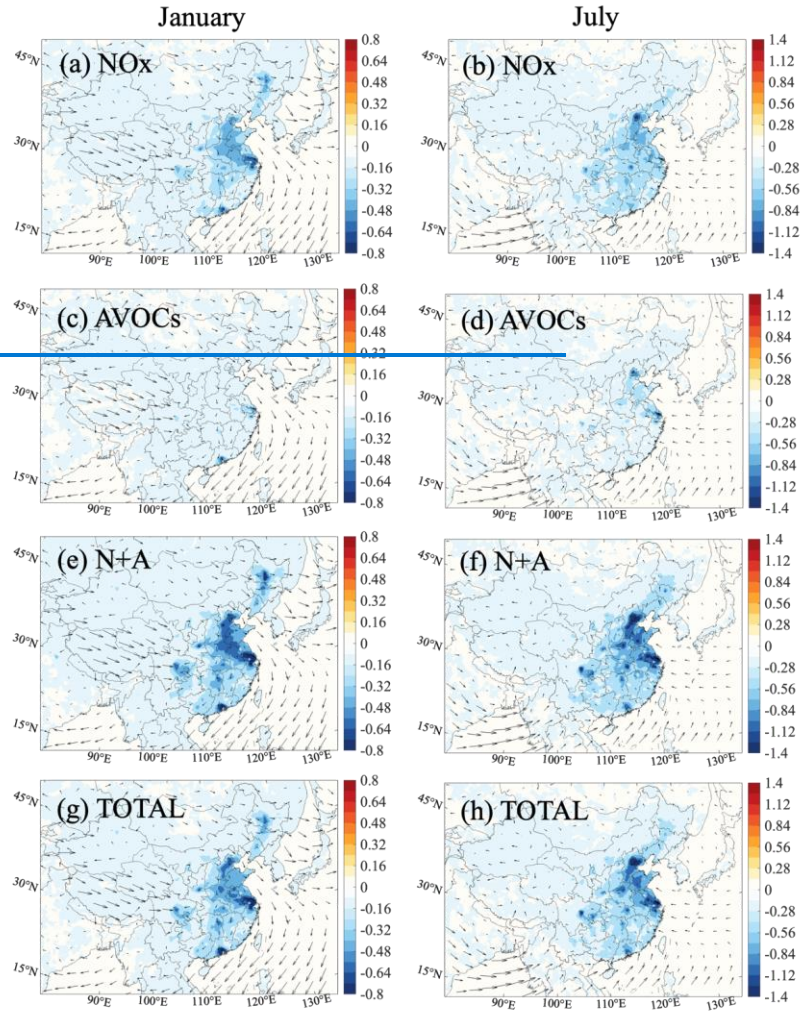

Figure 3. Changes in the averaged daytime surface production rate of RO_x (RO_2+HO_2+OH) [Unit: ppbv h^{-1}] response to a 50% reduction in NO_x emissions (a, b; NOx case), in anthropogenic VOCs (AVOCs) emissions (c, d; AVOCs case), in NO_x and AVOCs emissions (e, f; N+A case), and in all anthropogenic emissions (g, h, TOTAL case) relative to BASE case. Results are shown for January (a, c, e, g) and July (b, d, f, h) of 2018. Arrows represent the wind speed and wind direction.

Formatted: Font color: Text 1

Formatted: Font color: Text 1

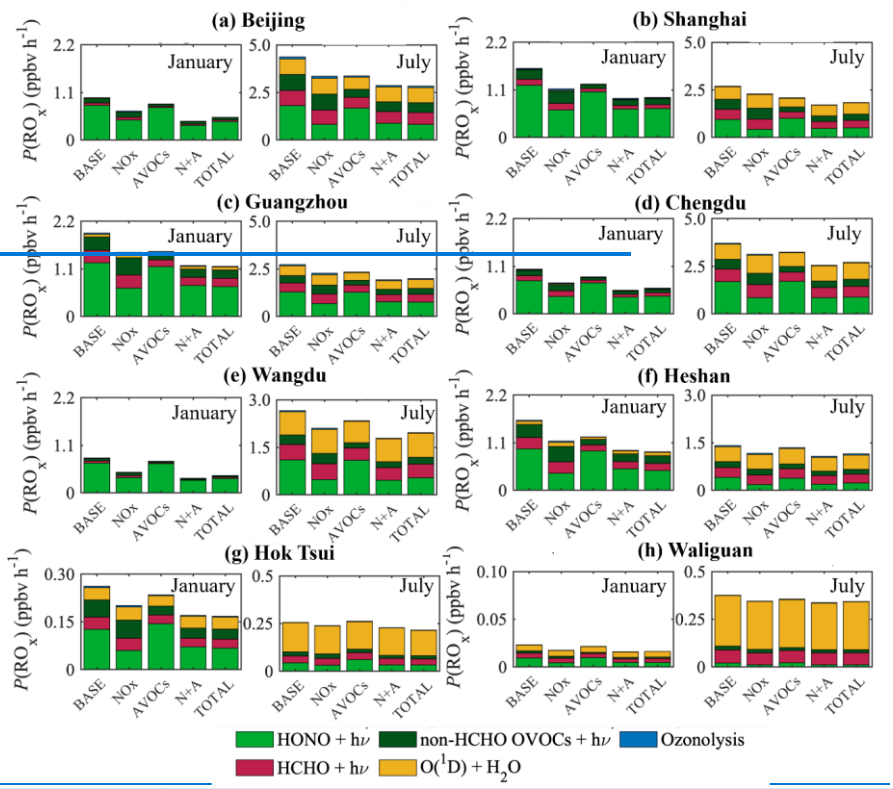

Figure 4. Averaged daytime value of production rate of RO_x ($P(RO_x)$) [Unit: ppbv h^{-1}] in five different simulated cases (BASE, NOx, AVOCs, N+A, TOTAL cases) and eight different sites (urban, rural, and remote sites) in January and July of 2018.

Formatted: Font color: Text 1

Formatted: Font color: Text 1

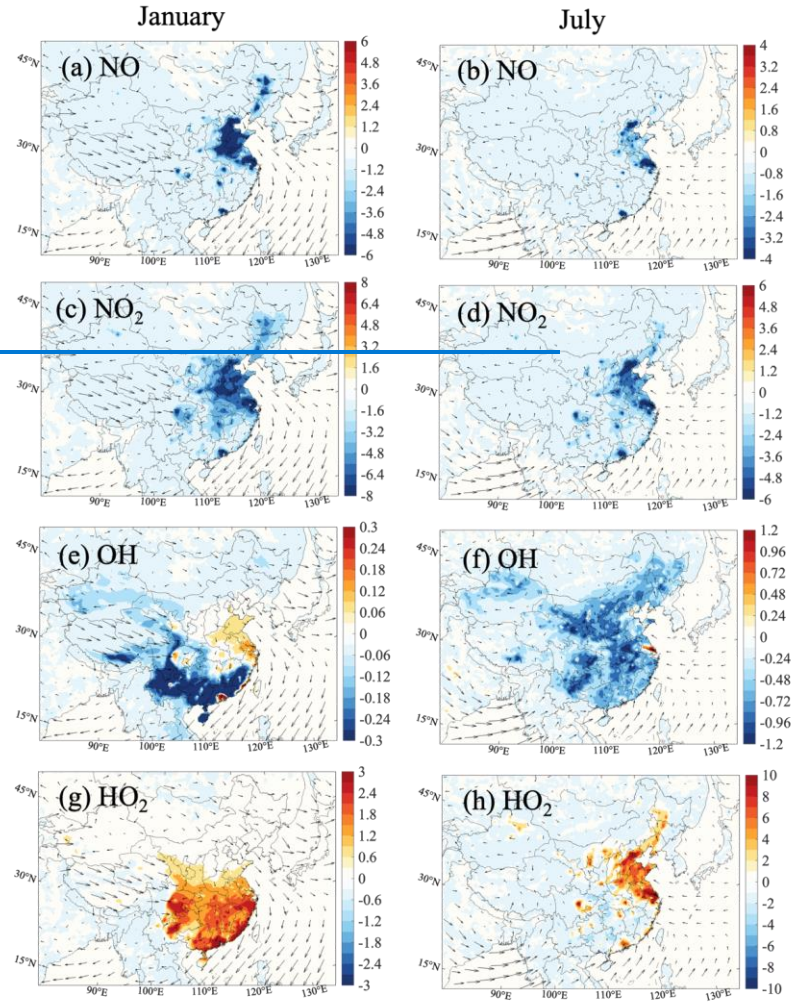

Figure 5. Changes in the surface mixing ratio of NO (a, b) [Unit: ppbv], NO_2 (c, d) [Unit: ppbv], OH radical (e, f) [Unit: 0.1 pptv] and HO_2 radical (g, h) [Unit: pptv] response to the NOx case relative to BASE case. The results are shown for January (a, c, e, g) and July (b, d, f, h) of 2018. Arrows represent the wind speed and wind direction.

Formatted: Font color: Text 1

Formatted: Font color: Text 1

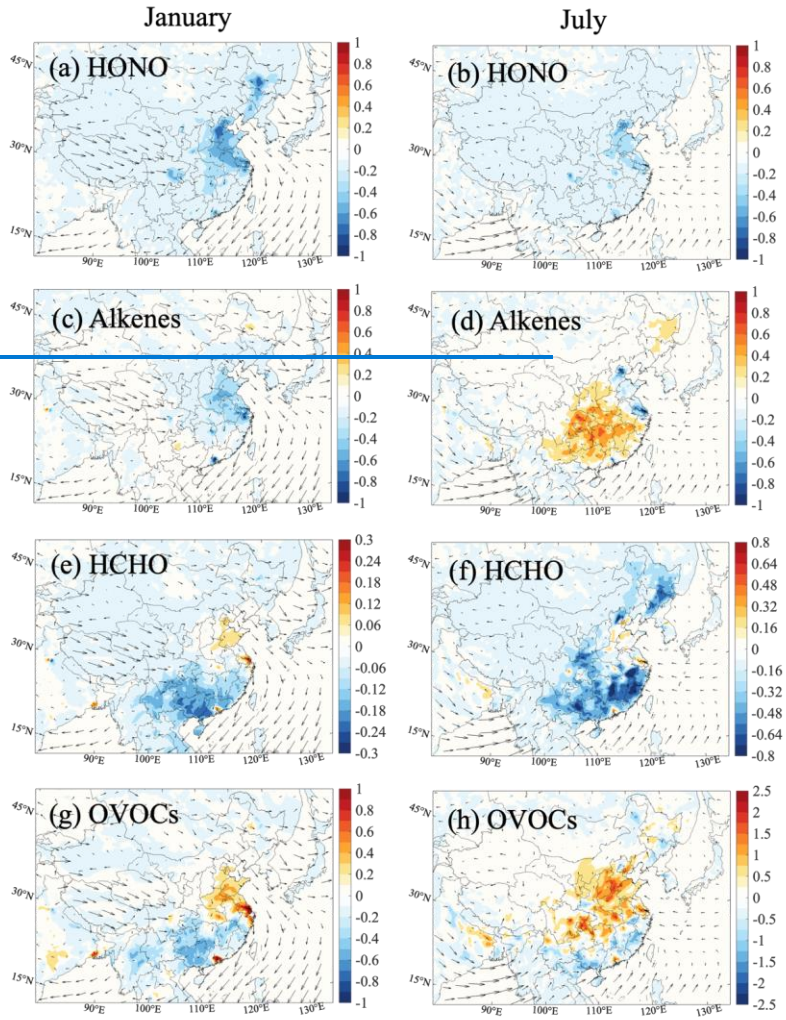

Figure 6. Changes in the surface mixing ratio of HONO (a, b) [Unit: ppbv], alkenes (c, d) [Unit: ppbv], formaldehyde (HCHO; e, f) [Unit: ppbv] and total oxidized VOCs (OVOCs; g, h) [Unit: ppbv] response to the NOx case relative to the BASE case. The results are shown for January (a, c, e, g) and July (b, d, f, h) of 2018. Arrows represent the wind speed and wind direction.

Formatted: Font color: Text 1

Formatted: Font color: Text 1

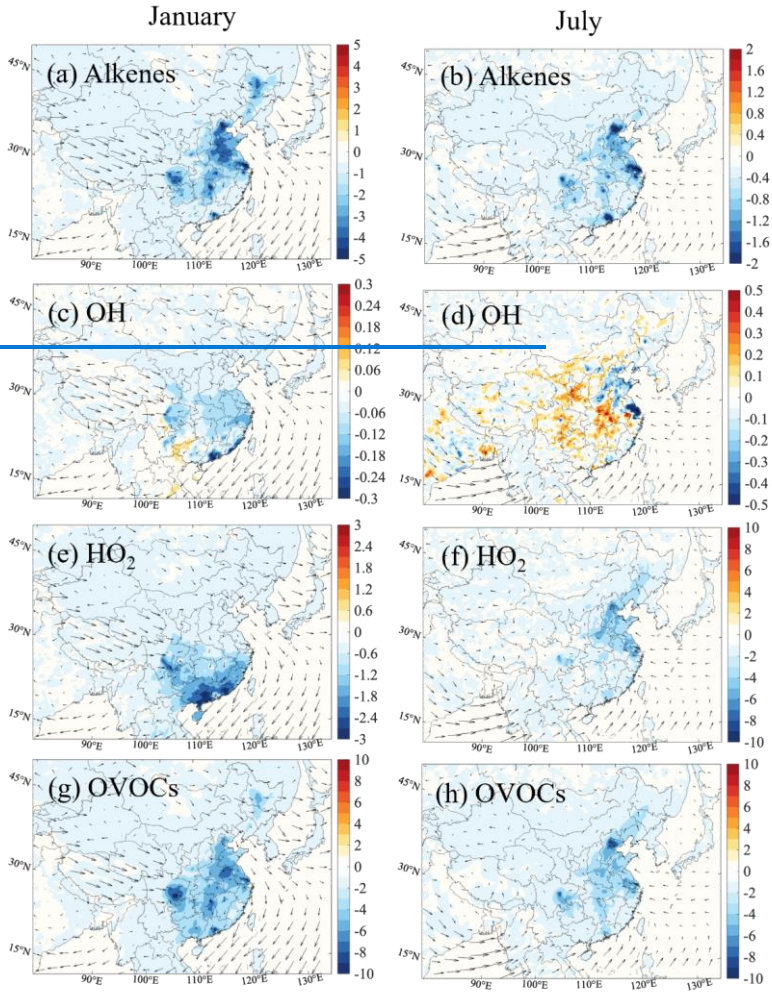

Figure 7. Changes in the surface mixing ratio of alkenes (a, b) [Unit: ppbv], OH radical (c, d) [Unit: 0.1 pptv], HO_2 radical (e, f) [Unit: pptv], and OVOCs (g, h) [Unit: pptv] response to the ratio of 0.5 in AVOCs emissions (AVOCs case) relative to BASE case. Results are shown for January (a, c, e, g) and July (b, d, f, h) of 2018. Arrows represent the wind speed and wind direction.

Formatted: Font color: Text 1

Formatted: Font color: Text 1

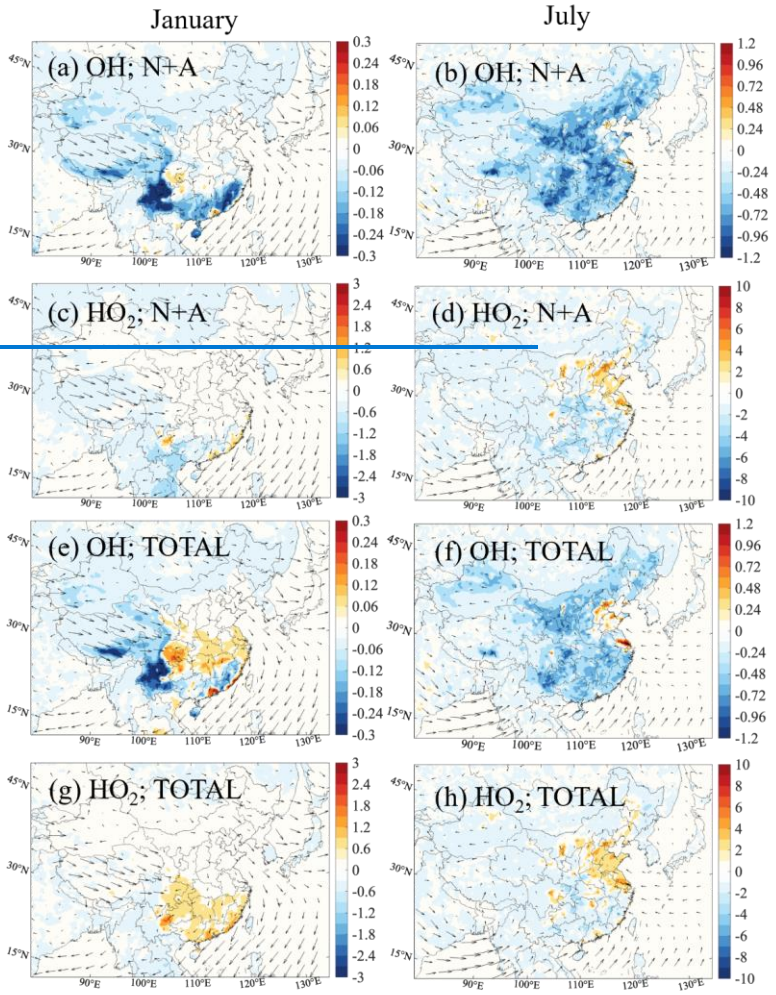

~~Figure 8. Changes in the surface mixing ratio of OH radical (a, b, e, f) [Unit: 0.1 pptv] and HO_2 radical (c, d, g, h) [Unit: pptv] response to the ratio of 0.5 in NO_x and AVOCs emissions (N+A case) and in all anthropogenic emissions (TOTAL case) relative to BASE case. Results are shown for January (a, c, e, g) and July (b, d, f, h) of 2018. Arrows represent the wind speed and wind direction.~~

Formatted: Font color: Text 1

Formatted: Font color: Text 1

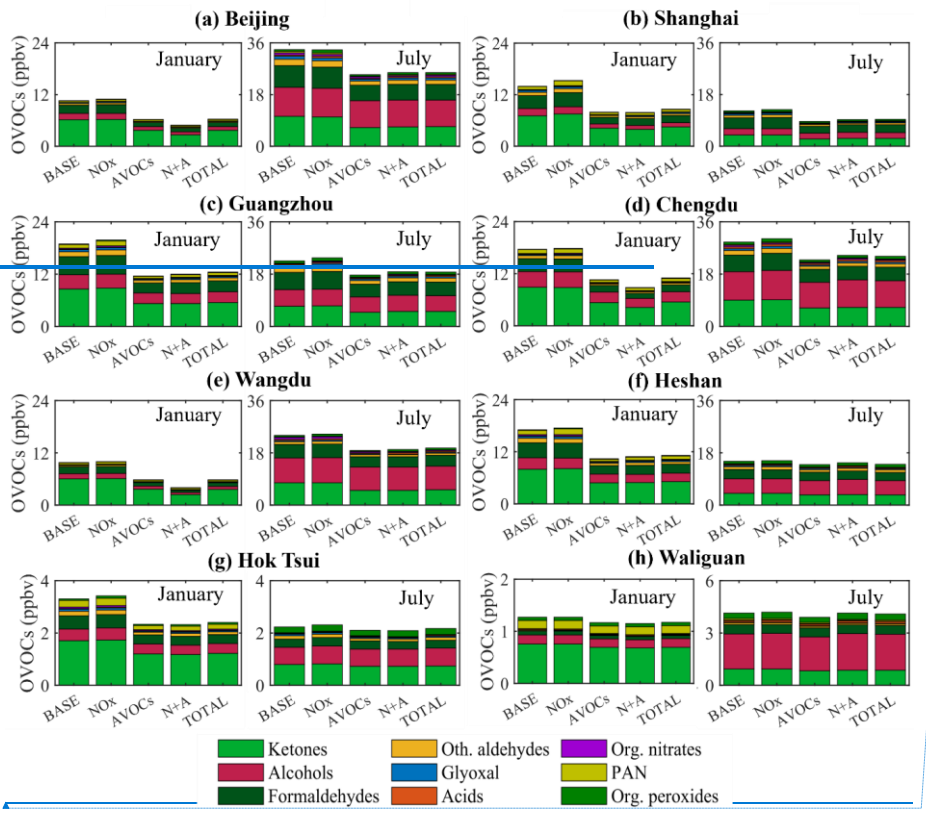

Figure 9. Averaged mixing ratio of oxidized VOCs (OVOCs; Unit: ppbv) with the contribution from nine types of species in five simulated cases (BASE, NOx, AVOCs, N+A, TOTAL cases) and at eight sites (urban, rural, and remote sites) in January and July of 2018.

Formatted: Font color: Text 1

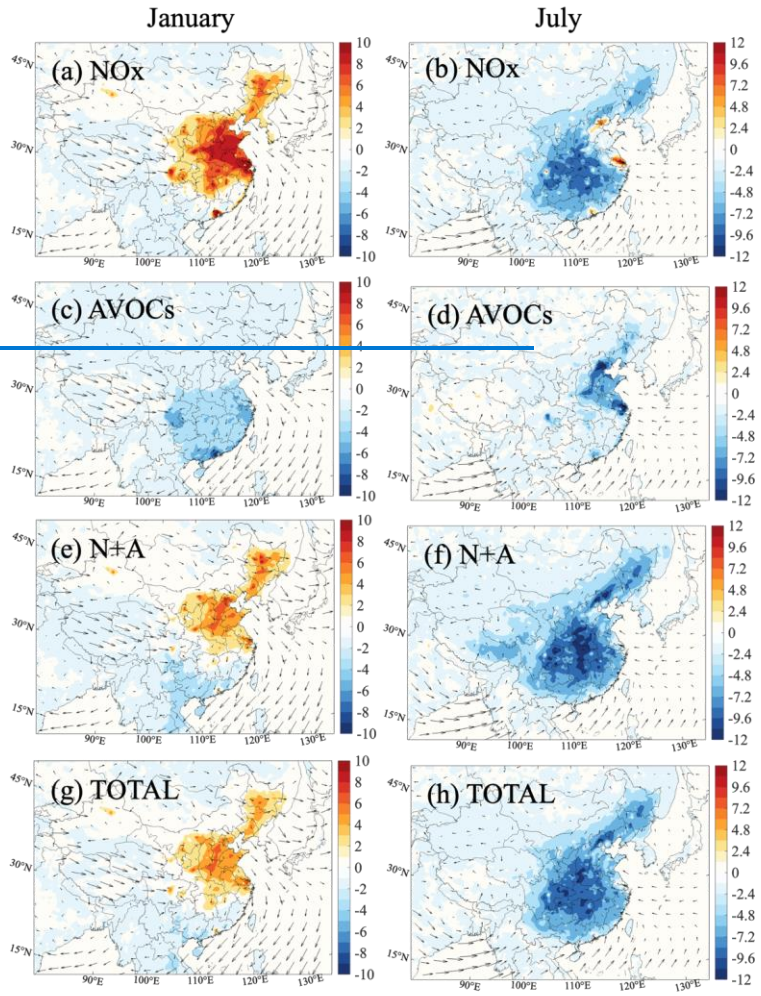

Figure 10. Changes in the averaged daytime surface mixing ratio of ozone [Unit: ppbv] response to the NOx case (a, b), AVOCs case (c, d), N+A case (e, f), and TOTAL case (g, h) relative to BASE case. The results are shown for January (a, c, e, g) and July (b, d, f, h) of 2018. Arrows represent the wind speed and wind direction.

Formatted: Font color: Text 1

Formatted: Font color: Text 1

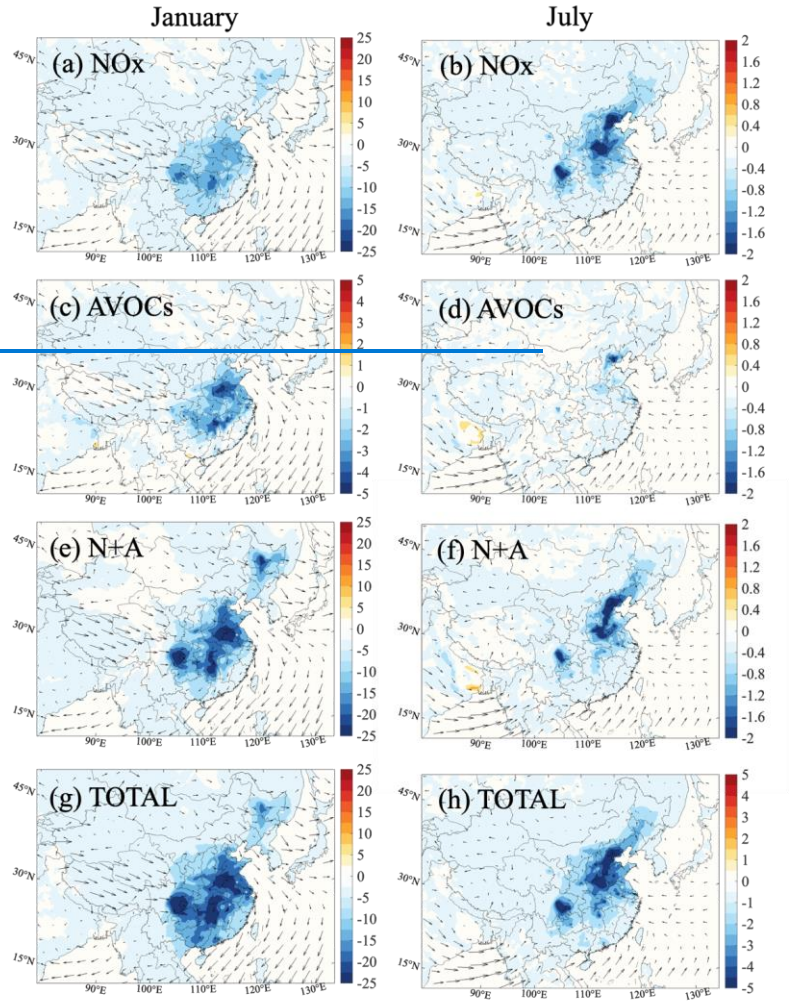

Figure 11. Changes in the surface concentration of Secondary Inorganic Aerosol [SIA, Unit: μg m^{-3}] response to NOx case (a, b), AVOCs case (c, d), N+A case (e, f), and TOTAL case (g, h) relative to BASE case. Results are shown for January (a, c, e, g) and July (b, d, f, h) of 2018. SIA represents the sum of nitrate, sulfate, and ammonia. Notice the inconsistency in the scale of Figure 11c and h. Arrows represent the wind speed and wind direction.

Formatted: Font color: Text 1

Formatted: Font color: Text 1

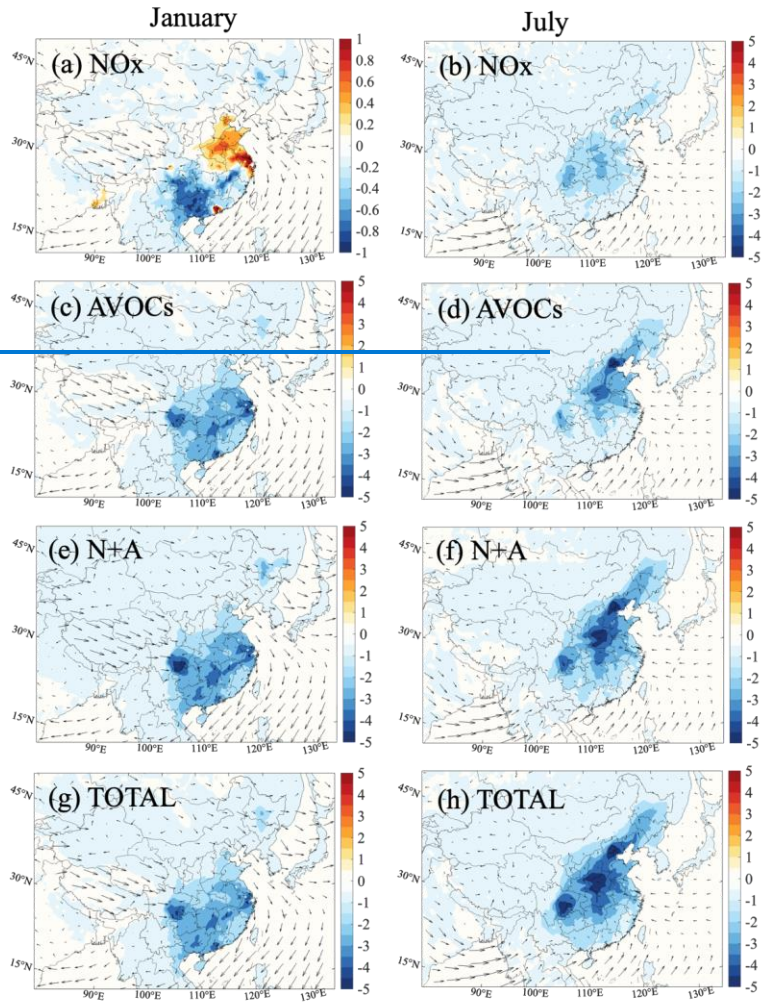

Figure 12. Changes in the surface concentration of Secondary Organic Aerosol [SOA, Unit: μg m^{-3}] response to NOx case (a, b), AVOCs case (c, d), N+A case (e, f), and TOTAL case (g, h) relative to BASE case. Results are shown for January (a, c, e, g) and July (b, d, f, h) of 2018. Notice the inconsistency in the scale of Figure 12a. Arrows represent the wind speed and wind direction.

Formatted: Font color: Text 1

Formatted: Font color: Text 1

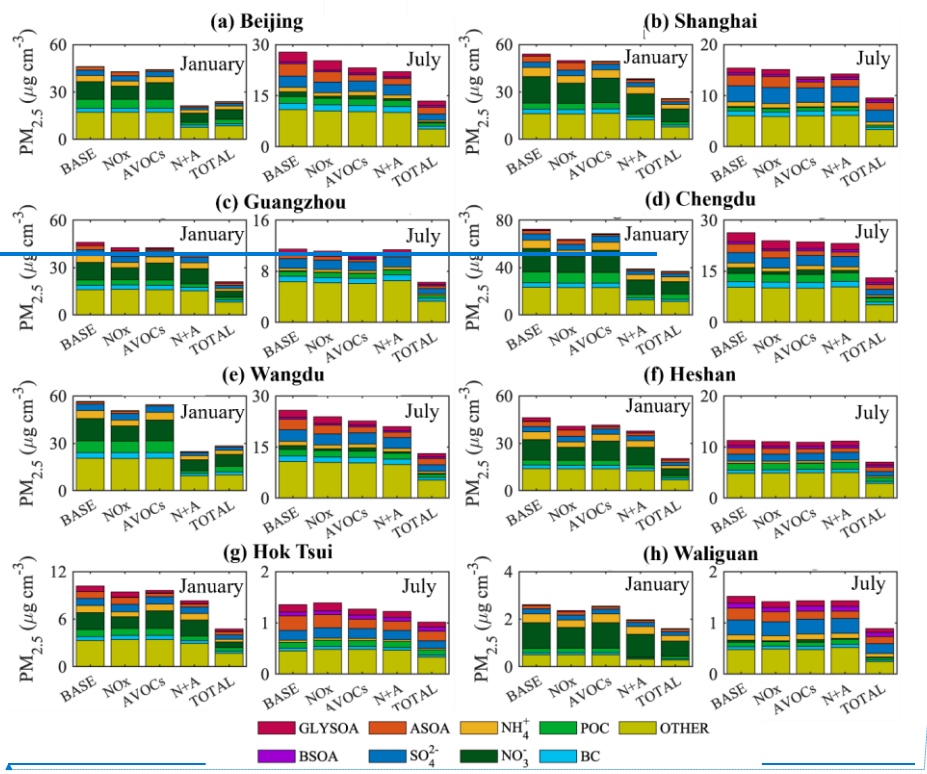

Figure 13. Averaged concentration of $PM_{2.5}$ [Unit: μg m^{-3}] with the contribution from different chemical compositions in five simulated cases and in eight sites for July 2018. The fine particle is composed of particulate nitrate (NO_3^-), particulate sulfate (SO_4^{2-}), particulate ammonia (NH_4^+), primary organic carbon (POC), black carbon (BC), anthropogenic secondary organic aerosol (ASOA), biogenic secondary organic aerosol (BSOA), secondary organic aerosol from glyoxal (GLYSOA), and other aerosol compositions (OTHER, including sea salt, carbonate, calcium, minerals, and other inorganic mass)

Formatted: Font color: Text 1

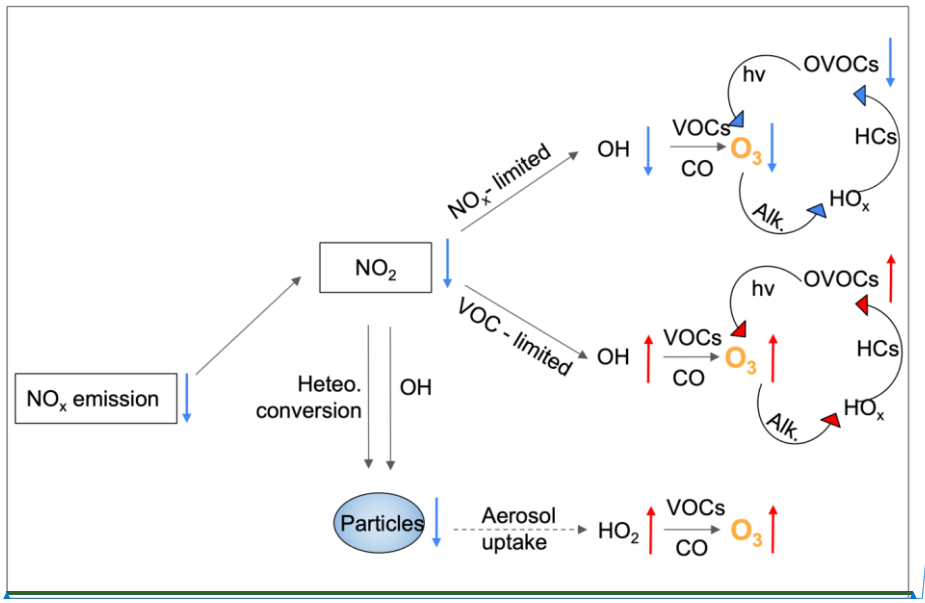

~~Figure 14. Schematics for the impact of NO_x emission reduction through aerosol effect and photochemical processes on ozone concentration. Arrows represent the changes in the concentration of chemicals associated with the reduction of NO_x emission (decrease trend shown in blue increase trend shown in red). HCs and Alk. are the abbreviations of hydrocarbons and alkenes.~~

Formatted: Font color: Text 1

Formatted: Font color: Text 1

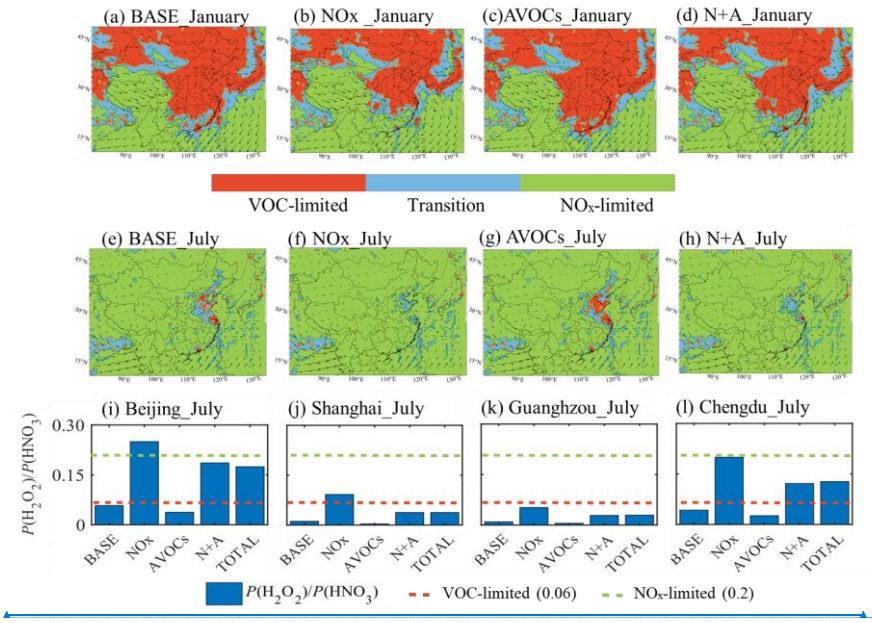

Figure 5. Ozone sensitivity regimes and their changes due to emissions reduction. (a-h) Display of regions in which ozone production is limited by the availability of nitrogen oxides (NO_x-limited, in green), and volatile organic components (VOC-limited, in red) from the TOTAL case under the emissions in case of BASE, NOx, AVOCs, and N+A conditions in January (a-d) and July (e-h) of 2018. The regions where ozone production is controlled by the availability of both NO_x and VOCs (transition) are shown in blue. (i-l) The daytime (06:00 to 19:00 Local Standard Time (LST)) value of ratio between the production rate of hydrogen peroxide (H_2O_2) and nitric acid (HNO_3) [$P(H_2O_2)/P(HNO_3)$] at four city sites (Beijing, Shanghai, Chengdu, Guangzhou) of China for July 2018 in the five emissions cases.

Formatted: Font color: Text 1
Formatted: Font color: Text 1
Formatted: Centered
Formatted: Font color: Text 1
Formatted: Font color: Text 1
Formatted: Font color: Text 1
Formatted: Font color: Text 1

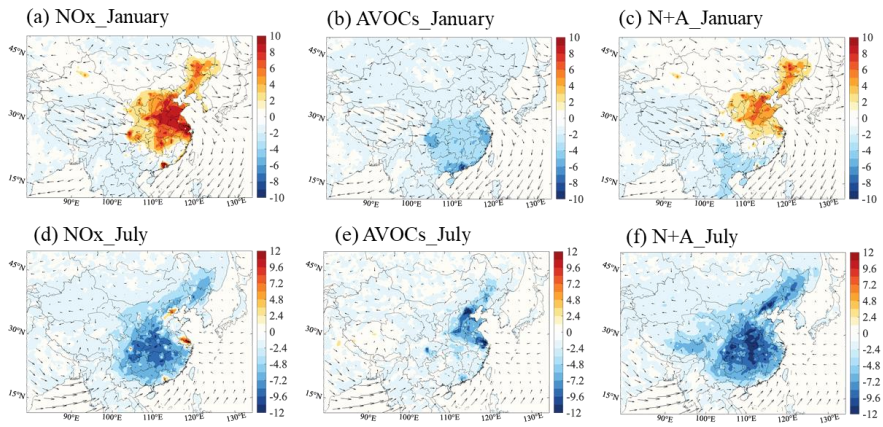

Figure 6. Changes in the averaged daytime surface mixing ratio ozone response to a 50% reduction in NO_x emissions (NOx case), in anthropogenic VOCs (AVOCs) emissions (AVOCs case) and in combined NO_x and AVOCs emissions (N+A case) relative to BASE case for January (a-c) and July (d-f) of 2018. Arrows represent the wind speed and wind direction.

Formatted: Font color: Text 1

Formatted: Font color: Text 1

Formatted: Font color: Text 1

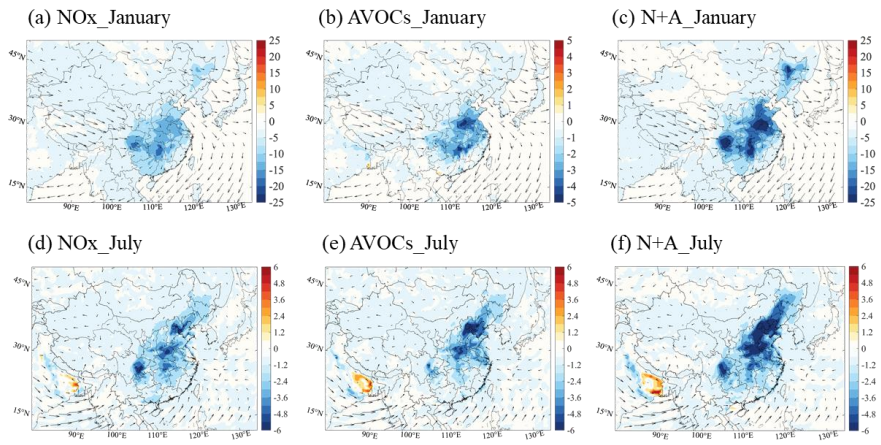

Figure 7. Changes in the surface concentration of fine particulate aerosol (Unit: μg m^{-3}) in response to NOx (a, d), AVOCs (b, e) and N+A case (c, f) relative to BASE case for January (a-c) and July (d-f) of 2018. Arrows represent the wind speed and wind direction. Notice the inconsistency in the scale of Figure 7b.

Formatted: Font color: Text 1

Formatted: Font color: Text 1

Formatted: Left

Formatted: Font color: Text 1

Formatted: Font: (Asian) +Body Asian (SimSun), (Asian) Chinese (Simplified, Mainland China)

Formatted: Font color: Text 1

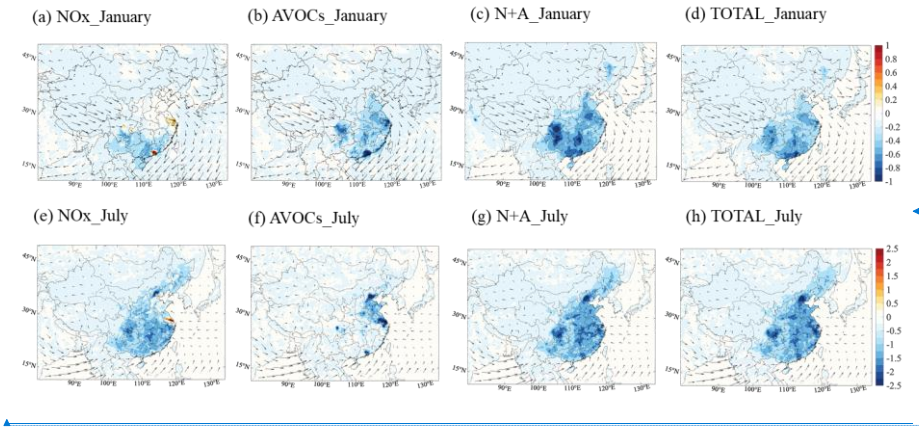

Formatted: Font color: Text 1

Formatted: Centered

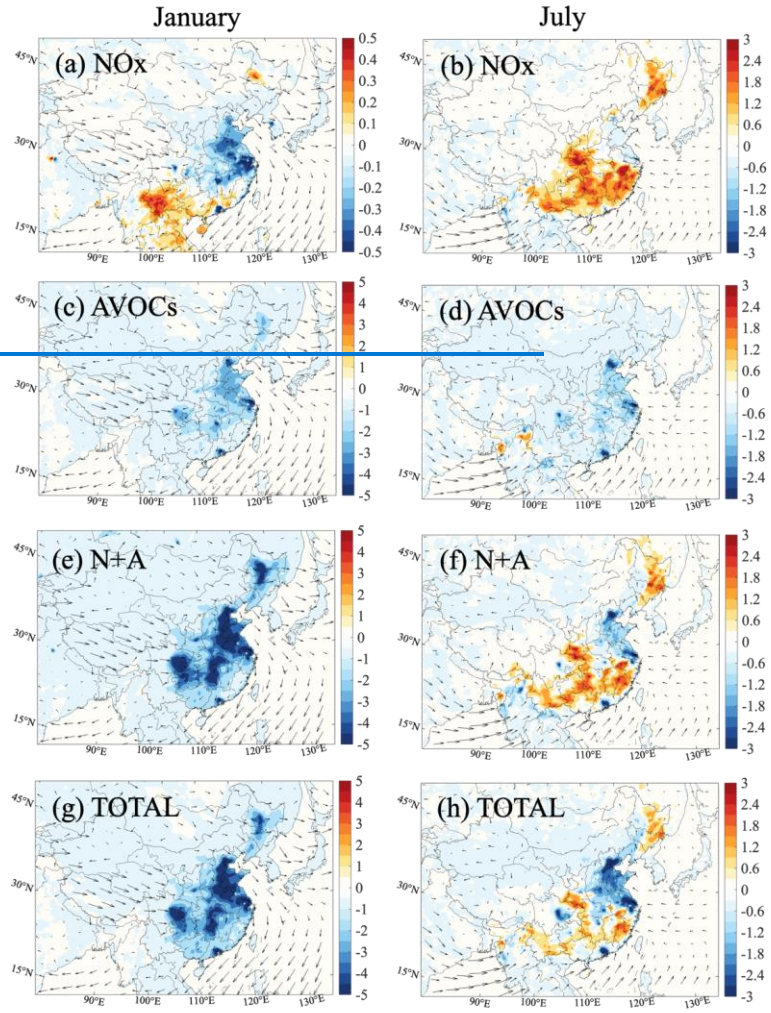

Figure 8. Changes in the average daytime atmospheric oxidizing capacity (*AOC*, Unit: 10^7 molec. cm^{-3} s^{-1}) response to NO_x (a, e), AVOCs (b, f), N+A (c, g), and TOTAL (d, h) cases relative to BASE case for January (a-d) and July (e-h) of 2018.

Formatted: Font color: Text 1

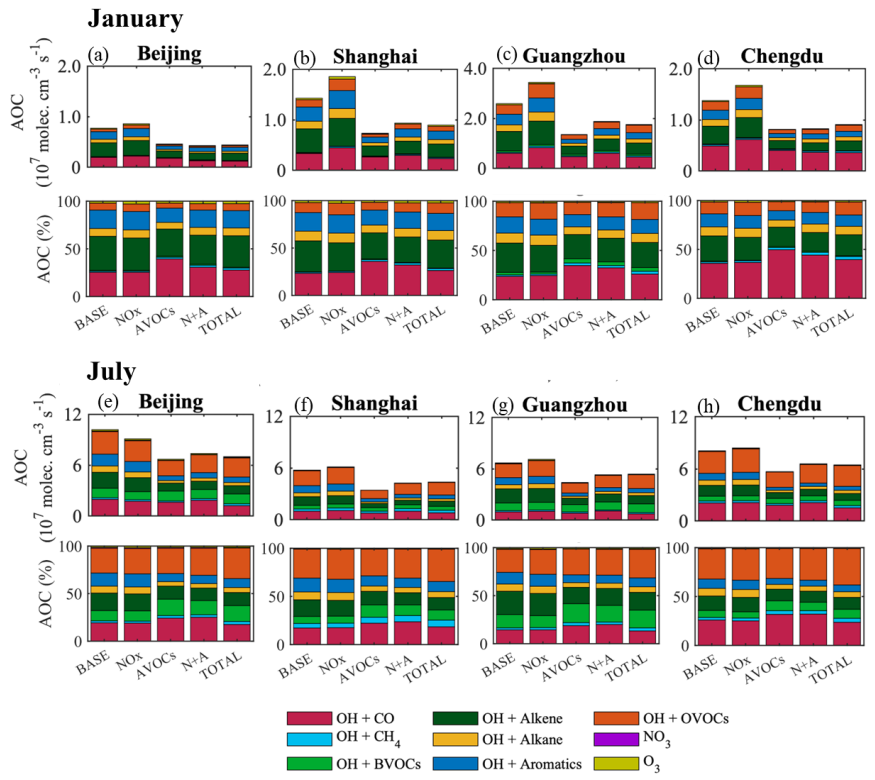

Figure 9. Averaged value and relative terms of daytime (06:00 to 19:00 Local Standard Time) *AOC* at the sites of Beijing (a, e), Shanghai (b, f), Guangzhou (c, g), and Chengdu (d, h) in five different simulated cases (BASE, NOx, AVOCs, N+A, TOTAL cases) in January (a-d) and July (e-h) of 2018. Notice the inconsistency in the scale of Figure 9c.

~~Figure 15. Changes in the average daytime OH reactivity from VOCs and CO [Unit: s^{-1}] response to the NOx case (a, b), AVOCs case (c, d), N+A case (e, f), and TOTAL case (g, h) relative to BASE case. Results are shown for January (a, c, e, g) and July (b, d, f, h) of 2018. Arrows represent the wind speed and wind direction.~~

Formatted: Font color: Text 1

Formatted: Font: (Asian) +Body Asian (SimSun), Font color: Text 1, (Asian) Chinese (Simplified, Mainland China)

Formatted: Font color: Text 1

Formatted: Font color: Text 1

Formatted: Font color: Text 1

Formatted: Font color: Text 1

Formatted: Justified

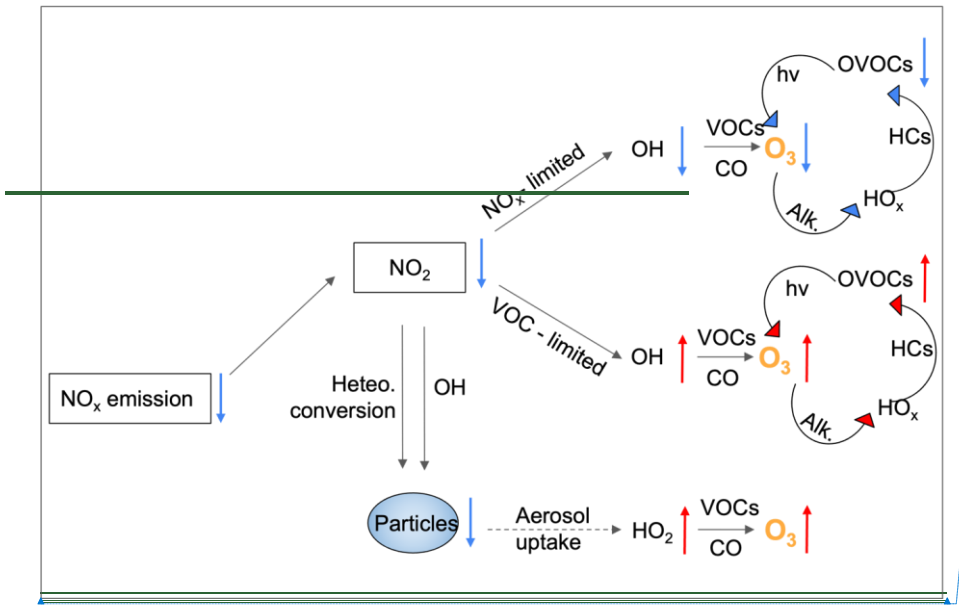

Formatted: Font color: Text 1

Formatted: Font color: Text 1

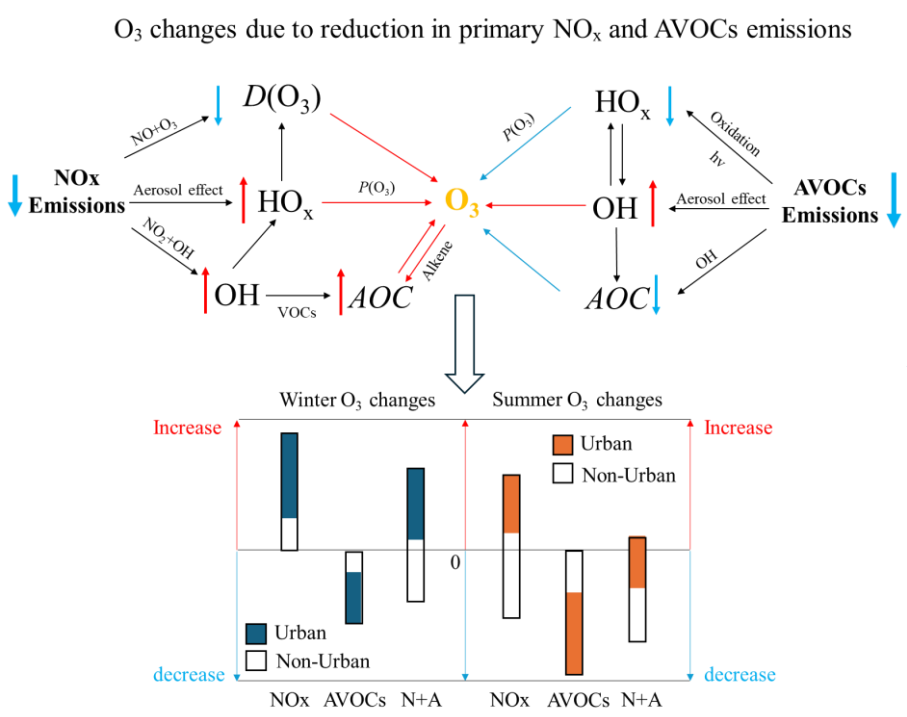

Figure 104. Schematics shows the responses of oxidative processes, associated with ozone formation, to the ~~for the impact of NO_x emission~~ reduction in primary emissions of NO_x and AVOCs in urban areas (VOC-limited) in winter and summer. ~~through aerosol effect and photochemical processes on ozone concentration.~~ Arrows besides the chemicals represent the changes ~~in the concentration of chemicals~~ associated with the reduction ~~of NO_x~~ in emission. (decrease trend shown in blue; increase trend shown in red) ~~.~~ Blue and red arrows closing to O_3 represent the positive and negative contributions to the ozone formations. *AOC*, ~~HCs and~~ $P(O_3)$, and $D(O_3)$ ~~Alk.~~ are the abbreviations of the Atmospheric Oxidative Capacity, production of ozone~~hydrocarbons and alkenes~~, and destruction of ozone. Bar figure shows the ranges of ozone changes in whole of China (black bar), in non-urban areas (white part in the bar) in four city sites in three emissions cases (NOx, AVOCs, and N+A represent the case with emissions reduction in NO_x, Anthropogenic VOCs (AVOCs), and the combined NO_x and AVOCs emissions, respectively) relative to BASE cases in winter and summer.

Formatted: Font color: Text 1
Formatted: Centered
Formatted: Font color: Text 1
Formatted: Font color: Text 1, Subscript
Formatted: Font color: Text 1
Formatted: Font color: Text 1
Formatted: Font color: Text 1
Formatted: Font color: Text 1, Subscript
Formatted: Font color: Text 1
Formatted: Font: Italic, Font color: Text 1
Formatted: Font color: Text 1
Formatted: Font: Italic, Font color: Text 1
Formatted: Font color: Text 1
Formatted: Font color: Text 1, Subscript
Formatted: Font color: Text 1
Formatted: Font color: Text 1
Formatted: Font color: Text 1
Formatted: Font color: Text 1, Subscript
Formatted: Font color: Text 1
Formatted: Font color: Text 1, Subscript
Formatted: Font color: Text 1

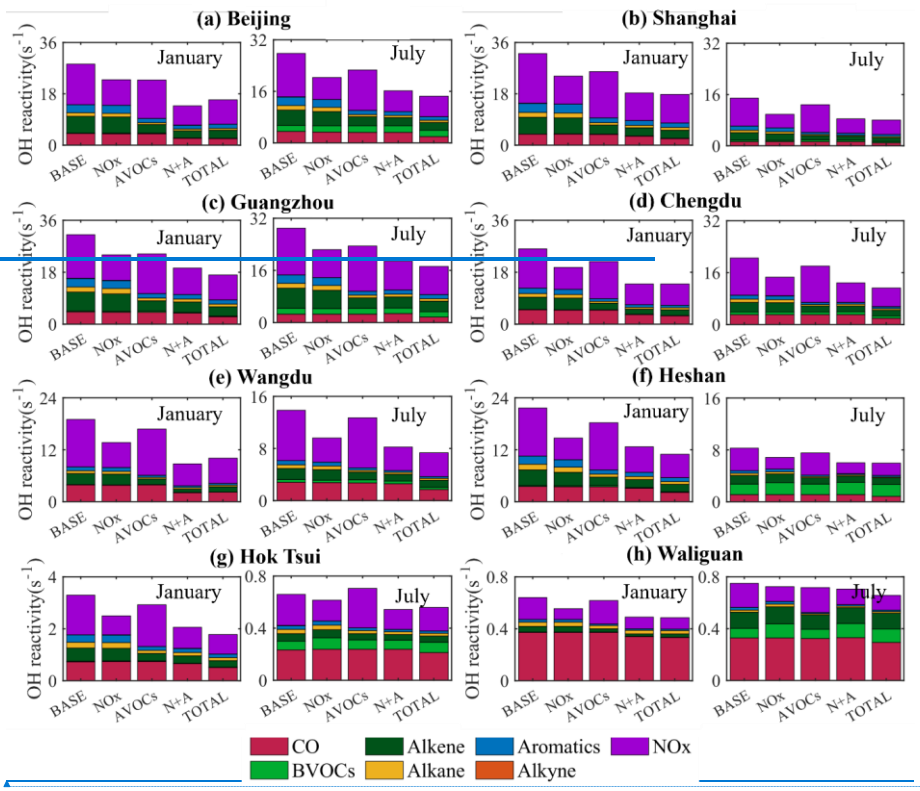

Figure 16. Averaged value of daytime OH reactivity [Unit: s^{-1}] with the contribution from seven different species in five different simulated cases (BASE, NOx, AVOCs, N+A, TOTAL cases) and in eight different sites in July.

Formatted: Font color: Text 1

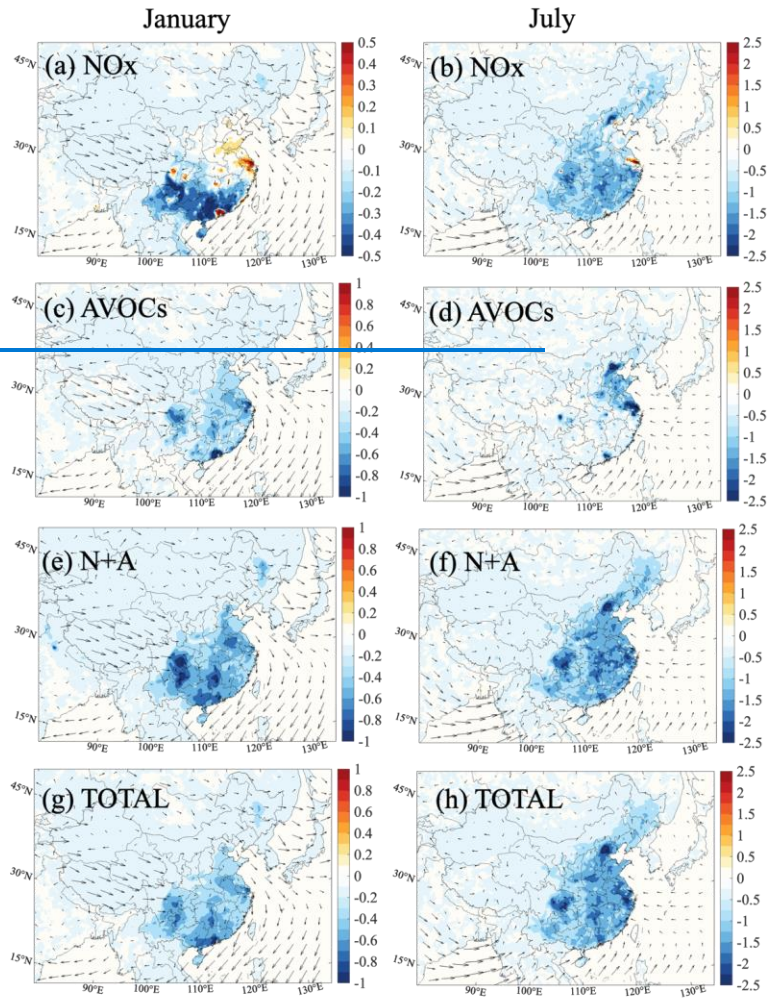

Figure 17. Changes in the daytime averaged atmospheric oxidizing capacity (*AOC*) [Unit: 10^7 molec. cm^{-3} s^{-1}] response to the NOx case (a, b), AVOCs case (c, d), N+A case (e, f), and TOTAL case (g, h) relative to BASE case. Results are shown for January (a, c, e, g) and July (b, d, f, h) of 2018. Arrows represent the wind speed and wind direction.

Formatted: Font color: Text 1

Formatted: Font color: Text 1

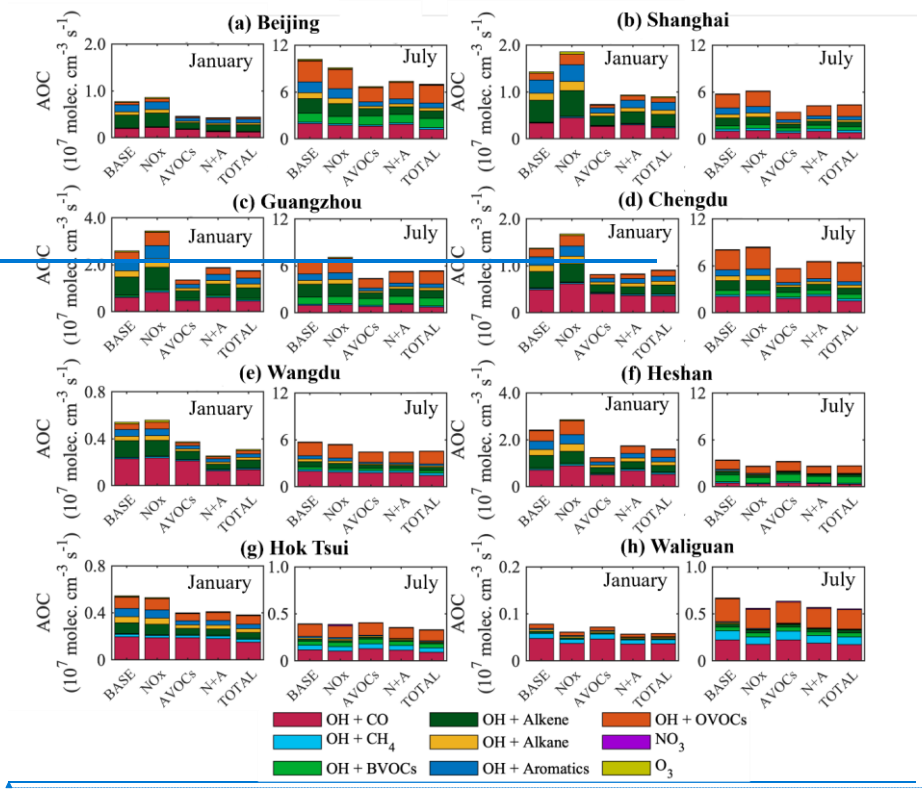

Figure 18. Averaged value of *AOC* [Unit: 10^7 molec. cm^{-3} s^{-1}] during daytime in nine different species in five different simulated cases (BASE, NOx, AVOCs, N+A, TOTAL cases) and in eight different sites in July.

Formatted: Font color: Text 1

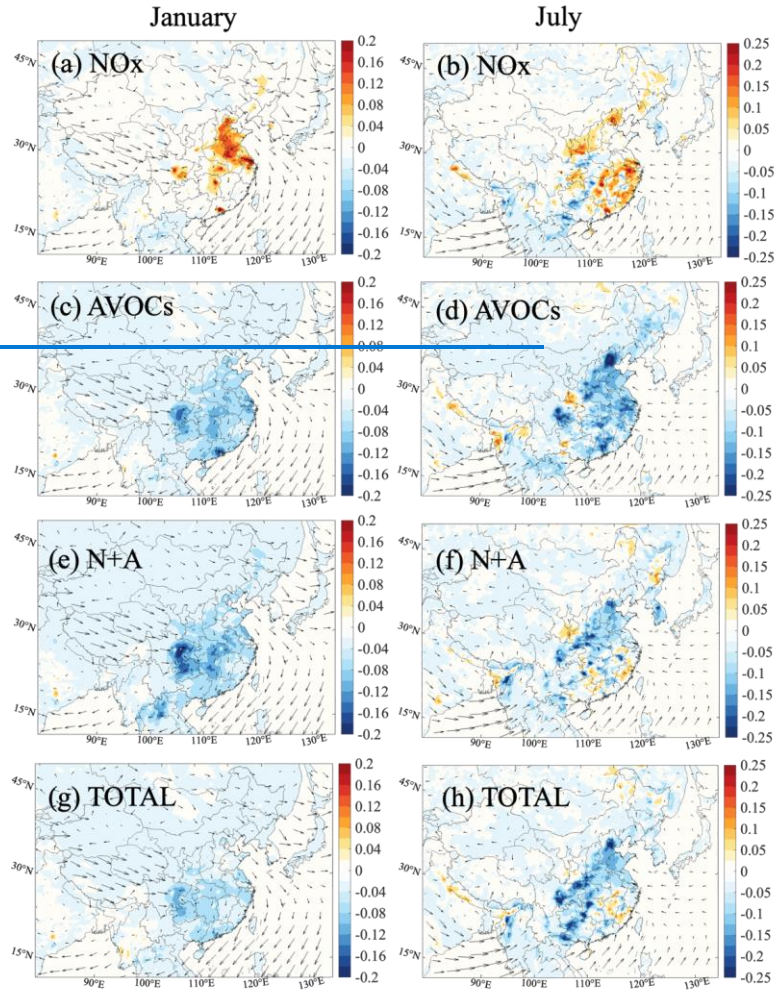

Figure 19. Spatial distribution of the averaged nighttime (20:00 to 05:00 LST) atmospheric oxidizing capacity (*AOC*) due to the reactions between ozone and alkenes [Unit: 10^6 molec. cm^{-3} s^{-1}] response to the ratio of 0.5 in NO_x emissions (a, b; NOx case), in Anthropogenic VOCs (AVOCs) emissions (c, d; AVOCs case), in NO_x and AVOCs emissions (e, f; N+A case), and all anthropogenic emissions (g, h, TOTAL case) relative to BASE case. Results are shown for January (a, c, e, g) and July (b, d, f, h) of 2018. Arrows represent the wind speed and wind direction.

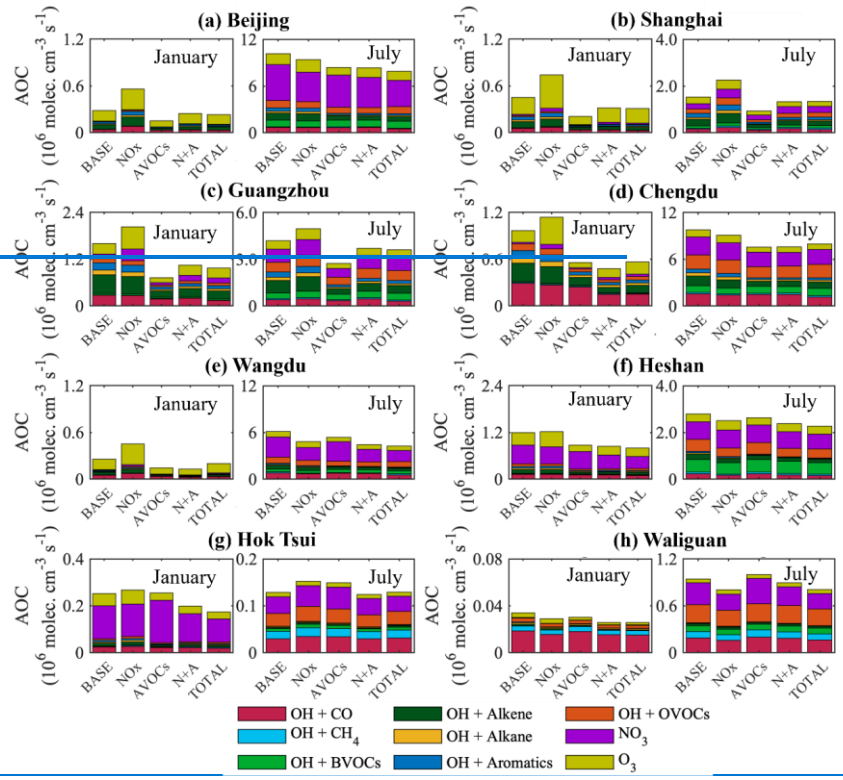

Figure 20. Averaged value of *AOC* [Unit: 10^6 molec. cm^{-3} s^{-1}] during nighttime in nine different species in five different simulated cases (BASE, NOx, AVOCs, N+A, TOTAL cases) and in eight different sites in July.

Formatted: Font color: Text 1